



UNIVERSIDADE FEDERAL DO CEARÁ
CENTRO DE TECNOLOGIA
DEPARTAMENTO DE ENGENHARIA METALÚRGICA E DE MATERIAIS
PROGRAMA DE PÓS-GRADUAÇÃO EM ENGENHARIA E CIÊNCIA DE
MATERIAIS

PAULO DEMÉTRIOS DA SILVA LIMA

**TEXTURAL PROPERTIES STUDY OF Mg-Al LAYERED DOUBLE
HYDROXIDES WITH DIFFERENT MOLAR RATIOS AND UPON
HYDROTHERMAL TREATMENTS**

FORTALEZA

2014

PAULO DEMÉTRIOS DA SILVA LIMA

**TEXTURAL PROPERTIES STUDY OF Mg-Al LAYERED DOUBLE
HYDROXIDE WITH DIFFERENT MOLAR RATIOS AND UPON
HYDROTHERMAL TREATMENTS**

Tese apresentada ao Programa de Pós-Graduação em Engenharia e Ciência de Materiais da Universidade Federal do Ceará, como requisito parcial à obtenção do título de doutor em engenharia e ciência dos materiais. Área de concentração: materiais não metálicos.

Orientador: Prof. Dr. Ricardo Emílio Ferreira Quevedo Nogueira

Co-orientador: Prof. Dr. Sebastião Mardônio Pereira de Lucena.

FORTALEZA

2014

Dados Internacionais de Catalogação na Publicação
Universidade Federal do Ceará
Biblioteca de Pós-Graduação em Engenharia - BPGE

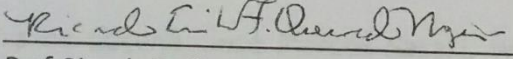
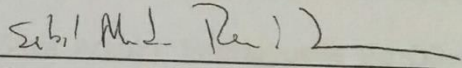
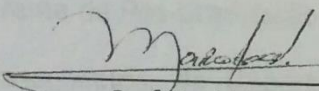
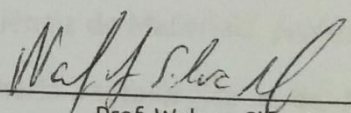
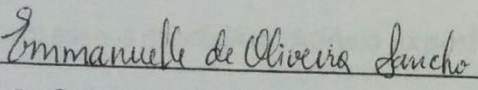
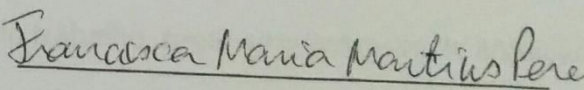
-
- L71t Lima, Paulo Demétrios da Silva.
Textural properties study of mg-al layered double hydroxides with different molar ratios and upon hydrothermal treatments / Paulo Demétrios da Silva Lima. – 2014.
122 f. : il. color. , enc. ; 30 cm.
- Tese (doutorado) – Universidade Federal do Ceará, Centro de Tecnologia, Departamento de Engenharia Metalúrgica e de Materiais, Programa de Pós-Graduação em Engenharia e Ciência de Materiais, Fortaleza, 2014.
Área de Concentração: Processos de Transformação e Degradação dos Materiais.
Orientação: Prof. Dr. Ricardo Emílio Ferreira Quevedo Nogueira.
Coorientação: Prof. Dr. Sebastião Mardônio Pereira de Lucena.
1. Ciência dos materiais. 2. Adsorção. 3. Cristalinização. I. Título.

PAULO DEMÉTRIOS DA SILVA LIMA

**TEXTURAL PROPERTIES STUDY OF Mg-Al LAYERED DOUBLE
HYDROXIDE WITH DIFFERENT MOLAR RATIOS AND UPON
HYDROTHERMAL TREATMENTS**

Tese apresentada ao Programa de Pós-Graduação em Engenharia e Ciência de Materiais da Universidade Federal do Ceará, como requisito parcial à obtenção do título de doutor em engenharia e ciência dos materiais Área de concentração: materiais não metálicos.

BANCA EXAMINADORA

<input checked="" type="checkbox"/> APROVADO	<input type="checkbox"/> NÃO APROVADO
Secretaria do Programa de Pós-Graduação em Engenharia e Ciência de Materiais da Universidade Federal do Ceará, em 28 de fevereiro de 2014.	
 Prof. Ricardo Emilio Ferreira Quevedo Nogueira Presidente e Orientador	 Prof. SebastiãoMardônio Pereira de Lucena Membro
 Prof. José Marcos Sasaki Membro	 Prof. Walney Silva Araujo Membro
 Prof.ª Emmanuelle de Oliveira Sancho Membro	 Prof.ª Francisca Maria Martins Pereira Membro

A Deus

A minha mãe que me ensinou a trabalhar e estudar.

A meu pai que me ensinou a estudar e trabalhar, não com palavras, mas com ações. Quando criança costumava vê-lo debruçado numa mesa à luz de um poste em frente de nossa casa, estudando. É a imagem que tenho dele e espero deixar o mesmo exemplo para meus descendentes.

AGRADECIMENTOS

A Deus

A meus pais Raimundo Nonato Cardoso Lima, Albanisa da Silva Lima e Maria Zenete Silva de Oliveira.

A minhas filhas, Karina e Lara Lima, que sentiram minha ausência em várias noites e fins de semana isolado no escritório. O sentimento foi recíproco. Vocês são meu motivo de tanto trabalho e estudo.

A meus irmãos que sempre me apoiaram Claudia Cristina, Sérgio Ricardo e Antônio André e seus respectivos cônjuges: Kleber, Silvânia e Andrea.

Ao meu amigo Daniel Paula de Sousa que sempre estudou muito e valorizou os amigos que estudam.

Ao meu orientador Ricardo Emilio Ferreira Quevedo Nogueira pela paciência, ajuda constante e confiança.

Ao meu coorientador Sebastião Mardônio Pereira de Lucena que me vem orientando desde a graduação como aluno do PET, orientação em pesquisas no NUTEC, coorientação na pesquisa do mestrado e coorientação nessa pesquisa do doutorado. Meu muito obrigado por todos esses anos de muita paciência em suportar minhas teimosias.

Ao professor Dr. Sasaki que esmiuçou e levantou vários pontos falhos em minha tese. Obrigado por sua contribuição professor Sasaki.

A Dra. Francisca Pereira pelas suas contribuições valiosas a minha tese.

Ao colega de graduação Dr. Walney Araujo pelas suas observações sinceras

A minha amiga Dra. Emmanuelle Sancho que tive a oportunidade de tê-la como membro da banca examinadora. Suas anotações engrandeceram muito minha pesquisa.

Ao Dr. Lindberg Lima Gonçalves que me aceitou no programa novamente mesmo depois de eu ter falhado no mestrado. Obrigado pela oportunidade.

A meus colegas do laboratório de Biomateriais e de Cerâmica pelo apoio nesses cinco anos de jornada: Erisandra, Jean, Eden, Fabiana, Claudia, Halison, Suely, Joelane.

Ao professor Dr. José de Araújo Nogueira Neto e seu aluno de graduação Allison Maia do departamento de Geologia da UFC pelos ensaios de MEV e EDS.

A Teresa Lima pelas análises de TG e Elis pelas análises de IR no departamento de Química da UFC.

A Teresa e os demais colegas do laboratório de DRX do departamento de Física da UFC pelas análises de difração de raios x:

Ao professor Dr. Ivanildo Silva que cedeu gentilmente o laboratório de sua responsabilidade para que ensaios de adsorção fossem realizados.

A minha amiga Bruna Cavalcante que realizou muitos dos ensaios de adsorção e elaborou vários gráficos de minha tese. Muito obrigado Bruninha.

Ao meu amigo Thiago Ribeiro que fez vários gráficos e refinamentos de minhas amostras. Sua habilidade computacional me poupou semanas de trabalho. Meu muito obrigado amigo Thiago.

A meu amigo Dr. Silvio Albuquerque que sempre me ajudou nessa caminhada. Obrigado pelos incontáveis favores e por ter feito as primeiras revisões de minha tese. Serei eternamente grato.

The work of a scientist is to reduce the
entropy of the information

Paulo D. S. Lima

RESUMO

Hidróxidos Duplos Lamelares (HDL) pertencem a uma classe de materiais cerâmicos formados por camadas empilhadas de hidróxidos metálicos com um ânion entre os espaços lamelares. Apresentam uma grande variedade de possíveis aplicações, na área industrial, ambiental, medicinal, entre outras. Hidróxidos Duplos Lamelares (HDL) não calcinados de Magnésio e Alumínio com razão molar $x = \text{Al} / (\text{Mg} + \text{Al})$, 0,20, 0,25 e 0,30 foram sintetizados utilizando o método de co-precipitação, seguido por tratamento hidrotérmico em temperatura fixa de 80 ° C e diferente tempos de maturação de 2 a 35 dias. O material obtido foi caracterizado por DRX, IV, TG, MEV e EDS. A cristalinidade das amostras foi avaliada e tamanho de partícula foi calculado usando a equação Scherrer. Foram investigadas adsorção de corantes ácido azul 25 e azul reativo 4 para algumas amostras de razão molar 0,25. O objetivo deste trabalho foi estudar o efeito do tratamento hidrotérmico e condições de tempo de maturação nas propriedades texturais de hidrotalcita sintetizada com diferentes razões molares e propor uma função matemática para prever o tamanho de cristalito e cristalinidade. Esta função leva apenas dois de muitos parâmetros em consideração: tempo de tratamento hidrotérmico e razão molar. As amostras obtidas com uma razão molar 0,20 e 0,25 apresentaram boa cristalinidade para todas as amostras. Por outro lado, as amostras com razão molar 0,30 apresentaram baixa cristalinidade, um pronunciado deslocamento nos picos basais 003 e 006, e um alargamento em todos os picos. O deslocamento desses picos para essa última amostra foi mostrado ser estatisticamente significativo em relação às outras duas. Um resultado não esperado foi encontrado em desacordo com a literatura: uma nova fase cristalina foi observada em duas amostras de razão molar 0,20. Os resultados do MEV e EDS indicam que há uma provável fase amorfa nas amostras de razão molar 0,30. A fase amorfa explicaria a redução da cristalinidade das amostras dessa série. Apenas a função para prever a cristalinidade foi obtida e mostrada em gráficos 3D e hipsométricos. Esta função pode ser usada para prever características de um HDL sintetizado para uma aplicação industrial, tal como a adsorção.

Palavras-Chaves: HDL, Hidrotalcita, Cristalinidade, Adsorção.

ABSTRACT

Layered Double Hydroxide (LDH) belongs to a class of ceramic materials that present structure formed by stacked layers of double metals hydroxides and an anion into the lamellar space. They present a large variety of applications possibilities, as industrial, environment, medicine, among others. Non-calcined Mg-Al layered double hydroxide (LDH) with molar ratio, $x = \text{Al} / (\text{Mg} + \text{Al})$, 0.20, 0.25 and 0.30 were synthesized using co-precipitation method, followed by hydrothermal treatment at a fixed temperature 80°C and different aging from 2 to 35 days. The material obtained was characterized by XRD, IR, TG, SEM and EDS. The samples crystallinity was evaluated and particle size was calculated using Scherrer equation. Sorption of anionic acid blue 25 and reactive blue 4 dyes from aqueous solution was investigated for some of the 0.25 molar ratio samples. The purpose of this research was to study the effect of hydrothermal treatment aging conditions on textural properties of synthetic hydrotalcite with different molar ratios and propose a mathematical function to predict crystallite size and crystallinity. This function takes just two of many parameters in consideration: hydrothermal treatment aging time and molar ratio. The obtained as-synthesized samples with a molar ratio 0.20 and 0.25 showed good crystallinity for all the samples. On the other hand the third samples with molar ratio 0.30 showed poor crystallinity, a pronounced shift in the correspondent basal planes peaks 003 and 006, and a broadening in all peaks. The shift in the basal planes was shown to be statistically significant to the others. A non-expected result was found in disagreement with literature: a new crystalline phase was observed in two 0.20 molar ratio samples. MEV and EDS results indicate the existence of a probable amorphous phase in the 0.30 molar ratio samples. The amorphous phase would explain the reduction in crystallinity of this series samples. Just the function to predict the crystallinity was obtained and showed in a 3D and hypsometric graphics. This function may be used to predict a characteristic of a synthesized LDH for an industrial application, like adsorption.

Key-Words: LDH, Hydrotalcite, Crystallinity, Adsorption.

FIGURES LIST

Figure 1.1 Brucite structure, Mg (OH) ₂ .	22
Figure 1.2 LDH general structures.	22
Figure 1.3 Hydrotalcite mineral from a mine in Middle Urals, Russia.	24
Figure 1.4 hydrotalcite rhombohedral structure.	25
Figure 1.5 Growth of LDH researches.	26
Figure 1.6 Cycles of adsorption and desorption.	28
Figure 1.7 Synthesis Influence in LDH crystallinity.	33
Figure 2.1 IUPAC adsorption isotherm classifications.	38
Figure 3.1 Diffraction of an incident beam	43
Figure 3.2 Scheme operation of the X-ray diffractometer	44
Figure 3.3 Diagram for particle and crystallite size	48
Figure 4.1 Flowchart of the obtained process to synthesize Mg-Al LDH.	51
Figure 5.1 XRD for 20 Mg-Al Series.	55
Figure 5.2 XRD for 25 Mg-Al Series.	56
Figure 5.3 XRD for 30 Mg-Al Series.	57
Figure 5.4 XRD for 20, 25, and 30 Mg-Al Series.	58
Figure 5.5 Cell parameter c obtained for 20 Mg-Al and 25 Mg-Al Series.	61
Figure 5.6 3D Surface Color Map (a, b and c) and hypsometric (d) for D003.	62
Figure 5.7 3D Surface Color Map (a, b and c) and hypsometric (d) for D006.	63
Figure 5.8 3D Surface Color Map (a, b and c) and hypsometric (d) for Ds.	64
Figure 5.9 Diagram for hypothesis test sequence.	70
Figure 5.10 3D Surface Color Map (a, b, c, d, e) and hypsometric (f) for I=f(x,t).	77
Figure 5.11 Function fit: Rational only (a) fit with I = f (x, t) (b, c, d).	79
Figure 5.12 XRD samples with brucite: 20 Mg-Al 28 (a) and 20 Mg-Al 35 (b).	82
Figure 6.1 Thermo Gravimetric (a) and derivative (b) for the 20 Series.	84
Figure 6.2 Thermo Gravimetric (a) and derivative (b) for the 25 Series.	85
Figure 6.3 Thermo Gravimetric (a) and derivative (b) for the 30 Series.	86
Figure 6.4 Infra-Red for 20 Series samples.	90
Figure 6.5 Infra-Red for 25 Series samples.	91
Figure 6.6 Infra-Red for 30 Series samples.	92
Figure 6.7 Micrographs: (a) 20Mg-Al 4 (b) 20Mg-Al 35	94
Figure 6.8 Element maps for: a) 20 Mg-Al 4 and b) 20 Mg-Al 35	94
Figure 6.9 Micrographs: a) 25Mg-Al 4; b) 25Mg-Al 14; c) 25Mg-Al 21; d) 25Mg-Al 28.	95
Figure 6.10 Micrographs for 25 Mg Al 4 sample without grinding. Magnification: a) 800 x; b) 1,000 x; c) 2,000 x; d) 5,000 x	96
Figure 6.11 Distribution of particle size in the not ground sample 25 Mg-Al 4.	98
Figure 6.12 Element maps for: a) 25 Mg-Al 4 and b) 25 Mg-Al 35	98
Figure 6.13 Element maps for 25 Mg-Al 4 (without grinding)	99
Figure 6.14 Micrographs for 30 Mg-Al 4 sample. Magnification: a) of 50x; b) 80x.	100
Figure 6.15 EDS for 30 Mg-Al 4 sample in different regions (a, b, c).	101
Figure 6.16 Micrographs for 30Mg-Al 35 sample. Magnification: (a) of 30x; (b) 1,000x.	102

Figure 6.17 EDS for 30 Mg-Al 35 samples in different regions (a, b).....	102
Figure 6.18 Element maps for: a) 30 Mg-Al 4 and b) 30 Mg-Al 35.	103
Figure 7.1. N ₂ adsorption-desorption isotherm of 25Mg-Al 4 at 77 K.....	104
Figure 7.2 Experimental adsorption results in a) AB 25 and b) RB 4.....	106

TABLES LIST

Table 2.1 Chemical and physical adsorption.....	37
Table 4.1 Dyes chemical structures and characteristics.....	53
Table 5.1 Refinement parameters from 20 Mg-Al LDH Series.....	60
Table 5.2 Refinement parameters from 25 Mg-Al LDH Series.....	60
Table 5.3 Mean (\bar{x}) and Standard Deviation (s) for 003 and 006 peaks.....	66
Table 5.4 Applied statistics to 2θ peaks shift at 003 planes.....	71
Table 5.5 Applied statistics to 2θ peaks shift at 006 planes.....	72
Table 5.6 Applied statistics to Crystallinity.....	74
Table 5.7 Parameter c for the 30 Series.....	75
Table 5.8 Parameters for the fit function.....	78
Table 5.9 Cell parameters and crystallite size for the samples with brucite.....	81
Table 6.1 Mass loss in the first stage.....	87
Table 6.2 Mass loss in the second stage.....	88
Table 7.1 Relative comparison among the experimental results.....	105
Table 7.2 Fit for dyes adsorption in LDH samples.....	107
Table 7.3 Isotherms parameters adsorption: Langmuir (L), Freundlich (F), Langmuir-Freundlich (LF) e Toth (T) for Acid Blue 25 (AB 25) and Reactive Blue 4(RB 4).....	108

ABBREVIATIONS

ANOVA	Analysis Of Variance
AB25	Acid Blue 25
BET	Brunauer Emmett Teller
CI	Color Index
EDS	Energy Dispersive Spectroscopy
FWHM	Full Width at Half Maximum
FCC	Fluid Catalytic cracking
IUPAC	International Union of Pure and Applied Chemistry
ICDD	International Center For Diffraction Data
ICSD	Inorganic Crystal Structure Database
LDH	Layered Double Hydroxides
RB4	Reactive Blue 4
SEM	Scanning Electron Micrograph
TG	Thermo Gravimetric
UV/VIS	Ultra Violet Visible
UFC	Universidade Federal do Ceará
XRD	X-Ray Diffraction
XRDP	X-Ray Diffraction Pattern
XRPD	X-Ray Powder Diffraction

SYMBOLS LIST

q_{\max}	Maximum Adsorption Capacity
k_l	Langmuir Equilibrium Constant
k_f	Freundlich Equilibrium Constant
k_{lf}	Langmuir-Freundlich Equilibrium Constant
k_t	Toth Equilibrium Constant
q	Adsorption Capacity
λ	Wave Length
θ	Angle
F_{hkl}	Structure Factor
β	Full Width At Half Maximum Intensity
D_{hkl}	Interplane Distance
\bar{x}	Mean Value
Md	Median Value
s	Sample Standard Deviation
CV	Coefficient Of Variance
σ^2	Population Variance
μ	Population Mean Value
s^2	Sample Variance
v	Degree of Freedom
T	Student Test
H_0	Null Hypothesis
H_1	Alternative Hypothesis
a	Cell Parameter
b	Cell Parameter
c	Cell Parameter
α	Angle with crystallographic axis
β	Angle with crystallographic axis
γ	Angle with crystallographic axis

CONTENTS

INTRODUCTION.....	18
1. LAYERED DOUBLE HYDROXIDES	21
1.1 Structure	21
1.2 Hydrotalcite.....	23
1.3 LDH Applications	25
1.3.1 <i>Industrial Applications</i>	26
1.3.2 <i>Environmental Applications</i>	27
1.3.3 <i>Medicine Applications</i>	29
1.4 Synthesis Methods	30
1.5 LDH Textural Properties and Crystallinity	32
2 ADSORPTION AND DYES	36
2.1 Adsorption Processes	36
2.1.1 <i>Chemical and Physical Adsorption</i>	36
2.1.2 <i>Adsorption Isotherm</i>	37
2.1.3 <i>Equilibrium Isotherms</i>	38
2.2 Dyes.....	40
2.2.1 <i>Dyes Nomenclature</i>	41
3 X-RAY DIFFRACTION.....	42
3.1 X-Ray Diffraction Theory	42
3.1.1 <i>Bragg's Law</i>	42
3.2 X-Ray Diffraction Techniques	43
3.3 Rietveld Method.....	46
3.3.1 <i>The Peak Intensity</i>	46
3.3.2 <i>The Pseudo-Voight Function</i>	47
3.4 Particle and Crystallite	48
4 MATERIAL AND METHODS	50
4.1 LDH Synthesis	50
4.2 LDH Characterization Analyses.....	50
4.3 Material and Procedures for LDH Adsorption	52
4.4 Software	53
5 X-RAY DIFFRACTION AND THE FIT FUNCTION	54
5.1 X-Ray Diffraction Patterns.....	55

5.2 Hydrotalcite Cell Parameters	59
5.3 Hydrotalcite Crystallite Size	62
5.4 Statistical Approach to XRD Results	65
5.5 FIT Function.....	76
5.5.1 FIT Function possible applications.....	79
5.6 The non-Expected Brucite.....	81
6 THERMOGRAVIMETRY, INFRA-RED AND MICROGRAPHY	83
6.1 Thermo Gravimetric Analysis	83
6.2 Infra-Red Spectroscopy.....	89
6.3 Scanning Electronic Microscopy and Energy Dispersive Spectroscopy.....	93
6.3.1 Micrographs and EDS for the 20 Series	93
6.3.2 Micrographs and EDS for the 25 Series	95
6.3.3 Micrographs and EDS for the 30 Series	99
7 ADSORPTION APPLICATIONS	104
7.1 Adsorption-Desorption Isotherm.....	104
7.2 Dyes Adsorption.....	105
CONCLUSIONS	109
PROPOSALS FOR FUTERES RESEARCH	112
REFERENCES.....	113
APPENDIX	122
A. Scientific Production	122
B. Presentation	123

INTRODUCTION

Chemical contamination of water from a variety of toxic derivatives, in particular heavy metals, pigments and aromatic, is a very serious problem presenting a high potential of human poisoning. Therefore there is a need to develop technologies that can remove pollutants from wastewater (SINGH et alli, 2009).

Fast commercial and industrial growth has resulted in more comfort for humans, but for many years man has not been concerned with the possible consequences of the environment. Consequently a very large amount of pollutants has been discharged creating serious impacts on soil and water (CHUANG et alli, 2008).

Textile dyes have been used for decades and are available in a great variety of colors. The process of dyeing consists of several steps which are chosen according to the nature of the textile fiber, structural features, and classification (GUARATINI and ZANONI, 2000). It is estimated that 40,000 tons of dyes are lost each year in wastewaters (MARSCH and REINOSO, 2006).

Most dyes are synthetic in origin and exhibit complex aromatic molecular structures that make them more stable and difficult to degrade (PONRAJ et alli, 2011). Textile industry dyes can be classified into three categories as follow: (a) anionic: direct, acid, reactive, (b) cationic: basic and (c) non-ionic: dispersed dyes (KYZAS et alli, 2013).

Traditionally, activated carbon has been used for adsorption of these dyes in complementary treatment. Studies indicate (PEREIRA et alli, 2003, AL-DEGS et alli, 2001) that activated carbon is more efficient in the removal of cationic dyes (such as methylene blue) than the anionic dyes (acid, direct and reactive dyes).

LOW and LEE (1997) have generalized that most biological sorbents (maize cob, bagasse pith, wood and peat) are more efficient in attracting cationic than anionic dyes. Studies with low cost inorganic materials such as clays and fuller's earth also indicate that inorganic materials have affinity for the cationic surfactants.

In the last decade, layered double hydroxides (LDHs) have been widely investigated due to their distinctive characteristic of having positive charges on the layers instead of negative charges, as in traditional clays. LDH is therefore a strong candidate to capture anionic dyes. Several studies have shown that the capacity of LDH to adsorb anionic dyes is of the same order of magnitude of the adsorption of cationic

dyes by activated carbons (ABDELKADER et alli, 2011; ZHU et alli, 2005; BOUDIAF et alli, 2012).

Calcined and non-calcined LDH, in particular are a promising candidate for adsorption because of its relative ease of preparation, high capacity of anion exchange, reuse, high surface area and porosity (AUXILIO et alli, 2009; SAIAH et alli, 2009).

LDH belongs to a class of ceramic materials that present a structure formed by stacked layers of double metals hydroxides and an anion into the lamellar space. Their general formula, $[M^{+2}_{1-x} M^{+3}_x (OH)_2]^{+x} A^{-m}_{x/m} \cdot nH_2O$, permits a large variety of combinations of different metals M^{+2} and M^{+3} (CREPALDI and VALIM, 1998; THEVENOT et alli, 1989; ALEJANDRE et alli, 1999; ARAÚJO, 2003; CHANG et alli, 2005; TRONTO, 2006).

The purposes of this research were to synthesize and study hydrotalcite in depth to verify how its textural properties are affected by molar ratio and aging time; to attempt to predict its crystallinity and crystallite size before synthesis (surface fit); and to evaluate its performance as a dye adsorbent.

This kind of investigation, although important to ensure a more thorough understanding of hydrotalcite, has not been reported in the literature.

In order to achieve these objectives it was necessary to characterize the materials in such a way as to enable a quantification of the textural properties. The main analysis employed was the X-ray diffraction, which allows determination and quantification of phases, calculation of cell parameters, crystallinity and crystallite size. Quantitative analyses were also important to confirm the result from X-ray diffraction and to get more information about the properties of the LDH studied.

Textural properties like crystallinity, crystallite size, particle size distribution, surface area and porosity are important to LDH applications. Some authors studied these characteristics and manifest interest in proposing a synthesis path that could impart specific properties to the LDH obtained (OH et alli, 2002; BRAVO-SUAREZ et alli, 2004; SHARMA et alli, 2007; SAIAH et alli, 2009; BENITO et alli, 2010; BERBER et alli, 2013). However, none of them has yet proposed the kind synthesis path pursued in neither this study nor a type of function to predict these characteristics as it was proposed in this research.

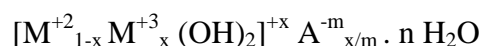
This thesis is divided into four parts: **Literature review**: LDH described in Chapter 1 with its characteristics and applications; Chapter 2 and 3 show the adsorption theme and X-ray diffraction, respectively; **Material and Methods** is seen in Chapter 4;

and **Results** that are divided into three chapters: 5, 6 and 7. Chapter 5 shows XRD results and the Fit function obtained for crystallinity. TG, IR, SEM and EDS results are reported in Chapter 6. Chapter 7 describes the results from adsorption studies.

1. LAYERED DOUBLE HYDROXIDES

1.1 Structure

Layered Double Hydroxide (LDH) belongs to a class of ceramic materials that present structure formed by stacked layers of double metals hydroxides and an anion into the lamellar space. Differently from common clays LDH presents positive charge on their surface and lamellar structure with a general formula (THEVENOT et alli, 1989; CREPALDI and VALIM, 1998; ALEJANDRE et alli, 1999; ARAÚJO, 2003; CHANG et alli, 2005; TRONTO, 2006):



where,

M^{+2} is a divalent metal cation (eg: Mg^{+2} , Mn^{+2} , Zn^{+2} , Ni^{+2} , Fe^{+2} , Cu^{+2} , Ca^{+2} , etc.);

M^{+3} is a trivalent metal cation (eg: Al^{+3} , Cr^{+3} , Co^{+3} , Ni^{+3} , Fe^{+3} , etc.);

A^{-m} is an interllamellar anion containing water molecules around it (CO_3^{-2} , NO_3^- , Cl^- , F^- , Br^- , I^- , SO_4^{-2} , CrO_4^{-2} , $[Fe(CN)_6]^{-4}$, $[NiCl_4]^{-2}$, etc.);

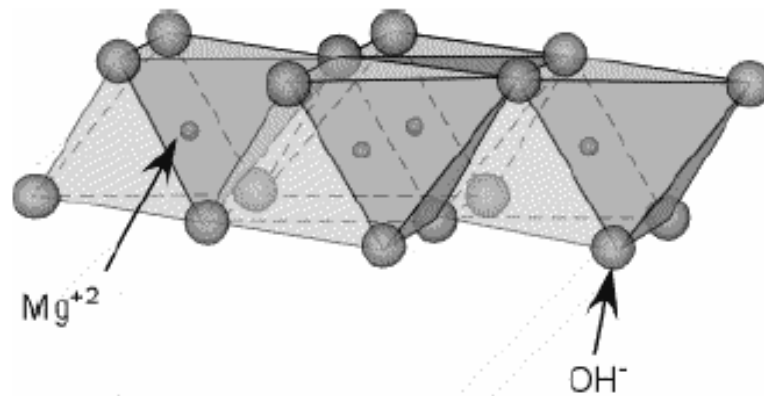
$x = M^{+3} / (M^{+2} + M^{+3})$ is the molar metal ratio.

LDH general formula shows that is possible a large variety of combinations of metals and interllamellar anions and consequently can be obtained many different kind of this cationic clay. Some authors say that the molar ratio varies from 0.20 to 0.33 to obtain pure LDH (SAIAH et alli, 2009; CAVANI et alli, 1991). KUSTROWSKI et alli (2005) suggest a range of 0.17 to 0.50 for some LDH. If it is combined just the examples of metals and anions listed above and vary the molar ratio from 0.20 to 0.33 in a tenth we obtain 4,900 different LDH.

Indeed a large number of natural or synthetic LDH has been studied. The most common divalent cations are Mg, Mn, Fe, Cu, Ca and Zn and trivalent ones are Al, Cr, Mn, Fe, Co and Ni. Some authors use various combinations of di and trivalent cations in LDH synthesis, obtaining different LDH depending on the composition and method (CHANG et alli, 2005).

LDH layers can be seen as having structures similar to that of brucite with the formula $[\text{Mg}(\text{OH})_2]$. Figure 1.1 shows brucite structure, where the Mg^{+2} ions have octahedral coordination with hydroxyl groups by edges that extend in infinite layers (GOLDANI, 2007).

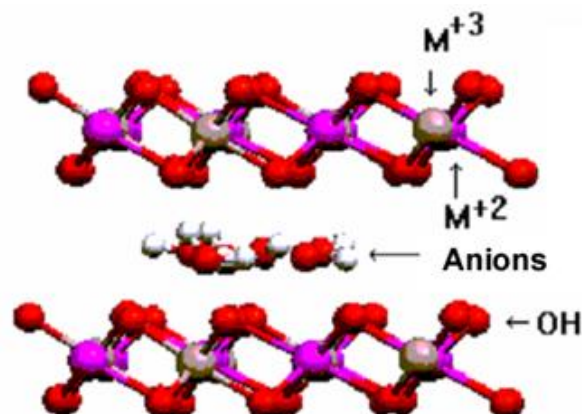
Figure 1.1 Brucite structure, $\text{Mg}(\text{OH})_2$.



Source: GOLDANI, 2007.

The divalent ions in LDH can be isomorphically replaced by trivalent ones, generating a residual positive charge that is compensated by anions located in the interlayer space (RIBEIRO, 2008; SAIAH et alli, 2009). Figure 1.2 shows the outline of a generic LDH structure with layers composed by a double hydroxide metals M^{+3} and M^{+2} and hydrated interlamellar anions.

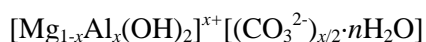
Figure 1.2 LDH general structures.



Source: RIBEIRO, 2008 (with adaptations).

1.2 Hydrotalcite

Hydrotalcite is a type of LDH with Mg and Al atoms in the lamellae structure and present the following general formula (FERREIRA, 2001; CHANG et alli, 2005; RODRIGUES, 2007; SILVA, 2008; PÉREZ et alli, 2009):



The metal ratio $x = \text{Al}^{+3}/(\text{Mg}^{+2} + \text{Al}^{+3})$ may vary, theoretically, in a large range, although, for some authors (FERREIRA, 2001; CHANG et alli, 2005; RODRIGUES, 2007; PÉREZ et alli, 2009) a range is limited from 0.2 to 0.33 to obtain a LDH as a unique phase. According to SILVA (2008) and ALEJANDRE et alli (1999), the metal ratio, x , may vary from 0.17 to 0.33.

Probably values above 0.33 to hydrotalcite is not possible because the elevated number of neighbor aluminum atoms could promote formation of amorphous bohemite ($\gamma\text{-AlO}(\text{OH})$) and/or gibbsite ($\text{Al}(\text{OH})_3$) that would not be detectable in X-rays Diffraction (CAVANI et alli, 1991; NODA PEREZ et alli, 2004). On the other hand low values of x could promote a high density of magnesium in the octahedral sheet and probably a brucite phase would be formed (CAVANI et alli, 1991)

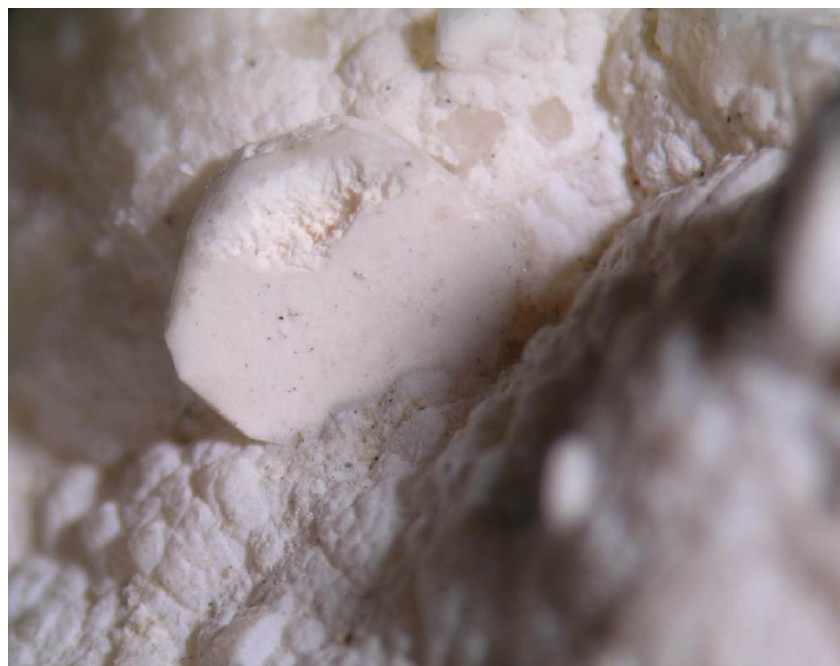
The metal ratio is an important parameter in this formula because it determines the charge density surface (AUXILIO et alli, 2009) and consequently the properties in adsorption applications (AGUIAR et alli, 2013). Furthermore adsorption, there are other industrial applications to hydrotalcite, like fluid catalytic cracking (POLATO et alli, 2009), hydrogenous oxidative catalyzer (MEIRA and CORTEZ, 2007), biomaterials (NAIME FILHO et alli, 2008), etc.

Hydrotalcite is described as a compound of brucite-like structure, where the ions Mg^{+2} and Al^{+3} are combined in octahedral sites of hydroxides sheets (CARJA et alli, 2001) and can be a natural or synthetic material (KUSTROWSKI et alli, 2005).

According to CAVANI et alli (1991), there were reports of the existence of a mineral similar to white powder that could be easily crushed as the same way to talc discovered by the year 1842 in Sweden. It was a layered double hydroxide of magnesium and aluminum, known as hydrotalcite because it appears to talc and has water in its constitution.

FRONDEL (1941) described hydrotalcite as a foliated and contorted platy and fibrous mineral. Figure 1.3 shows the hydrotalcite mineral from a mine at Urals, Russia.

Figure 1.3 Hydrotalcite mineral from a mine in Middle Urals, Russia.

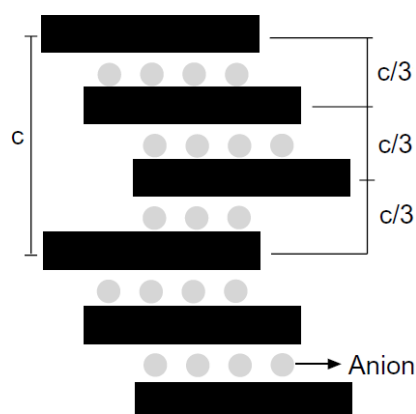


Source: <http://www.mindat.org/photo-68315.html> (access in October, 20th, 2013).

Such a clay presents a molar metal proportion of 3:1 of Mg and Al and the formula, $[\text{Mg}_6\text{Al}_2(\text{OH})_{16}]\text{CO}_3 \cdot 4\text{H}_2\text{O}$. It consists of layers of magnesium and aluminum hydroxides intercalated with hydrated carbonate ions (CO_3^{-2}) (ALEJANDRE, 1999; REIS, 2009).

Hydrotalcite shows a stack layer sequence that classifies it as rhombohedral crystal system with c parameter equal to three times the basal space belonging to $R\bar{3}m$ space group (CREPALDI and VALIM, 1997) and cell parameters $a = b = 3.054(3)$ nm and $c = 22.81(2)$ nm; α , β , and $\gamma = 90^\circ$, 90° and 120° , respectively (ALLMAN and JEPSEN, 1969) The Figure 1.4 shows the hydrotalcite rhombohedral structure

Figure 1.4 hydrotalcite rhombohedral structure.



Source: CREPALDI and VALIM, 1997 (with adaptations).

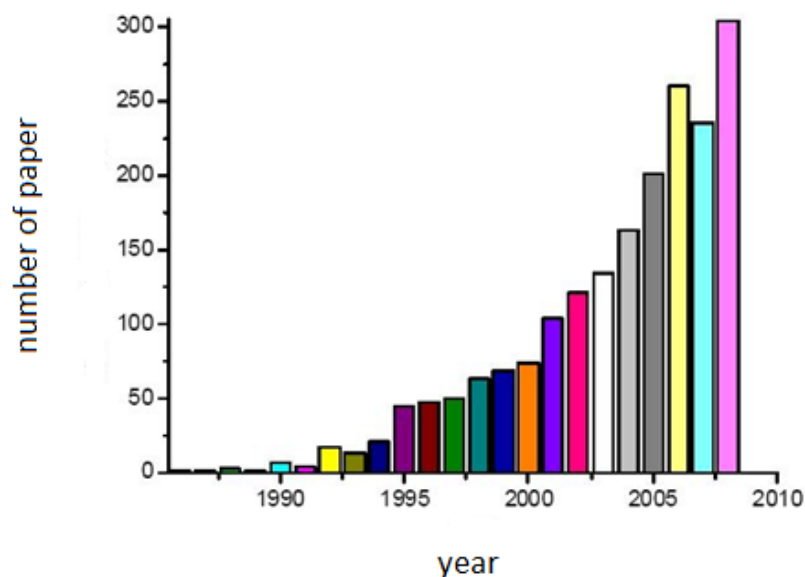
Hydrotalcite is the most known and studied LDH and it is taken as a reference for many isomorphous compounds even with different metals than Mg and Al. LDH with the similar structure is known as hydrotalcite-like compounds (KOVANDA et alii, 2005) and present many industrial and medicinal applications that is covered in the next section.

1.3 LDH Applications

LDH has been studied extensively in recent decades because they present several applications, properties and versatility. Figure 1.5 shows a histogram with the number of papers per year since 1980 to 2009. It shows the development of the number of researches performed on LDH clay type.

A search for “Layered Double Hydroxides” at www.periodicos.capes.gov.br resulted in 5,117 papers in October, the 20th 2013. Comparing with the graphic in figure 1.5, just 300 papers in 2009, it can be concluded that there are a global interest in LDH study. The reason is based in the large variety of LDH applications possibilities, as industrial, environment, medicine, among others.

Figure 1.5 Growth of LDH researches.



Source: REIS (2009).

1.3.1 Industrial Applications

LDH clays, mainly hydrotalcite, used in this research, shows high surface area, therefore are used as adsorbents of industrial contaminants as dyes (CONCEIÇÃO et alli, 2007 SAIHAH et alli, 2009; AGUIAR, et alli, 2013). AUXILIO et alli (2009) used calcined hydrotalcite to uptake acid blue 9 and obtained the best result in a 5.6 molar ratio.

SANTOS (2007) studied hydrotalcite with a molar proportion 3:1 (Mg:Al) modified as heterogeneous catalyst for biodiesel production. Modification of Hydrotalcite occurred with the addition of some elements (zinc, tin, barium, cerium and calcium) and subsequent calcination. The survey revealed great potential for use of hydrotalcite conversion of soybean oil to methyl esters according to the European standard for biodiesel.

POLATO et alii (2009) studied the effect of currents conversion FCC units (Fluid Catalytic Cracking) performance with hydrotalcite as catalyst partially replaced by copper, and manganese. It was concluded that initially 1:1 (Mg:Al) hydrotalcite partially replaced by copper or manganese redox properties showed more efficiency.

Hydrotalcite was also used as substrates for catalysts for oxidative dehydrogenation of light paraffins. The mixed oxide catalysts of vanadium and molybdenum were prepared and evaluated in different proportions in the decomposition reaction of isopropanol (MEIRA and CORTEZ, 2007).

Calcined hydrotalcite was used in the catalytic conversion of ethanol in the fixed bed reactor by VILLANUEVA (2000 and 2005). LDH calcination significantly increased surface area of the product formed, magnesium and aluminum double oxides. The author set a variation in the composition of the metal ions magnesium and aluminum as the same way as AUXILIO et alli (2009) did, but with different applications. The results just showed, for both cases, that the calcination can increase LDH surface and consequently improve their adsorption characteristics.

KAGUNYA and JONES (1995) used various types of calcined LDH as catalyst from aldol condensation of acetaldehyde. The authors observed that the large surface area of LDH favors the activity of self-condensation of acetaldehyde.

This sub-section shows that some parameters are important in LDH industrial applications: calcination, molar metal ratio and the nature of metal ion.

1.3.2 Environmental Applications

Contamination of water and soil from a variety of toxic derivatives, in particular heavy metals, pigments and aromatics, is a very serious problem presenting a potential of human poisoning. So there is a need to develop technologies that can remove pollutants from wastewater (SINGH et alli, 2009). There are many researches with applications of LDH uptake of many chemicals released into waters and soils, including industrial dyes that have a great concern for many researchers.

Phenylalanine is an amino acid and has various uses such as in the field of foods, pharmaceutical and medical purposes. However, in some uses, such as in food fermentation, waste water containing this amino acid should be treated. SILVÉRIO et alli (2008) had studied the effect of temperature and ionic concentration in the adsorption of phenylalanine by hydrotalcite. The researchers concluded that the phenylalanine adsorption increase when temperature decreasing and a reduction in ionic strength cause an increasing in adsorption. The new approach provides a potential use in the treatment of wastewater.

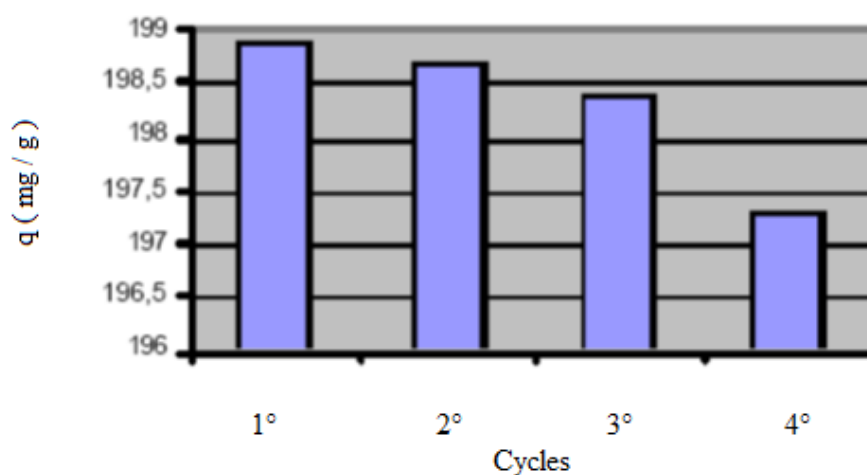
CONCEIÇÃO et alli (2007) synthesized hydrotalcite with a composite iron hydroxide. They used the pure clay and composite for removal of reactive red dye and chromate under varying pH conditions. The aim was to compare the adsorption isotherms of pure clay and composite clay for a possible magnetic field separation process.

GOLDANI (2007) developed a methodology for extract metallic elements manganese and iron effluents from coal mining. In this study, adsorption isotherms were compared to three types of clays: natural bentonite, montmorillonite and synthetic hydrotalcite. The author has found a significant difference in the adsorption from hydrotalcite compared to bentonite and montmorillonite, especially for manganese adsorption. Hydrotalcite showed a 90% greater efficiency than the others two clays.

The adsorption of industrial contaminants by LDH shows wide application, but it is necessary to analyze how many cycles LDH can be used in a process of adsorption-desorption. ZAMBONI et alli (2005) studied calcined hydrotalcite in relation to the cycles of adsorption of anionic contaminants from textile industries.

Figure 1.6 shows that the adsorption capacity varies slowly with the number of adsorption-calcination cycles. The reduction in uptake was 99.9%, 99.7% and 99.2% from the first cycle to the 2th, 3th, and 4th cycles, respectively, showing that LDH can be regenerate to be used in many cycles.

Figure 1.6 Cycles of adsorption and desorption.



Source: ZAMBONI et alli (2005).

MIOTTO et alli (2008) have studied and compared the adsorption of methylene blue and direct blue textile dyes with and without added surfactant SDS (sodium dodecyl sulfate) on hydrotalcite. They found that with the addition of SDS to hydrotalcite, methylene blue adsorption varies from 26% to 98%. On the other hand SDS did not affect the adsorption of direct blue that increased from 97.6% to 97.7%. Thus the nature of the dyes is important in LDH adsorption.

In this research methylene blue was also studied on hydrotalcite adsorption and compared with acid blue 25 and reactive blue 4 in just one cycle. Studies of a larger number of cycles must be performed to verify the economic feasibility of using hydrotalcite and other LDH as adsorption of contaminants from industrial wastewater.

The following parameters are important in environment applications: temperature, ionic concentration, pH conditions, and nature of contaminant adsorbed.

1.3.3 Medicine Applications

Many researches are focused on health using LDH, mainly hydrotalcite that among different applications is also used as a drug to combat reflux and as antacid. Hydrotalcite is patented as antacid by the name Talcid ® from Bayer.

CUNHA et alli (2009) conducted a quite interesting study showing the varied applications of LDH as biomaterials. The article approaches LDH applications for storage and release of species of biological and therapeutic interest. It shows a list of 44 intercalated drugs on hydrotalcite and Zn-Al-LDH.

LDH have specific characteristics that allow its use as carrier of drugs: biocompatibility, low toxicity and high integration of ionic species. With these features it is possible to promote the sustained release of inserted species. The cholic acid is the main acid produced by the bile and acts as aiding in the digestion of fats. SILVA and VALIM (2007) studied the intercalation of this acid in hydrotalcite to release it in the body of patients with deficiency of this substance.

Hydrotalcite was studied by RIBEIRO (2008) in controlled release of the drug enalaprilate in simulation of the passage through the gastrointestinal. The process occurred with the intercalation of enalaprilate in the interlayer region of LDH by ion-exchange method and the coating with a xiloglucan. In this research was used clay type Mg-Al LDH (2:1) with interlayer nitrate ion (NO_3^-) because it is more easily replaced than the carbonate (CO_3^-) (MARANGONI, 2005; RODRIGUES, 2007; COSTA, 2007;

RIBEIRO, 2008; REIS, 2009). The study concluded that it is possible to use the system described, however it is necessary to coat LDH to prevent acid attack from gastrointestinal tract.

Conjugated porphyrins are macrocyclic compounds possessing four pyrrole rings. They are present in some proteins and are essential for biological activities in the transport and storage of oxygen promoted by hemoglobin. HALMA (2004) studied different ways of ironporphyrins immobilization in LDH in order to check the catalytic activity.

A study comparing calcined and non-calcined hydrotalcite in adsorption of cholate anion (produced by the bile) under different conditions of pH and temperature were made by NAIME FILHO et alli (2008). This study found that the calcined hydrotalcite presents considerably more adsorption of cholate anion than the non-calcined one.

This section shows that LDH can be used as drug storage and a delivery agent, antacid and an adsorbent for substances in excess in a human body. As the same way as the industrial application (KAGUNYA and JONES, 1995; VILLANUEVA, 2000 and 2005; AUXILIO et alli, 2009) the calcination of LDH can improve their surface area and increase the adsorption capacity. Furthermore calcination, temperature and pH are important in medicinal applications.

1.4 Synthesis Methods

There are different methods of LDH synthesis that are mentioned by several authors. Among various methods are highlighted the most common (SANTOS, 2007; RODRIGUES, 2007; CREPALDI and VALIM, 1998; REIS, 2009; FERREIRA, 2001; HE et alli, 2005):

- 1. Co-precipitation at constant pH**
- 2. Co-precipitation at variable pH or salt-based method**
- 3. Salt-oxide method**
- 4. Hydrothermal synthesis**
- 5. Intercalation method**

Co-precipitation at constant pH: in this method the solutions of cation salts are simultaneously added to the anion to be intercalated. It is necessary to use a potentiometer to be able to control pH. This method has the advantage of achieving greater homogeneity of the product synthesized (CREPALDI and VALIM, 1998; NODA PEREZ et alli, 2004; KUSTROWSKI et alli, 2005; SANTOS, 2007).

Co-precipitation at variable pH: consists in addition of a solution containing salts of the divalent and trivalent cations mixed to a solution of the anion to be intercalated. The parameters such as initial concentration of salt and anion to be intercalated, agitation, temperature must be controlled in order to avoid the formation of undesirable phases, as simple hydroxides (NODA PEREZ et alli, 2004; HE et alli, 2005; KOVANDA et alli, 2005; RODRIGUES, 2007; SHARMA et alli, 2007; KOVANDA et alli, 2009;).

Salt-oxide method: this method basically consists of a reaction between oxides of divalent and trivalent metal salt cations. In this type of reaction the addition of reactants is controlled in order to obtain a constant pH (FERREIRA, 2001; HE et alli, 2005).

Hydrothermal synthesis: it is a kind of synthesis which occurs at higher temperatures. It uses two oxides of di and trivalent metals to form a suspension that is added in an acid with the ion wanted in the interlamellar space (RODRIGUES, 2007). It is important to differentiate it from hydrothermal treatment that occurs after synthesis.

Intercalation method is a method of obtaining new LDH from an existing precursor. It is used a concentrated anion solution to be intercalated. It is also very common to use precursors containing carbonate that can be protonated at high pH and thus avoids the destruction of the lamellae hydroxides (CREPALDI and VALIM, 1998; HE et alli, 2005).

In addition to the methods listed before there are other methods to synthesize LDH: sol-gel synthesis and electrochemical synthesis (RODRIGUES, 2007), urea hydrolysis (BENITO et alli, 2008; MEIS, 2010), synthesis using microwave (HERRERO et alli, 2007), and reconstruction method (LI et alli, 2010; CHANG^a et alli, 2011).

The co-precipitation at variable pH method was used in this research followed by hydrothermal treatment at constant temperature.

1.5 LDH Textural Properties and Crystallinity

The methods listed in the previous section for all LDH syntheses are shown relatively simple. However, many factors can influence the outcome textural characteristics of the products. Thus it is necessary to control these parameters to obtain the wanted LDH with crystallinity and purity (CREPALDI and VALIM, 1998).

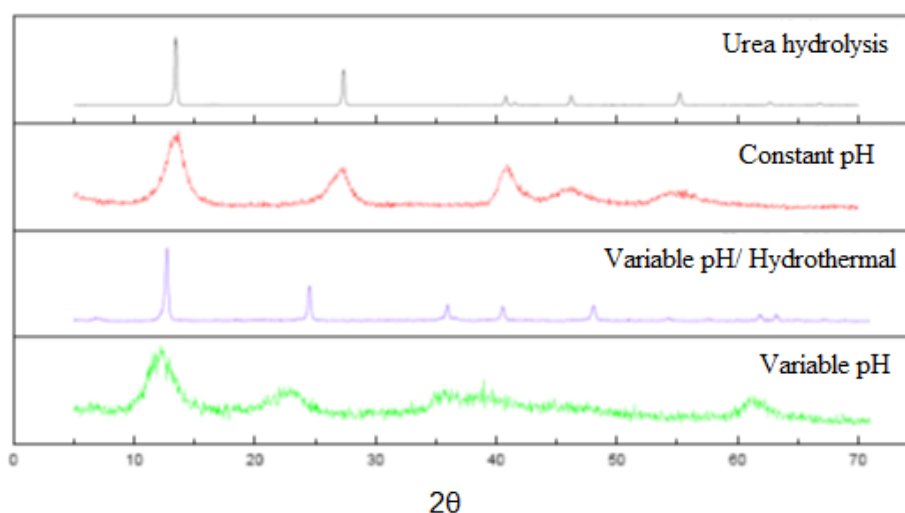
Several factors must be taken into account for LDH synthesis, for example: the degree of substitution of cations M^{+2} for M^{+3} , the nature of the cations, the nature of the interlayer anion, pH synthesis, and in some cases, the synthesis atmosphere. Furthermore, to obtain more crystalline material the following parameters must be controlled: concentrations of the salt solutions, the rate of addition of solution, the degree of agitation (RODRIGUES, 2007; REIS, 2009).

FARIAS et alli (2009) have discovered that the synthesis method influence on the obtained LDH crystallinity. Figure 1.7 shows a comparison of some LDH syntheses. The urea hydrolysis and the synthesis at variable pH accompanied by hydrothermal treatment seem to be better than the others syntheses.

SAIAH et alli (2009) carried out a study of the hydrothermal effect on Ni- $FeCO_3$ LDH treatment under various conditions of temperature and aging. They concluded that there was an increase in crystallinity as the temperature and aging were raised and accompanied by a reduction in LDH surface area. It was also noticed that there was an increase in the amount of amorphous material when the temperature of the hydrothermal treatment approach 200 °C.

LDH textural properties are not only dependent upon the synthesis parameters. It is important to consider the aging time and aging temperature (SHARMA et alli, 2007; SAIAH et alli, 2009; LIMA et alli, 2012). Textural properties in LDH are known in literature as: surface area, pore diameter, mean porosity and distribution (GÉRAUD et alli, 2007; SAIAH, 2009; BERBER at alli, 2013), crystallinity, crystallite size, crystallite agglomeration size (BRAVO-SUAREZ et alli, 2004; BENITO et alli, 2006; SHARMA et alli, 2007). Among all these properties, crystallinity is one of the most difficult to define.

Figure 1.7 Synthesis Influence in LDH crystallinity.



Source: FARIAS et alli, 2009.

The terms crystallinity and degree of crystallinity are used in this text as a textural property of clays (OH et alli, 2002; BRAVO-SUAREZ et alli, 2004; SHARMA et alli, 2007; SAIAH et alli, 2009; BENITO et alli, 2010; CHANG^b et alli, 2011; BERBER et alli, 2013) however, there are no definition accepted by the scientific community in this field. There are some equation and definitions for polymers crystallinity and procedures to obtain the crystallinity for some clay minerals like kaolinite, illite, smectite, etc.

Crystallinity for polymers is defined by IUPAC (ALLERA et alli, 1989) as the presence of three-dimensional order on the level of atomic dimensions; the term “degree of crystallinity” is also defined as the fractional amount of crystalline phase in the polymer sample relatively to the total of polymer crystalline and amorphous phase. It may be calculated for mass fraction (W_c) or volume fraction (ϕ_c).

There are some methods recommended to calculate the degree of crystallinity in polymers: by calorimetry, density measurements, infra-red spectroscopy and by X-Ray diffraction. The equation to calculate the degree of crystallinity by X-Ray diffraction is given as follows (ALLERA et alli, 1989):

$$W_c = I_c / (I_c + K_x I_a) \quad 1.1$$

where I_c and I_a are the integrated intensities scattered over a suitable angular interval by the crystalline and amorphous phase. K_x is a calibration constant (ALLERA et alli, 1989). A similar and simpler equation is proposed by KAVESH and SCHULTZ (1969):

$$W_c = I_c / (I_c + I_a) \quad 1.2$$

where I_c and I_a are the area under certain selected crystalline peaks and peaks considered amorphous, respectively.

In general, X-ray diffraction can provide information about the atomic arrangement in materials with high organization, low organization and materials that may also present part of its constitution crystalline and amorphous (HE, 2009). Thus a measure of Full Width at Half Maximum (FWHM) of the peaks could be related with crystallinity. It was done for some authors like AMIGÓ et alli (1994) and CONSTANTINO et alli (1998).

Clays like kaolinite present some definition and methods to measure its crystallinity. APARICIO and GALÁN (1999) have summarized some methods for the XRD determination of kaolinite crystallinity indices: Hincley, Stoch, Range & Weiss, Lietard, Hughes & Brown, Plançon & Zacharie and Indices of Amigó. They compared statistically the methods to found the better one to measure crystallinity indices of eight different kaolinites. All of them utilize relations of areas and height of peaks from the patterns, except for the Indice of Amigó that uses a relation of FWHM between 001 and 002 peaks (AMIGÓ et alli, 1994).

Crystallinity degrees were indicated in a qualitative way: very low, low, good and very good by CONSTANTINO et alli (1998). They synthesized hydrotalcites-like compounds and analyzed properties of crystallinity degree of the samples by evaluation of the X-ray diffraction pattern based on the number of reflections, their intensity and their FWHM.

KÜHNEL et alli (1975) studied crystallinity of goethite samples associated with silicates. They quantified the crystallinity of these minerals on the basis of statistical measures from the analysis of their X-ray line profiles.

The crystallinity is said to be proportional to the sharpness and intensity of the XRD peak by OH and co-workers (2002). They carried out an interesting research with hydrotalcite synthesized in different conditions like metal ion concentration, aging

time and reaction temperature. It was evaluated how the particles size varied with the conditions of synthesis.

Hydrotalcites like compounds with nickel and aluminum were synthesized by KANNAN et alli (1996) with molar ratio varying from 0.20 to 0.33. They compared the intensity of the 006 peaks in their XRD pattern and associated them with their degree of crystallinity. Furthermore they performed hydrothermal treatments on aged samples to study the change in textural properties. They verified an increase in the intensity and sharpness of the peaks in XRD and concluded that the crystallinity was enhanced.

SHARMA et alli (2007) had done a summation of 003 and 006 peaks intensity to measure crystallinity in hydrotalcite with different molar ratio. In previous work (LIMA et alli, 2012) a study with Mg-Al LDH adsorption was carried out with adsorption of reactive blue 4 and acid blue 25 in different aging times: 4, 14 and 28 days. Crystallinity was measured by the intensity of the 003 peaks of the XRD patterns. The XRD diffraction showed a reduction in crystallinity with aging time as the same way a reduction in adsorption took place.

Maybe crystallinity could be better measured by FWHM of their peaks, this parameter is directly associated with particles size through the Scherrer equation (3.11). However one of the samples series could not be refined to obtain the correspondent particle size. Thus in this research crystallinity was adopted as a measure of the intensity of the 003 peaks of the XRD patterns the same way as LIMA and co-workers (2012) did.

2 ADSORPTION AND DYES

This chapter describes the fundamental of adsorption process, adsorption isotherms and the classification of dyes that were used in this research.

2.1 Adsorption Processes

Adsorption is a process of mass transfer and occurs between a fluid and a solid adsorbent which retain molecules of liquids or gases on its surface. The solid that adsorbs is known as adsorbent while the fluid is adsorbate (MARSH and REINOSO, 2006).

The adsorbents are natural or synthetic substances with microcrystalline structure whose pore inner surface is accessible to a selective combination between the solid and solute. The adsorbents used in more large scale are activated carbon, silica gel, activated alumina and various types of clays (PERRY and GREEN, 2008).

The process is related to the interaction energy of adsorbent and adsorbate and is classified in chemical and physical adsorption depending upon some criteria, showed in Table 2.1, like heat of adsorption, mono or multilayer formation, etc.

2.1.1 Chemical and Physical Adsorption

The adsorption process can present different characteristics with respect to the energy between the adsorbent and the fluid molecules adsorbed. Depending on the magnitude of this energy the process is classified as physical adsorption or chemical adsorption. Table 2.1 shows the major differences: heat of adsorption, specificity, number of adsorption layer, electron transfer and temperature range (RUTHVEN, 1984).

It is important to industrial application, in the majority of the cases, that the adsorbent presents a physical adsorption. This characteristic implies in its reuse in many cycles. Obviously, it is important other characteristics like, ease of preparation, high capacity anion exchange, high surface area and porosity (AUXILIO et alli, 2009; SAIAH et alli, 2009).

Table 2.1 Chemical and physical adsorption.

Physical Adsorption	Chemical Adsorption
<ul style="list-style-type: none"> • Low heat of adsorption • (< 2 to 3 times the latent heat of evaporation) • Not specific • Monolayer or multilayer • Without dissociation • No electron transfer • Significant at low temperatures 	<ul style="list-style-type: none"> • High heat of adsorption • (> 2 or 3 times the latent heat of evaporation) • Highly specific • Only monolayer • Dissociation can occur • Electron transfer • Wide temperature range

Source: RUTHVEN, 1984.

2.1.2 Adsorption Isotherm

Adsorption is a mass transfer process and it is necessary to know how far it reaches. Such information can be obtained from the adsorption isotherms. In physical adsorption the isotherm is a graph between the amount adsorbed (mmol.g^{-1}) against the relative pressure (p/p^0) of the adsorbate (MARSH and REINOSO, 2006).

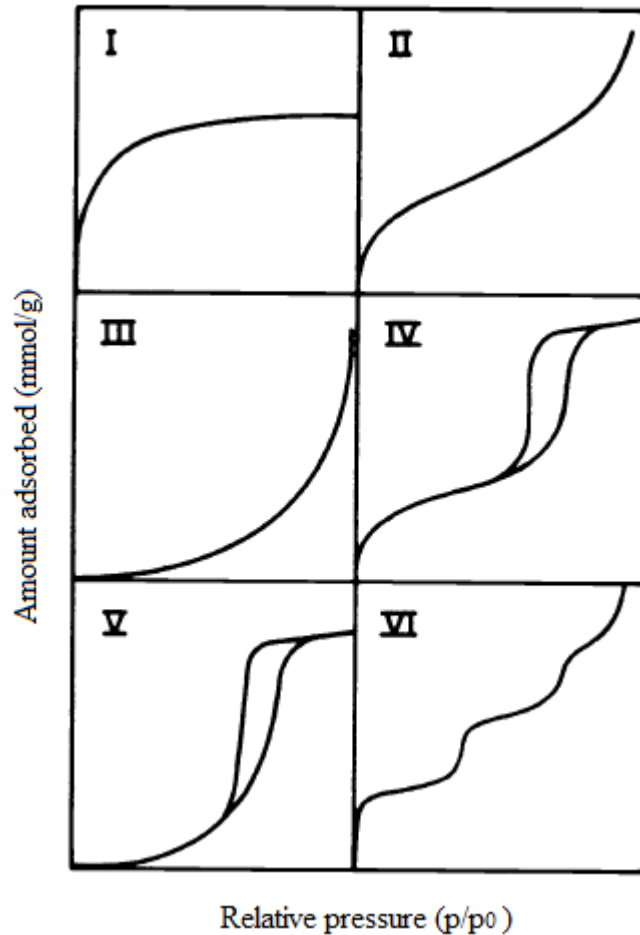
The most common physisorption isotherms are described by one of the six types showed in Figure 2.1. All of them obey to Henry's law in region of low pressure, i.e., the amount of gas adsorbed is proportional to pressure (SINGH et alli, 1985).

Figure 2.1 shows the IUPAC (International Union of Pure and Applied Chemistry) classification of physical adsorption isotherms. In the case of isotherm I adsorption represents only one layer that can occur in micro porous materials, the amount adsorbed approaches a limiting value as (p/p^0) tends to unity. The model II shows the adsorption in a non-porous material. In the beginning is formed a monolayer and as the relative pressure increases the multilayer adsorbed predominates.

In III type is possible to see that the adsorption is difficult, i.e., the adsorption energy is weak. The number IV resembles II with the difference that there is hysteresis due to the process of filling by capillary condensation is different from the emptying and it is common in mesoporous materials.

Type V shows low energy in adsorption and it is related to the type III where the adsorbent-adsorbate interaction is weak and the hysteresis shows the presence of mesopores. The type VI isotherm represents a stepwise multilayer on a uniform non-porous surface (GUELF, 2007; MARSH and REINOSO, 2006; SINGH et alli, 1985).

Figure 2.1 IUPAC adsorption isotherm classifications.



Source: SINGH et alli, 1985.

2.1.3 Equilibrium Isotherms

There are many mathematical models to describe adsorption isotherm, among them, the following are highlighted: Langmuir, Freundlich, Langmuir-Freundlich e Toth.

The simplest model of adsorption is described by Langmuir and occurs in an energetically uniform surface without interaction between the molecules of adsorbate. Thus Langmuir isotherm assumes monolayer coverage of adsorbate onto adsorbent.

Langmuir model is written as follows (KYZAS and LAZARIDIS, 2009; RUTHVEN, 1984):

$$q = \frac{q_{\max} k_L C_{eq}}{1 + k_L C_{eq}} \quad 2.1$$

where

q_{\max} (mg/g) is the maximum adsorption capacity,

k_L (mL/mg) is the Langmuir equilibrium constant.

Freundlich isotherm model encompasses the heterogeneity and the exponential distribution of active sites and their energies. The isotherm provides no saturation of the adsorbent surface, it is expected an endless coverage. Freundlich model is described as follows (KYZAS and LAZARIDIS, 2009):

$$q = k_F C_{eq}^{1/n} \quad 2.2$$

where k_F ($\text{mg}^{1-1/n} \text{L}^{1/n}/\text{g}$) is the Freundlich constant associated to adsorption capacity and $1/n$ is the heterogeneity factor.

The third model combines the previous two models and is known as the Langmuir-Freundlich isotherm model that describes heterogeneous surface. Essentially the Langmuir-Freundlich isotherm is a Freundlich isotherm with an asymptotic property that approaches the maximum at high concentrations.

Furthermore, Langmuir-Freundlich isotherm tends to Langmuir when the parameter of heterogeneity "b" tends to unity. The mathematical expression for the Langmuir-Freundlich model is described by equation 2.3 (KYZAS and LAZARIDIS, 2009):

$$q = \frac{q_{\max} (k_{LF} C_{eq})^b}{1 + (k_{LF} C_{eq})^b} \quad 2.3$$

where k_{LF} (mL/mg)^{1/b} is the Langmuir-Freundlich constant and b is the heterogeneity factor.

Toth isotherm model is an enhancement of Langmuir and Freundlich isotherms. It originated from the potential theory and is applied in heterogeneous adsorption where it assumes a nearly Gaussian energy distribution. Toth model is described as follows (ALLEN et alli, 2004; MOUZDAHIR et alli, 2010):

$$q = \frac{q_{\max} k_T c_{eq}}{\left(1 + (k_T c_{eq})^{m_T}\right)^{1/m_T}} \quad 2.4$$

where k_T is the Toth constant and m_T is the heterogeneity factor.

Similarly to the model of Langmuir-Freundlich, Toth model tends to Langmuir model when constant m_T tends to unity.

2.2 Dyes

Dyes are classified according to **chemical structure** (used for the organic chemist) or by its **application method** that depends upon the kind of substrate it is applied (IQBAL, 2008). Textile industries dyes can be classified into three categories as follow: (a) anionic: direct, acid, reactive, (b) cationic: basic, and (c) non-ionic: dispersed dyes (KYZAS et alli, 2013). The applied method definition for dyes is described according to HUNGER (2003):

Direct dyes are used mainly in materials from cellulose, for example: cotton, viscose or paper. They can be used on cellulosic fiber “directly” without any previous treatment like metal salts that are used with others categories of dyes. Their water solubility is less than the acid dyes.

Acid dyes are water-solubilizing and easily to dissociate in a wide acidity range. Used in acidic dye baths in nylon, paper, leather, silk, etc.

Reactive dyes are compounds that contain groups capable to form covalent bonds with substrate. It is used in cotton, wool, silk, and nylon. The reaction to bind covalently to the fiber occurs under influence of heat and alkaline pH.

Basic dyes are cationic and form positively charged dye ions by dissociation and its positive electric charge is delocalized over the entire molecule. Some of them are used in paper industry and on synthetic fibers like polyacrylonitrile, modified nylon and polyester. They are applied in acidic dye baths.

Disperse dyes are colorants that present a disperse colloidal form and a low water solubility or water-insoluble in some of them. They are used in hydrophobic fibers and synthetic one, like polyester, cellulose acetate, polyamide, and acrylic. It is often applied at high temperatures and or pressure.

2.2.1 Dyes Nomenclature

Dyes can be named by the Color Index (C.I.) or by their commercial trade name. The commercial names are usually composed of three parts: the first is a trademark that designates the manufacturer and the dye's class; the second is the color; and the third one is a number and or letters used as a code that indicate the properties of the dye. These codes are not standardized and so their properties associated with their number (HUNGER, 2003).

For example: acid blue 25, reactive blue 4 were used in this research, can be abbreviating to AB25 and RB4. The C.I. name for a dye derives from the application class that the dye belongs, its color and hue. It is represented by five numbers in this index. For example, AB25 has its Color Index, C.I. 62055.; RB4, C.I. 61205.

The chapter seven show adsorption results with these two different kinds of dyes: acid, and reactive, AB25 and RB4, respectively. Their chemical structures are shown in chapter 4, Material and Methods.

3 X-RAY DIFFRACTION

This chapter aims to describe to the reader, in a superficial way, the principles of the most important analysis for materials science, X-Ray Diffraction (XRD) and the theory for determination of crystallite size using the well-known Scherrer equation.

3.1 X-Ray Diffraction Theory

X-ray diffraction is one of the most important and most widespread techniques for materials characterization and gives information on atomic scale structure of crystalline compounds (WASEDA et alli, 2011).

The X-ray diffraction is the phenomenon of interaction between an incident X-ray beam and the electrons of the atoms of a material, related to coherent scattering. The term coherent is associated with Thompson scattering of diffracted beam which present the same wavelength as the incident beam (WOOLFSON, 1997).

3.1.1 Bragg's Law

In a material where the atoms are arranged periodically in space, characteristic of crystalline structures, the phenomenon of diffraction X-ray scattering occurs in directions that obey Bragg's law, Equation 3.1 (CULLITY, 1956).

Assuming a monochromatic beam of a specific wavelength (λ) relates to a crystal at an angle θ , called the Bragg angle, equation 3.1 is the Bragg's law:

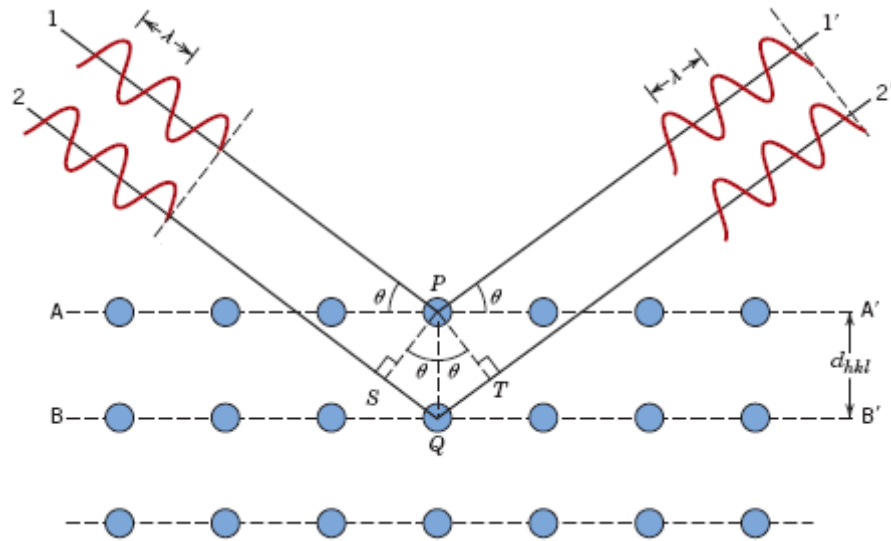
$$n\lambda = 2 |d_{hkl}| \sin\theta \quad 3.1$$

where θ corresponds to the angle measured between the incident beam and a crystal plane, " d_{hkl} " is the distance between the planes of atoms and "n" the diffraction order, an integer.

The phenomenon of X-rays diffraction occurs when there is constructive interaction between two or more diffracted waves. Figure 3.1 illustrates the effect of two parallel beams 1 and 2 with wavelength λ and incident angle θ and the respective diffracted beams 1' and 2'.

d_{hkl} is the distance between two consecutive planes, so the difference in the path 1-1' and the path 2-2' will be the distance SQT equivalent to $2|d_{hkl}|\sin\theta$. It is necessary that this distance, $2|d_{hkl}|\sin\theta$, be an integer multiple of the wavelength to satisfy a constructive interference (WASEDA et alli, 2011).

Figure 3.1 Diffraction of an incident beam



Source: CALLISTER JR. and RETHWISCH, 2012.

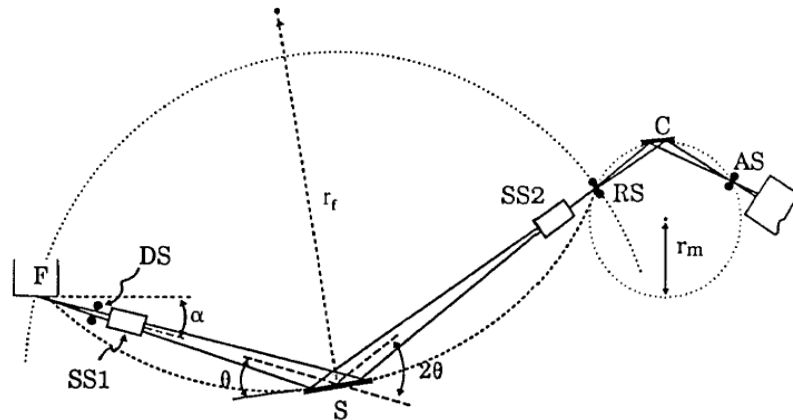
3.2 X-Ray Diffraction Techniques

Diffractometer is the traditional instrument used to discover the internal structure of a crystalline substance. For samples powder analysis basically consists in measuring the intensity of the diffracted X-rays from the sample as a function of diffraction angle for a known wavelength X-ray (WASEDA et alli, 2011).

Figure 3.2 shows a flow chart of a diffractometer. A monochromatic beam of X-rays emitted by the source F while the sample powder is placed on the point S that rotates together with the detector in C that counts the number of photons. As they move the counter in a constant angular velocity, it is recorded the number of counts of the diffracted beam as a function of 2θ (JENKINS and SNYDER, 1996).

According to LENG (2008), most commercially available diffractometers show the geometric arrangement known as the Bragg-Brentano geometry, showed in Figure 3.2:

Figure 3.2 Scheme operation of the X-ray diffractometer



Source: JENKINS and SNYDER, 1996.

A divergent X-ray beam from F passes through a divergence slit (DS), then through a collimator, Soller Slit (SS1), before it gets the specimen (S) at an angle θ . The X-rays are diffracted at an angle 2θ and pass through a second parallel collimator (SS2), through the receiving slit (RS), to the detector slit (AS) (JENKINS and SNYDER, 1996).

The diffracted beam is usually expressed through peaks that stand out, recorded a spectrum of intensity versus angle 2θ , constituting diffraction pattern. The intensities obtained at angles 2θ represented by the diffraction peaks correspond to diffraction of the incident beam of a particular set of crystal planes, which have the same interplanar distance, each with Miller indices hkl (WASEDA et alli, 2011).

The information obtained from each peak is the intensity and the angular position (2θ) and consequently the substance pattern. Each crystalline compound shows a characteristic diffractometric pattern, allowing their identification through the angular positions and relative intensities of the diffracted peaks (LENG, 2008).

X-ray diffraction can provide information about the atomic arrangement in different levels of organizations, high, medium and low and may also present part of its constitution crystalline and amorphous (HE, 2009).

According to WASEDA et alli (2011), there are several methods to measure the intensity of the diffracted beams in crystal structures. The most common method is to measure the intensities of the samples using the powder diffractometer. To analyze

the samples with this technique is necessary to evaluate some structural information as the structure factor.

It is wave function of the beam reflected by the hkl plane of a unit cell (PAIVA-SANTOS, 2001). The equation is defined by HAMMOND (2009):

$$F_{hkl} = \sum_{n=0}^N f_n \exp 2i\pi(hx_n + ky_n + lz_n) \quad 3.2$$

where f_n is the atomic scattering factor and $2i\pi(hx_n + ky_n + lz_n)$ is the phase φ_n of the n^{th} atom in the motif with fractional coordinates (x_n, y_n, z_n) . The scattering factor can be calculated by the following equation (PAIVA-SANTOS, 2001):

$$f_n = f_{n0} \exp\left(\frac{-B \sin^2 \theta}{\lambda}\right) \quad 3.3$$

where f_{n0} the scattering factor for the rest atom and B is the thermal parameter.

This structure factor is used to evaluate the relationship between the structures of crystals and the intensity of the diffracted X-rays of each crystallographic plane measured. In addition to the structure factor, it is also important to consider the polarization, multiplicity, Lorentz, absorption and temperature factor (WASEDA et alli, 2011).

The identification of a crystalline compound is obtained by comparing the XRD patterns with individual phase's pattern based on the set of d spaces in terms of θ or 2θ and their relative intensities (RIBEIRO, 2010).

There are several programs that permit a collection of diffraction patterns allowing the application of diffraction refinement of the crystal structures and quantification of polyphase compounds.

The patterns are available in specialist databases sites as the International Center for Diffraction Data (ICDD) or Inorganic Crystal Structure Database (ICSD).

The information to generate the diffraction patterns are affected not only by overlapping the reflection planes, but also by physical effects and instrumental effect, as well as the preparation of the sample, particularly changes leading to intensity profile of peaks (CULLITY, 1956).

3.3 Rietveld Method

It is a crystalline structural refinement used with X-ray or neutron diffraction and it is based on the better approximation of the calculated and the observed diffractogram. The diffraction pattern is obtained from a constant 2θ increment in a scan process (PAIVA-SANTOS, 2001).

Instrumental and structural parameters are used in the Rietveld method to calculate a phase pattern of diffraction. The structural parameters are: atomic coordinates (x,y,z) in unit cell, thermal vibration, occupational density, cell parameters (a,b,c) and the angles with crystallographic axis (α,β,γ). The instrumental parameters are: reflections profile, global parameters, intensity parameters and the crystallite preferential orientation parameter (YOUNG et alli, 1993).

3.3.1 The Peak Intensity

The refinement is based on the least squares method that minimizes the square difference between the observed and calculated intensity for all the peaks in the analyzed pattern. The following equation shows how it is calculated (PAIVA-SANTOS, 2001).

$$M = \sum_i w_i (I_i^{obs} - I_i^{calc})^2 \quad 3.4$$

where I_i^{obs} and I_i^{calc} are the intensities of the observed and calculated for the i^{th} point and w_i is the weight, $w_i = 1/I_i^{obs}$.

The refinement provides indicators to measure the adjust quality: the weighted pattern R index, R_{wp} , and the expected R index, R_e , defined by (YOUNG et alli, 1993):

$$R_{wp} = \sqrt{\frac{\sum_i w_i (I_i^{obs} - I_i^{calc})^2}{\sum_i w_i I_i^{obs}}} \quad 3.5$$

$$R_e = \sqrt{\frac{n-p}{\sum_i w_i I_i^{obs}}} \quad 3.6$$

where n is the number of observed points and p is the number of adjusted parameters. The ratio R_{wp}/R_e is known as the goodness of fit or “ χ factor” and is a measure of how well the fitted model accounts for the data (YOUNG et alli, 1993).

$$S = \frac{R_{wp}}{R_e} \quad 3.7$$

Values of the quality of the fit (S) about 1.0 mean a good adjust of the data.

3.3.2 The Pseudo-Voight Function

The Rietveld method is based in a function to adjust the shape of the peak. The intensity of the diffraction peak is distributed by a profile function. There are many functions that depend on the characteristics of the equipment and the kind of radiation used. In this work was used a pseudo-Voight(p-V) function. It is a linear combination of a Lorentzian (L) and a Gaussian (G) defined by the following equation (PAIVA-SANTOS, 2001):

$$p-V = \eta L(x) + (1-\eta)G(x) \quad 3.8$$

The η parameter defines the contribution of each function and is calculated by the following equation:

$$\eta = N_A + 2\theta N_B \quad 3.9$$

N_A and N_B are refineable parameters.

The full width at half maximum intensity H_k depends on 2θ , the experimental conditions and on the sample physical characteristics (PAIVA-SANTOS, 2001).

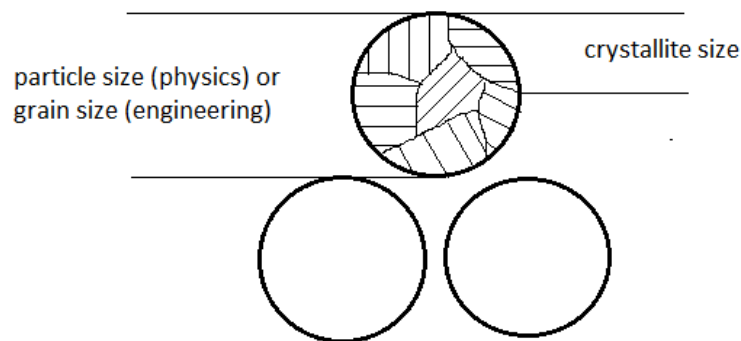
$$H_k = U \tan^2 \theta + V \tan \theta + W \quad 3.10$$

Where U, V and W are the refinement parameters from the standard crystal (LaB₆) used in this research.

3.4 Particle and Crystallite

The term particle size is used in physics as the same meaning of grain size in engineering and refers to a set of many fine units of single crystals known as crystallites (WASEDA et alli, 2011). Figure 3.3 shows the differences from particle size and crystallite size. It is noteworthy to mention the term particle used in engineering as a discrete and solid unit that can present a single or multiphase (REED, 1988) and according to RAHAMAN (2003), it can be a single crystal, polycrystalline or a glass.

Figure 3.3 Diagram for particle and crystallite size



Source: adapted from WASEDA and co-workers, 2011

The width of a diffraction peak can be a result of crystallite size and micro strain. The crystallite size (D) can be estimated by Scherrer's equation that does not consider the micro strain (WASEDA et alli, 2011):

$$D = \frac{k\lambda}{\beta \cos \theta} \quad 3.11$$

where D is the average crystallite size; λ is the radiation wavelength; k is a constant that is related to the shape of the particles (it is adopted $k = 1$ in this research, a discussion about it is in 5.2 section); θ is the diffraction angle and β is the full width at half maximum intensity (FWHM).

β parameter has to be corrected for instrumental broadening by the following equation assuming that the shape of the peaks have approximately a Gaussian distribution (WASEDA et alli, 2011):

$$\beta^2 = \beta_{obs}^2 - \beta_{inst}^2 \quad 3.12$$

where β is the peak width related only to the size of crystallites; β_{obs} is the observed width and β_{inst} is the instrumental width which is extracted from a standard crystal (LaB₆ was used in this work).

4 MATERIAL AND METHODS

Non-calcined Mg-Al LDH with Mg/Al molar proportion 4:1, 3:1, and 7:3 (with respectively molar ratio 0.20, 0.25, and 0.30) were synthesized using co-precipitation method, followed by hydrothermal treatment at a fixed temperature 80° C and different aging: 2, 4, 7, 14, 21, 28, and 35 days. The material obtained was characterized by X-Ray Diffraction (XRD), Scanning Electron Micrograph (SEM), Energy Dispersive Spectroscopy (EDS), Infra-Red (IR) and Thermo Gravimetric analysis (TG).

The samples were namely by the codes xx Mg-Al t where “xx” means the molar ratio multiplied by a hundred, 0.20, 0.25 or 0.30, and “t” the time from 2 to 35 days. For example: 25 Mg-Al 7 means a sample with molar ratio 0.25 (molar proportion 3:1) and seven days aging time.

4.1 LDH Synthesis

All the reagents for the Mg-Al LDH syntheses were analytical standard and purchased from Sigma-Aldrich: $\text{Mg}(\text{NO}_3)_2 \cdot 6\text{H}_2\text{O}$, $\text{Al}(\text{NO}_3)_3 \cdot 9\text{H}_2\text{O}$ and NaHCO_3 .

Mg-Al LDH with molar ratio 0.20, 0.25 and 0.30 were synthesized by co-precipitation method at variable pH using corresponding metal nitrate salts. An aqueous solution of $\text{Mg}(\text{NO}_3)_2 \cdot 6\text{H}_2\text{O}$ and $\text{Al}(\text{NO}_3)_3 \cdot 9\text{H}_2\text{O}$ was added drop wise to a solution containing NaHCO_3 , in excess, at 60 °C (± 2 °C), under vigorous stirring.

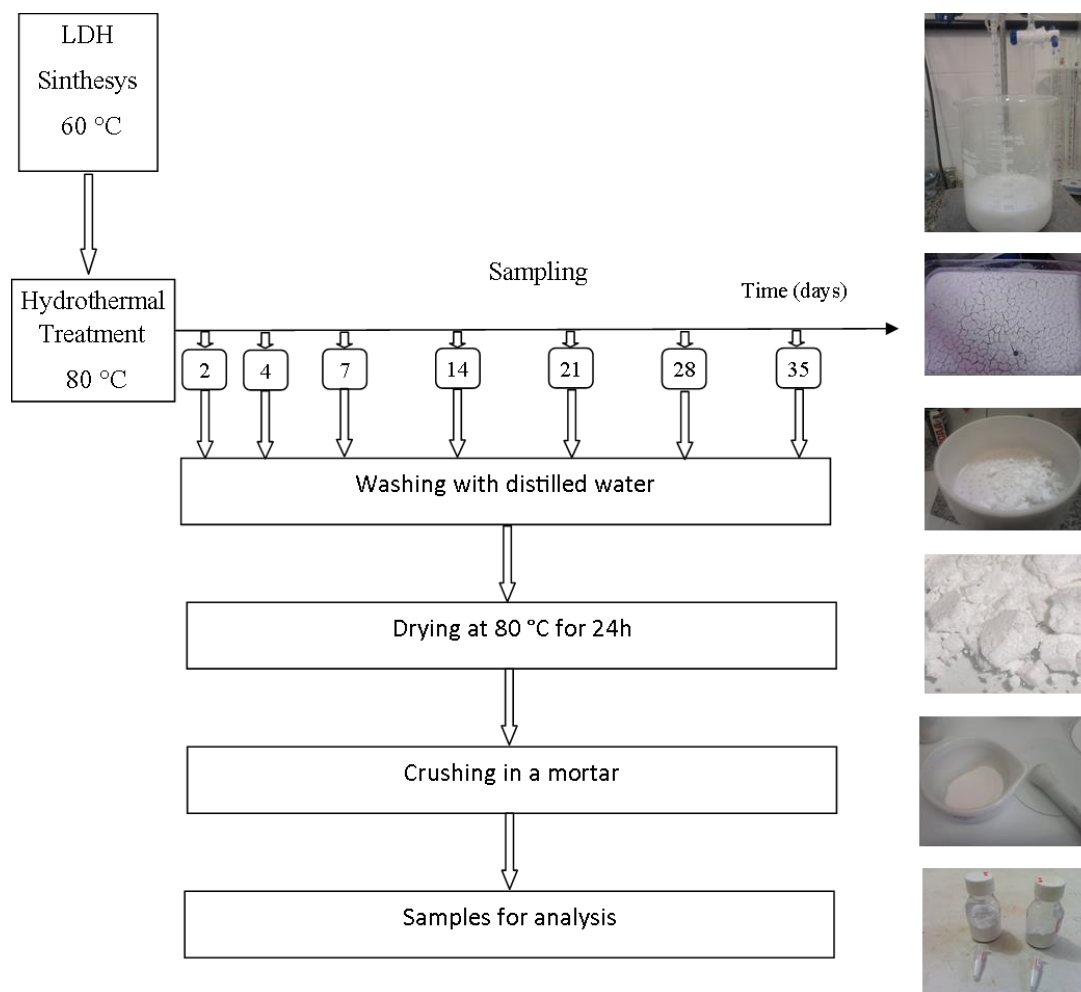
Figure 4.1 shows a flowchart of the synthesis process of the Mg-Al LDH in Biomaterials Laboratory of Universidade Federal do Ceará (UFC). This flowchart shows photographs of the synthesis process; the as-synthesized material in a tray and the samples before and after crushing.

4.2 LDH Characterization Analyses

Mg-Al LDH samples were characterized by XRD in a X-Pert Pro MPD-Panalytical X-ray Diffraction System from Physics Department of UFC with a copper tube $\text{CuK}\alpha$ ($\lambda = 0.1542$ nm) operating at a voltage of 40 kV and a current of 45 mA.

The program X'Pert High Score Plus with powder diffraction data from International Center for Diffraction Data (ICDD), CIF-6296, was used to identify the samples phase from the Panalytical equipment with 1/2" slit and the values for (U,V,W) =(0.014783, -0.042093, 0.057882).

Figure 4.1 Flowchart of the obtained process to synthesize Mg-Al LDH.



The obtained material was passed through a hydrothermal treatment at 80°C. After the corresponding aging it was filtered and washed with deionized water until the filtered reach pH 7. Then, all the 21 samples were dried again at 80 °C for 24h and ground in a mortar for exactly 2 minutes.

The microstructural analysis was carried out in a scanning electron microscope (SEM) Philips XL-30 from Materials Science and Engineering Department of UFC and HITACHI TM 3000 TableTop Microscope and the HITACHI ED 3000 X-Stream for Energy Dispersive Spectroscopy (EDS) analyses from Geology Department of UFC.

Infra-Red (IR) analyses were carried out in ABB-BOMEM FTLA 2000-102, from 400 to 4,000 cm^{-1} using 1% KBr proportion to the samples.

Thermo gravimetric analyses (TG) were performed with Universal V4.7A TA Instruments. The measurements were carried out at 10 $^{\circ}\text{C}/\text{min}$ rate temperature, from 30 to 800 $^{\circ}\text{C}$ in a synthetic air atmosphere. Both IR and TG were performed in Chemical Department of UFC.

One of the Mg-Al LDH samples were measured by N_2 adsorption experiments at 77 K, using an automatic sorptometer Autosorb 1 C (Quantachome, USA) from Chemical Engineering Department of UFC.

4.3 Material and Procedures for LDH Adsorption

The reagents reactive blue 4 (RB4) and acid blue 25 (AB25) dyes with analytical standard were purchased from Sigma-Aldrich. Table 4.1 shows the chemical structure and some properties of the dyes. The solutions were prepared in distilled water.

Adsorption experiments were performed in a rotatory shaker (Tecnal TE-165, Brazil) using conical tubes containing 20 mL of dye solutions in contact with 0.015 g of Mg-Al LDH. At the end of experiments the supernatant were collected and centrifuged for 10 min at 10,000 rpm (refrigerated microcentrifuge Cientec CT – 15000R).

The concentration of each dye in the supernatant solutions, before and after the adsorption experiments, was determined in UV/Vis spectrophotometer (Thermo Scientific BioMate 3, USA, from Chemical Engineering Department of UFC) after finding out the absorbance at the characteristic wavelength.

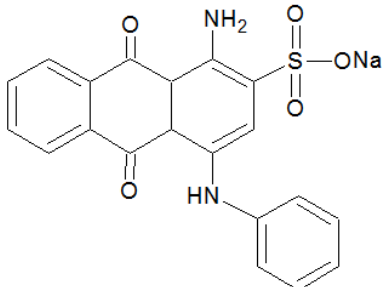
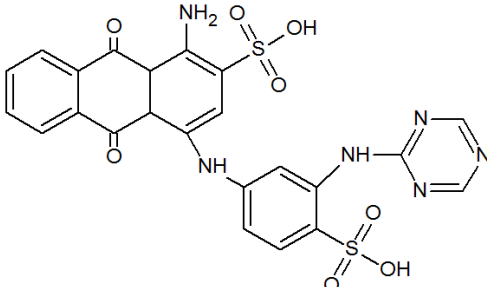
The maximum wavelength (λ_{max}) was observed at 600 nm for RB4 and AB25. All the adsorption experiments were performed twice at controlled temperature ($22^{\circ}\text{C} \pm 1^{\circ}\text{C}$).

Adsorption isotherms were determined by analyzing the residual dye concentration from aqueous solution at increasing initial concentrations. Each batch rests for a specific time interval necessary to reach the equilibrium. Dye amount adsorbed in the solid phase (adsorption capacity – q) was calculated according to Equation 4.1:

$$q = \frac{V(c_0 - c_{eq})}{m_{ads}} \quad 4.1$$

where c_0 (mg/mL) and c_{eq} (mg/mL) are the initial and the final (equilibrium) concentration of dye in liquid phase, V (mL) is the volume of solution, and m_{ads} (g) is the dried-weight of the sample.

Table 4.1 – Dyes chemical structures and characteristics.

ACID BLUE 25							
	<table border="1"> <tr> <td>Molecular formula</td> <td>$C_{20}H_{13}N_2NaO_5S$</td> </tr> <tr> <td>Molar Mass</td> <td>416.38</td> </tr> <tr> <td>λ_{max} (nm)</td> <td>605</td> </tr> </table>	Molecular formula	$C_{20}H_{13}N_2NaO_5S$	Molar Mass	416.38	λ_{max} (nm)	605
Molecular formula	$C_{20}H_{13}N_2NaO_5S$						
Molar Mass	416.38						
λ_{max} (nm)	605						
REACTIVE BLUE 4							
	<table border="1"> <tr> <td>Molecular formula</td> <td>$C_{23}H_{14}Cl_2N_6O_8S_2$</td> </tr> <tr> <td>Molar Mass</td> <td>637.43</td> </tr> <tr> <td>λ_{max} (nm)</td> <td>600</td> </tr> </table>	Molecular formula	$C_{23}H_{14}Cl_2N_6O_8S_2$	Molar Mass	637.43	λ_{max} (nm)	600
Molecular formula	$C_{23}H_{14}Cl_2N_6O_8S_2$						
Molar Mass	637.43						
λ_{max} (nm)	600						

4.4 Software

The data were refined by Rietveld method with the program DBWSTools 2.3 and it was used a pseudo Voight function to fit the results. The identification of phases was carried out by HighScore Plus; Statistical analysis, graphics of XRDP, the fit function was evaluated by the program Origin Pro 8.0. Image J was used to measure the dimensions of the particles of the SEM pictures. Word from Office 2010 was used as text editor.

5 X-RAY DIFFRACTION AND THE FIT FUNCTION

The results and discussion of this chapter approach just XRD, refinement and their results like cell parameter, crystallite size and the fit function. The other analyses will be discussed in the next chapter: IR, TG, SEM and EDS.

The samples codes “(xx) Mg-Al (t)” established in previous chapter (Material and Methods) are used in the remaining text and it is introduced a new term, the “xx Series” that refer to all the samples from a molar proportion. It will be used when is mentioned some quantitative parameter analyzed in all the samples, results like mean value, confidence interval or just a qualitative results compared between the series.

A statistical approach was used to verify the existence of a significant shift in two peaks relatively to the planes 003 and 006, observed in the 30 Series compared to the others. Furthermore the crystallinity analysis was evaluated to verify differences among the three series.

Initially was carried out ANOVA test to verify three hypothesis tests: crystallinity and the shift peaks in the planes 003 and 006; however the conditions of the data did not permit the use of this statistical test. ANOVA test has two presuppositions to be applied: the normality of the measures values in every set and similar variances of the set compared among them. At least one of them failed and ANOVA could not be used as a hypothesis test. Thus three hypothesis tests were carried out separately and the results are shown in Tables 5.4, 5.5 and 5.6 that show parametric and non-parametric tests.

Non-parametric test was carried out for the three hypothesis test although it was really necessary just in crystallinity test where the set did not show Gaussian origin. Thus a Wilcoxon Paired Rank Test was chosen to verify it and confirmed the other results with the parametric test for the shift in 003 and 006 planes.

All the hypothesis tests, parametric and non-parametric, were carried out as a one-tale test, or rather, it was tested the null hypothesis of a first sample mean or median to be equal to the second one against the alternative hypothesis where first sample mean or median be greater than the second one.

For statistical tests a 5% level of significance is applied and the same value for confidence coefficient is used in some confidence intervals. The symbol “ $t_{5\%}$ ” representing a t-Student with 95% confidence interval.

5.1 X-Ray Diffraction Patterns

The obtained 21 samples from the three different molar ratio syntheses were characterized by XRD and Figures 5.1 and 5.2 shows their XRPD pattern (2, 4, 7, 14, 21, 28 and 35days) for 20 Mg-Al Series and 25 Mg-Al Series. The best refinements were achieved through the Rietveld method using the program DBWSTools (BLEICHER et alli, 2000).

Figure 5.1 XRD for 20 Mg-Al Series.

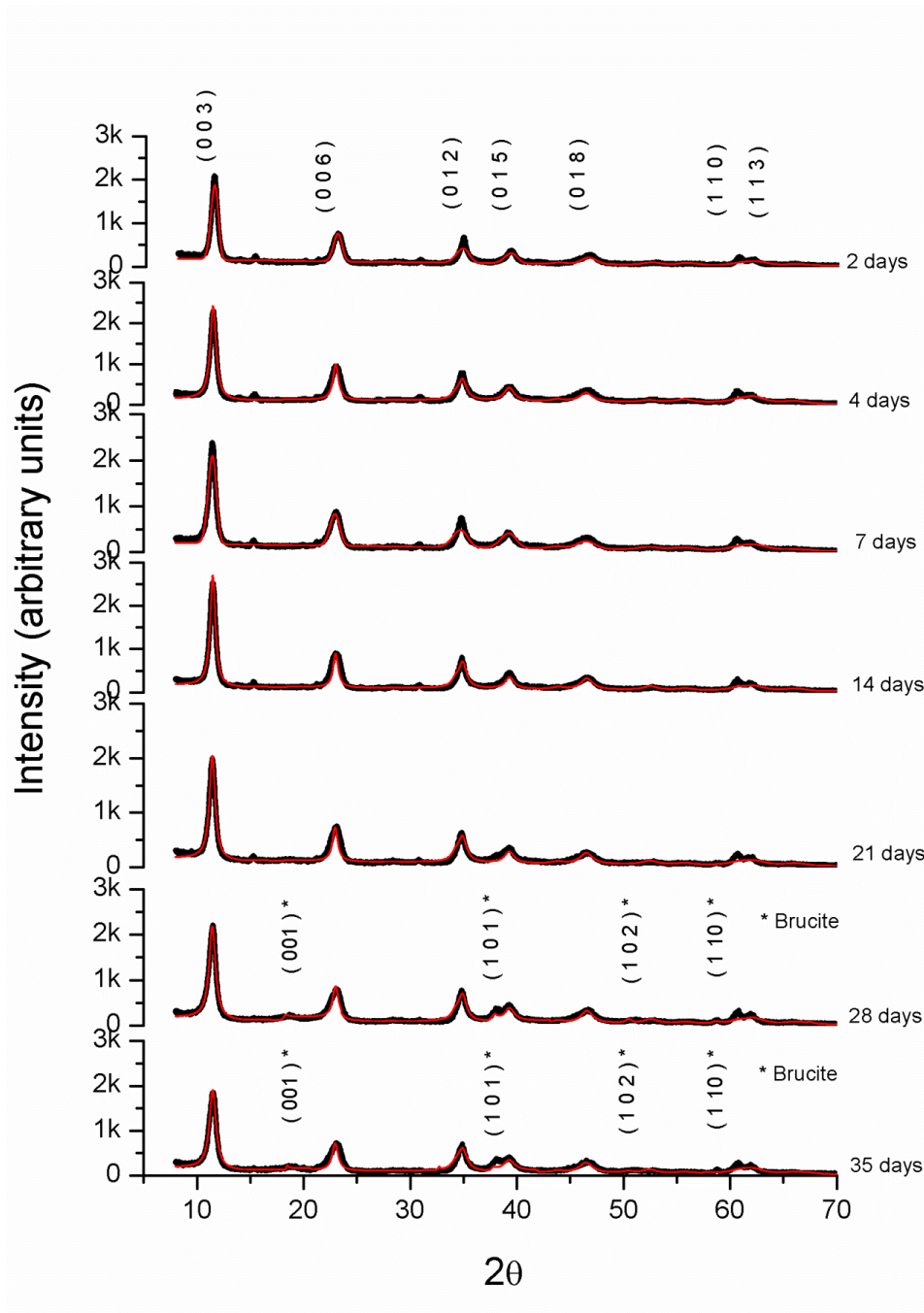


Figure 5.2 XRD for 25 Mg-Al Series.

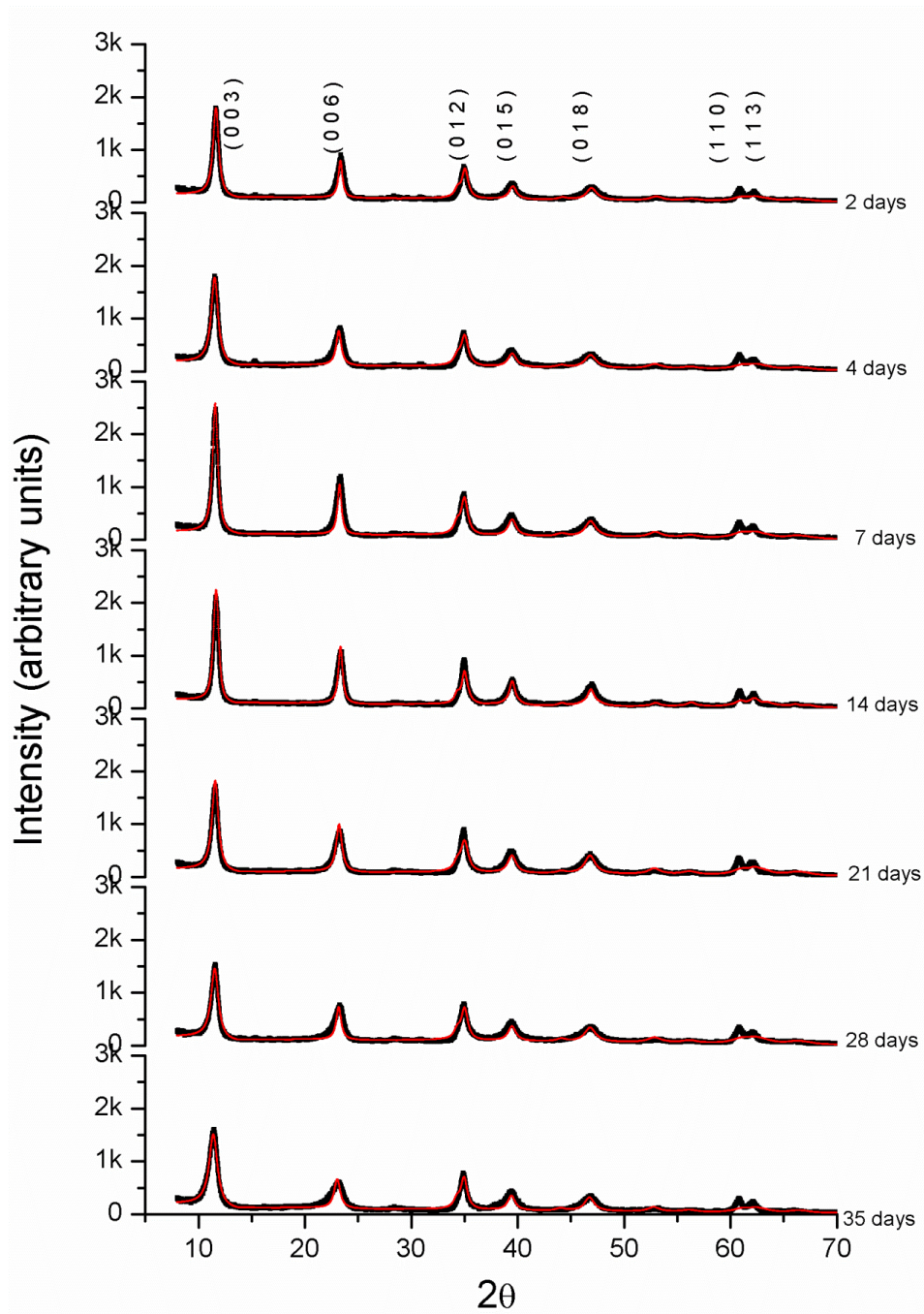
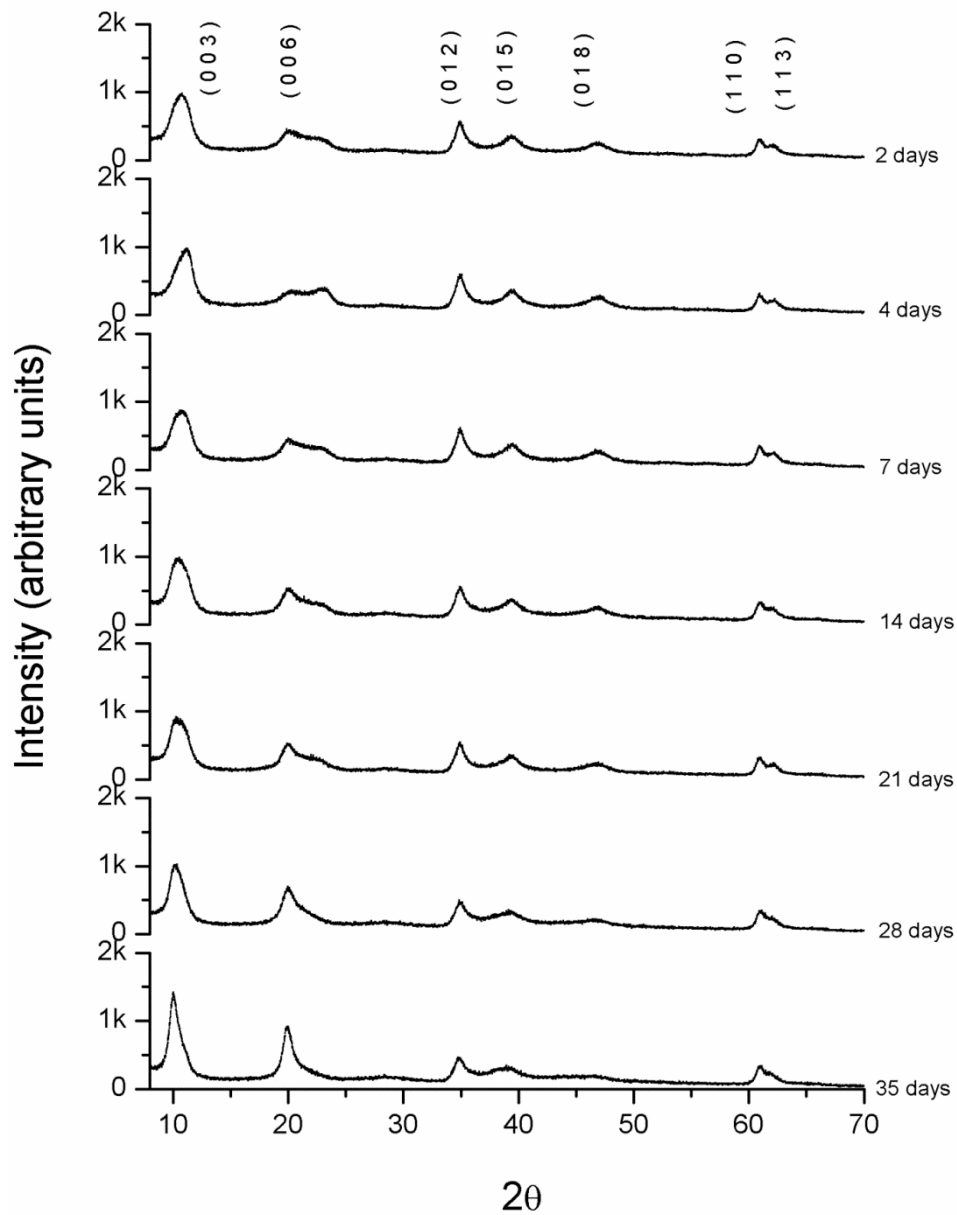


Figure 5.3 shows only the XRD pattern for the 30 Mg-Al Series. Anyone of the seven samples could be refined.

The XRD pattern for all 21 samples shows seven well-defined peaks 003, 006, 012, 015, 018, 110 and 113 that are characteristics reflections which correspond to hydrotalcite structure (CAVANI, 1991; FERREIRA, 2001; OH et alli, 2002; RODRIGUES, 2007; PÉREZ et alli, 2009; SILVA, 2008; CHANG et alli, 2005).

Figure 5.3 XRD for 30 Mg-Al Series.



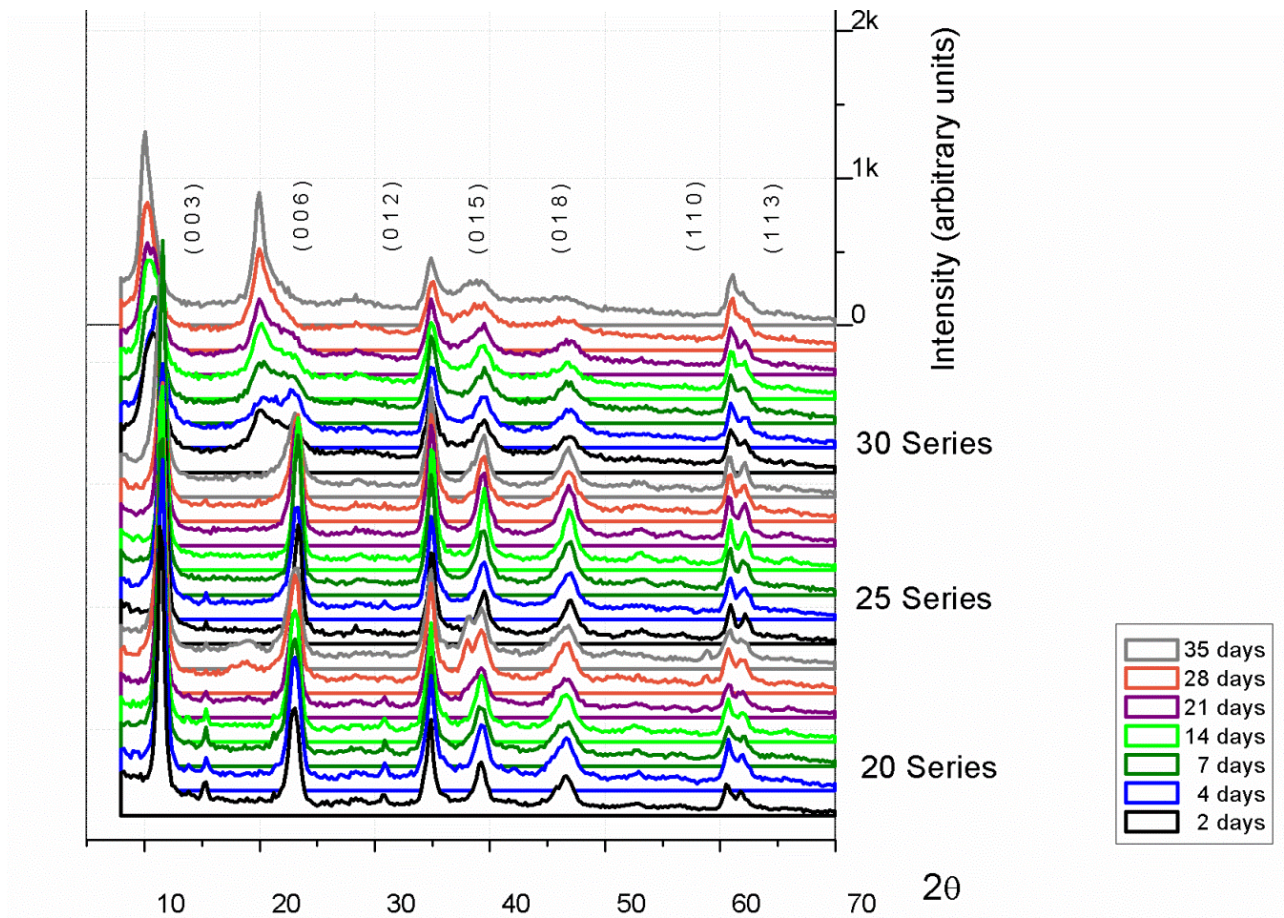
The presence of carbonate anions (CO_3^{2-}) can be confirmed by the basal d-spacing for the 20 and 25 Mg-Al Series, $d_{003} = 0.775 \text{ nm} (\pm 0.0014 t_{5\%})$ and $0.766 \text{ nm} (\pm 0.0015 t_{5\%})$ respectively. Similar results can be found in literature (CARJA et alli, 2001; NODA PÉREZ et alli, 2004; GÉRAUD et alli, 2007; LI et alli, 2010).

It can be seen from the Figures 5.1 and 5.2 that the 20 and 25 Series present apparently similar crystallinity evidenced by the height of their peaks (the next section shows a hypothesis test that was carried out to verify it).

Those results are better than de 30 Series that showed a very low intensity of their peaks in all seven samples. It is important to underline that the scales in the graphs correspond to 20 and 25 Series are the same varying from zero to 3,000 counts whereas the 30 Series varies from zero until 2,000 counts.

A better visualization for comparison can be seen in Figure 5.4 that shows 21 samples XRD pattern in perspective way where you can see a great difference in the peak position of 003 and 006 planes.

Figure 5.4 XRD for 20, 25, and 30 Mg-Al Series.



The non-basal peaks 012, 015 and 018 did not change their position for the three series; and the 012 peaks are well defined for all samples whereas in the 30 Series there was a reduction in sharpness and a broad for the 015 and 018 peaks. The alignment is visible also in the planes relative to the lamellae 110 and 113.

The samples 20 Mg-Al 2 to 21 and 25 Mg-Al 2 and 4 showed little peaks at 2θ angles 15.35° and 30.85° with the respectively 169 and 121 average counts. The identification of this phase was not accomplished by the program used. Thus it can be assumed to be just contamination with no identified origin.

Figure 5.1 shows another phase than hydrotalcite in the samples with 28 and 35 days aging. Four peaks correspondent to the planes 001, 101, 102 and 110 were identified as a brucite crystalline phase $[\text{Mg}(\text{OH})_2]$, a non-expected result that is discussed in the last section.

5.2 Hydrotalcite Cell Parameters

Table 5.1 and 5.2 present the results from the refinement for the 20 and 25 Series, respectively: cell parameters (a and c), crystallite size for the basal planes D_{003} and D_{006} ; a lamellar plane D_{110} , and a mean value for the seven planes, D_s .

The cell parameter a showed a disperse result in both Series. It begins with an intermediate value, gets the maximum and then reaches smaller values. The parameter a for 20 Series present a mean value of 0.3045 nm ($\pm 0.0003 t_{5\%}$) and for the 25 Series a 0.3034 nm ($\pm 0.0005 t_{5\%}$) and low standard deviation for both series. This result in 5% confidence interval to mean population (μ) ($0.3042\text{nm} < \mu < 0.3048\text{nm}$) and ($0.3029\text{nm} < \mu < 0.3039\text{nm}$) respectively for 20 and 25 Series present a short range for both series and a reduction in the mean value.

The isomorphic substitution of Mg^{+2} in the octahedral structure of a brucite like-layer for Al^{+3} of smaller ionic radius probably is the reason for the reduction in the cell parameter a . Thus the reduction in a cell parameter is expected for molar ratio (x) increasing from 0.20 to 0.25 owing to the differences in their ionic radius. Mg^{+2} has 0.65 Å ionic radius whereas Al^{+3} has 0.50 Å (CAVANI et alli, 1991).

Similar results were found by NODA PÉREZ et alli (2004); PÉREZ et alli (2009) in two of three syntheses in different pH and temperature. They synthesized hydrotalcite with 0.20, 0.25 and 0.33 molar ratio. KUSTROWSKY et alli (2005) led a research with synthesized hydrotalcite in four different molar ratios 0.20, 0.22, 0.25, and 0.33 and the same reduction in a parameter with the increasing in molar ratio was observed.

The crystallite size of the 20 and 25 Series samples were calculated from the X-ray line broadening according to the Scherrer equation (3.11) with the full width at half maximum intensity (FWHM) and the constant k was set equal to unity.

The constant k , relative to the particles shape in Scherrer equation, was arbitrarily chosen to be equal to unity, although this value is not true, because it would represent a spherical shape particle. LI et alli (2006) used a 0.89 whereas KOVANDA et alli (2005) had chosen 0.90 for this parameter. Any of them explained mathematically their chosen. Thus $k = 1$ will serve just for comparison between other works.

Table 5.1 Refinement parameters from 20 Mg-Al LDH Series.

Cell parameters			Crystallite size			
time	a	c	D_{003}	D_{006}	D_{110}	D_s
days	nm					
2	0.3047	2.319	11.6 ± 0.1	10.0 ± 0.1	4.41 ± 0.05	7.2 ± 0.1
4	0.3050	2.328	14.4 ± 0.2	15.6 ± 0.2	4.88 ± 0.05	8.4 ± 0.2
7	0.3046	2.330	10.2 ± 0.1	8.5 ± 0.1	3.67 ± 0.04	5.4 ± 0.1
14	0.3042	2.322	16.5 ± 0.2	17.1 ± 0.3	5.22 ± 0.06	10.2 ± 0.3
21	0.3042	2.324	14.5 ± 0.2	16.3 ± 0.2	4.80 ± 0.05	9.5 ± 0.2
28	0.3041	2.328	12.9 ± 0.2	14.9 ± 0.2	5.36 ± 0.06	9.5 ± 0.2
35	0.3046	2.332	12.5 ± 0.1	14.4 ± 0.2	4.65 ± 0.05	8.7 ± 0.2

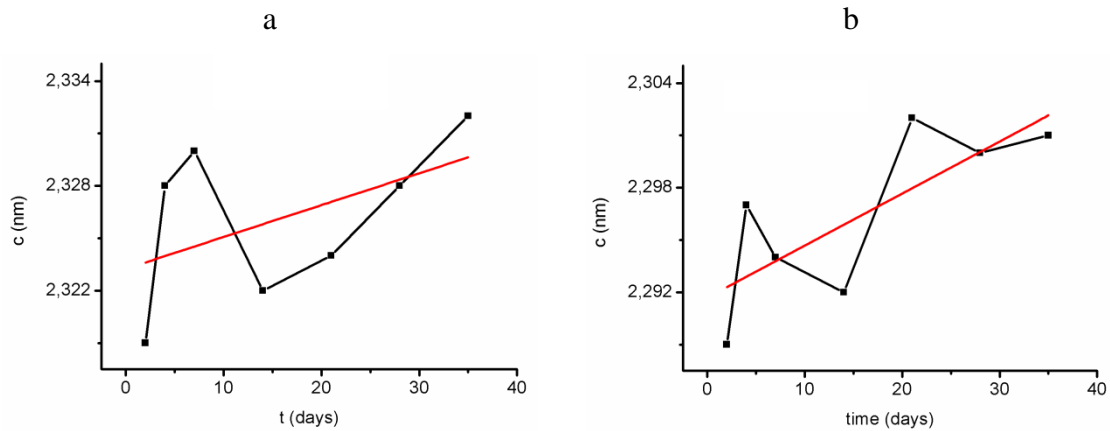
Table 5.2 Refinement parameters from 25 Mg-Al LDH Series

Cell parameters			Crystallite size			
time	a	c	D_{003}	D_{006}	D_{110}	D_s
days	nm					
2	0.3035	2.289	14.9 ± 0.2	22.8 ± 0.4	5.76 ± 0.07	11.9 ± 0.4
4	0.3030	2.297	12.0 ± 0.1	16.9 ± 0.3	5.23 ± 0.06	9.9 ± 0.3
7	0.3036	2.294	16.9 ± 0.2	23.3 ± 0.4	5.53 ± 0.06	11.9 ± 0.4
14	0.3042	2.292	16.0 ± 0.2	21.6 ± 0.4	7.60 ± 0.10	13.5 ± 0.4
21	0.3038	2.302	13.1 ± 0.2	15.0 ± 0.2	5.97 ± 0.07	10.0 ± 0.2
28	0.3033	2.300	11.1 ± 0.1	17.8 ± 0.3	5.20 ± 0.06	10.2 ± 0.3
35	0.3026	2.301	9.7 ± 0.1	14.0 ± 0.2	6.02 ± 0.07	10.0 ± 0.2

The parameter c in both series presents a behavior with apparently tendency of growing as aging time increases. The mean values are 2.326 nm ($\pm 0.0043 t_{5\%}$) and 2.296 nm ($\pm 0.0046 t_{5\%}$), respectively, for 20 and 25 Series. They present a short range.

The supposition of c parameter growing with aging time was tested by constructing tendency line (Figure 5.5) with the result for coefficient of determination (R^2) just 9.58% and 50.3%, respectively for 20 and 25 Series. Low values to support this supposition.

Figure 5.5 Cell parameter c obtained for 20 Mg-Al and 25 Mg-Al Series.



Comparing cell parameter c between this series, it is also verified a reduction in their values as the molar ratio increases. According to AUXILIO et alli (2009) the molar ratio determines the layer charge density. So the reason for this aspect is due to the elevation in the residual charge observed as the Al^{+3} atoms are substituted by Mg^{+2} atoms in the lamellae. The increase in positive charge is favorable to a strong interaction between the layer and the interlamellar anion causing a reduction in the layer-interlayer distance. The same behavior was observed in others works (NODA PÉREZ et alli, 2004; PÉREZ et alli, 2009; KUSTROWSKY et alli, 2005).

The cell parameter may change little with molar ratio however it was not expected to vary with aging time because it is an intrinsic characteristic of the crystalline structure. This little change can be evidenced by the order of the standard deviation 10^{-3} and 10^{-4} for a and c cell parameters for the two series.

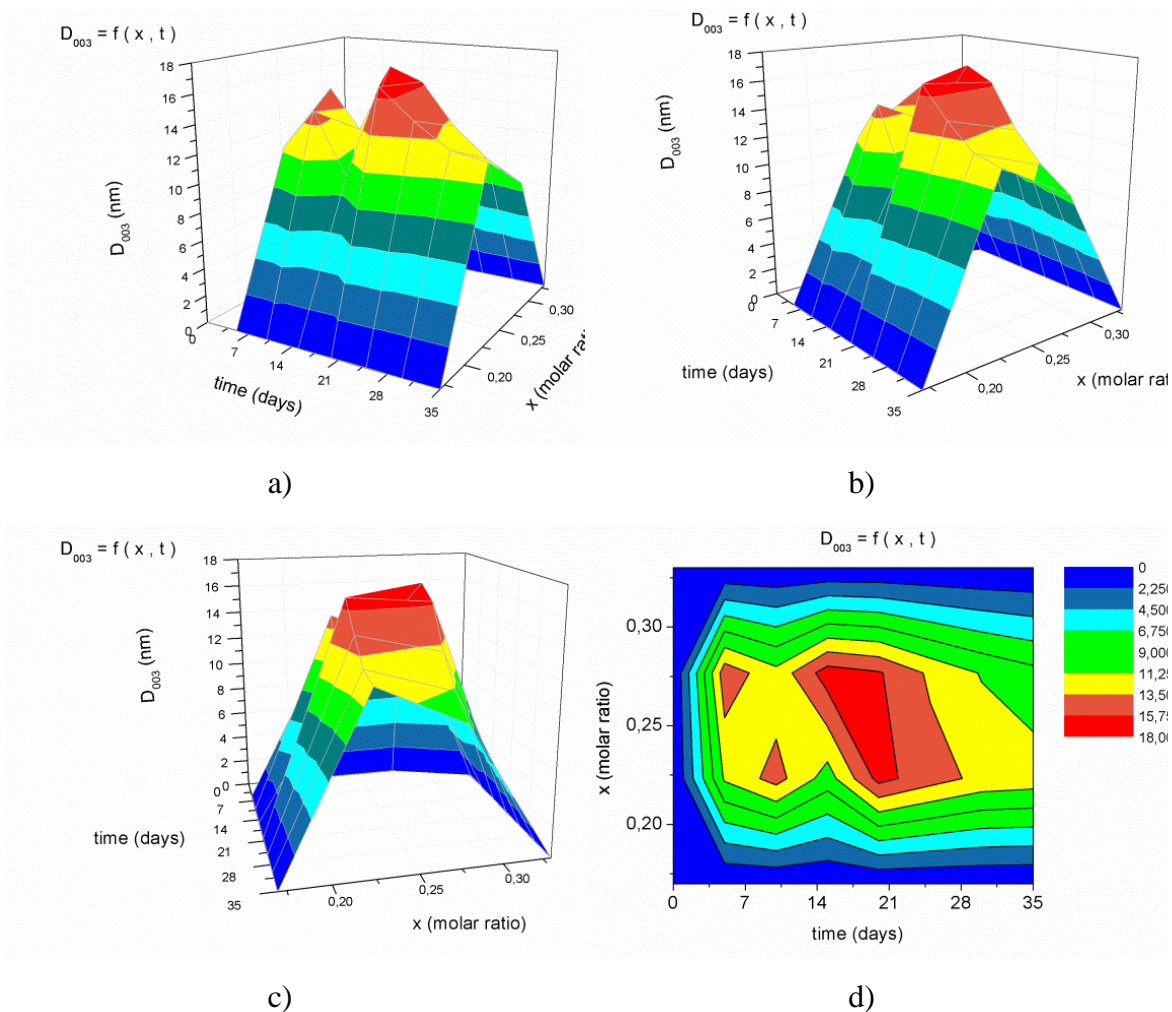
On the other hand, there are reasons to believe a significant change in textural properties with variation in molar ratio and aging, as discussed before (section 1.5).

Although there are many of these parameters like specific surface area, particle size distribution, porosity, etc., it was expected to observe a change in two of these studied parameters: crystallinity and crystallite size as the synthesis conditions modify (molar ratio and aging). The other parameters were not evaluated in this research.

5.3 Hydrotalcite Crystallite Size

To better visualization of the crystallite size in results from Tables 5.1 and 5.2, three 3D surface color and hypsometric maps were drawing in three different angles for D_{003} , D_{006} and D_s .

Figure 5.6 3D Surface Color Map (a, b and c) and hypsometric (d) for D_{003} .

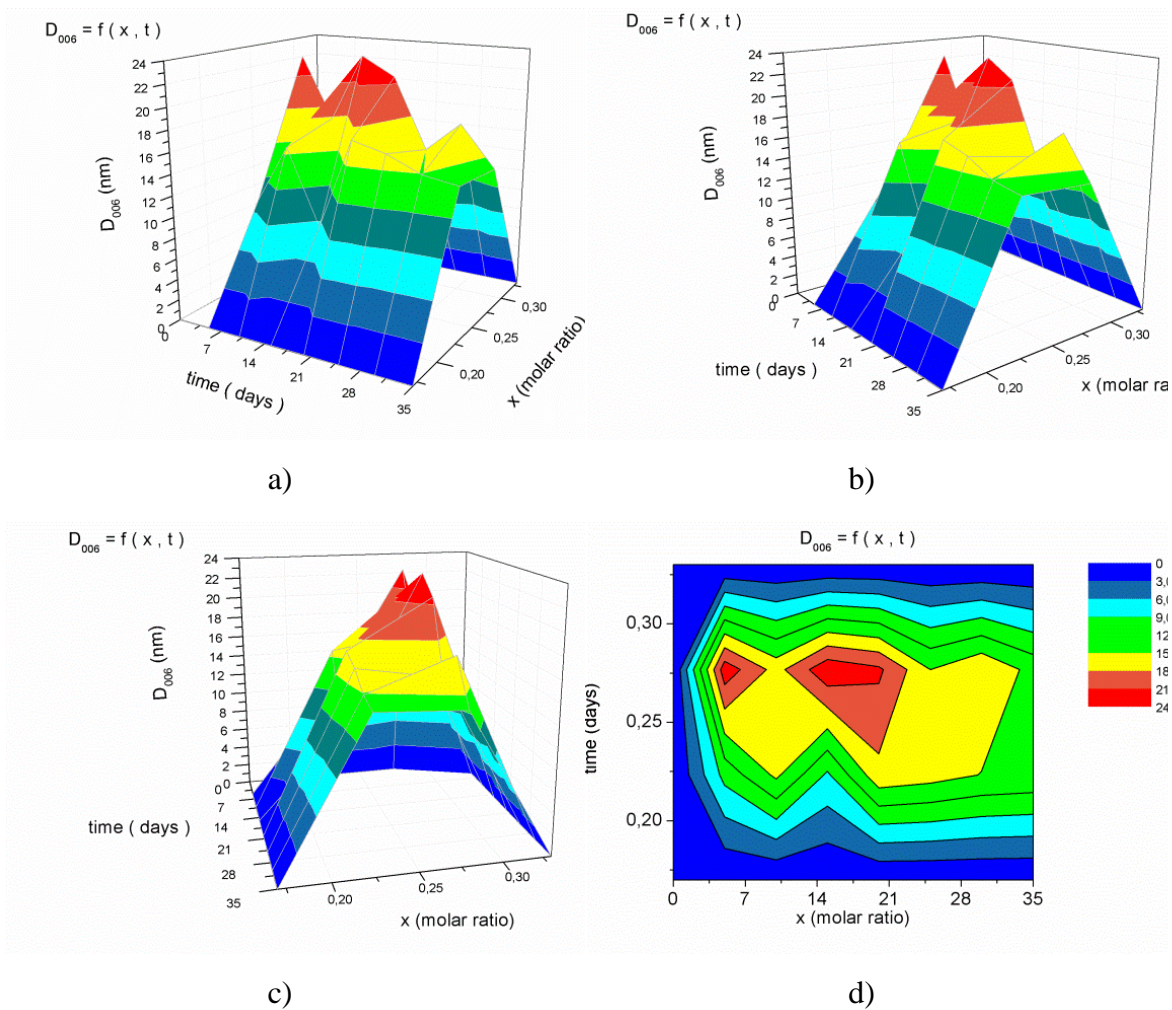


The color scale is drawn together with the hypsometric maps in Figures 5.6, 5.7 and 5.8. It is important to highlight again about the different scale used in these figures: 18 nm, 24 nm and 14 nm respectively for D_{003} , D_{006} and D_s .

The surface Map and hypsometric for D_{003} in Figure 5.6 showed a region of maximum between 14 and 21 days between 0.20 and 0.30 molar ratio and it reaches almost 18 nm for the crystallite size. There are another two regions with low values peaks: a region between 4 and 7 days and correspondent molar ratio varying from 0.25 to 0.30; and another between 7 and 14 days with molar ratio varying from 0.20 to 0.25.

A similar behavior was observed for surface map from the D_{006} showed in Figure 5.7. However there were two regions of maximum: one above 7 days and between 0.25 and 0.30 molar ratio; and another between 14 and 21 days that shows just a difference in the maximum region area that is less than the respective area from D_{003} .

Figure 5.7 3D Surface Color Map (a, b and c) and hypsometric (d) for D_{006} .

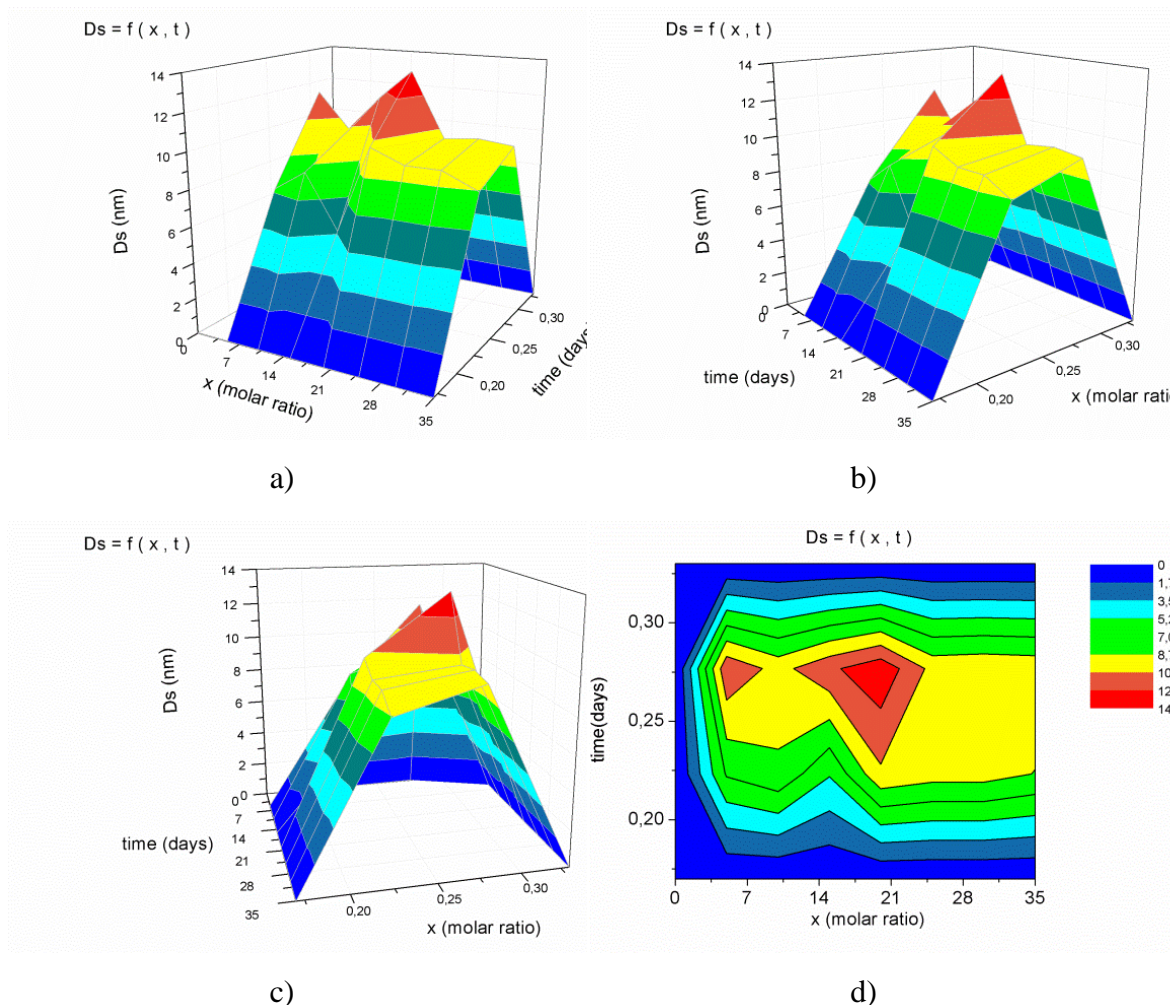


In the initial times between zero and 2 days can be observed that occurs a quick growth in the crystallite size that is better visualized in the hypsometric maps, for D_{003} , D_{006} and D_s , showed by the proximity lines. It could be wrongly interpreted that crystallite size would grow linearly with time as shown.

Maybe it is important to know how the variation happens in the beginning. SHARMA et alli (2007) carried out a research accompanying the crystallite size from zero to 11 hours and they found that the growth varies almost like a logarithm function with time.

D_s measures in Figure 5.8 present a unique region of maximum and it is possible to imagine that the yellow region will extend for extras days until it decreases. Thus there is probably a tendency of crystallite size decreasing with time. The limited time analyzed, until 35 days, shows the need to explain what could happen to crystallite size with a long time aging.

Figure 5.8 3D Surface Color Map (a, b and c) and hypsometric (d) for D_s .



Ds measures present the lowest scale as it was a mean for seven planes. Although the scales are different, there is an apparent common aspect between the 3D surfaces: there is a similarity about their shape and Ds could represent better the crystallite size for LDH varying with molar ratio and time.

The graphics were constructing with a matrix considering the values zero for the crystallite size in the low and high molar ratios limits, as mentioned in literature, 0.17 (SILVA, 2008; ALEJANDRE et alli, 1999) and 0.33 (RODRIGUES, 2007; PÉREZ et alli, 2009; FERREIRA, 2001; SILVA, 2008; CHANG et alli, 2005).

Obviously the most common value accepted for the low limit to obtain pure LDH is 0.20 but for a simple matter of symmetry it was chosen a justified value 0.17. So the matrix of input data consisted of four lines (correspondent to molar ratios 0.17, 0.20, 0.25 and 0.33) and eight times (0, 2, 4, 7, 14, 21, 28 and 35 days).

It is important to underline that the matrix used was 4x8 and not a 5x8, as expected, (0.17, 0.20, 0.25, 0.30 and 0.33). The values for the third series, 30 Series, were not obtained, as the refinement did not run and consequently the molar ratio 0.30 was not included.

As was seen before there is another phase in at least two samples from the 20 Series and the discussion above is about pure LDH. However the crystallite size was calculated for hydroxalcite and for brucite, separately (it will be approached in the final section). Thus the author believes that the discussion about the results is relevant.

5.4 Statistical Approach to XRD Results

It is known from literature and discussed before that it does exist a suggest range of obtaining pure LDH that varies from a molar ratio 0.20 to 0.33 relative to Al/(Mg+Al) atoms in the hydroxalcite structure for some authors (FERREIRA, 2001; CHANG et alli, 2005; RODRIGUES, 2007; PÉREZ et alli, 2009; SILVA, 2008) and 0.17 to 0.33 for SILVA (2008) and ALEJANDRE et alli (1999).

Based on the last range (0.17 to 0.33) it was chosen the values in-between and symmetrical 0.20, 0.25 and 0.30 to be analyzed in this research. Thus it is reasonable to imagine that the extremes values 0.20 and 0.30 would give minimum values of crystallinity and crystallite size and molar ratios in-between would give

maximum values. Unfortunately it was not possible to obtain the structural parameters from the 30 Series. Thus, just the crystallinity was analyzed and compared.

The obtained as-synthesized samples from 20 Series showed apparently the same crystallinity as the 25 Series samples and both present a visible superior crystallinity than the 30 Series. This result was not expected (for the author) since the molar ratio 0.20 is in the low limit of synthesis to obtain pure LDH for the majority of the references described in previous chapters of this work.

Furthermore the 30 Series showed poor crystallinity, evidenced by a count reduction (expected result for the author), a broadening in all peaks and a shifting to lower values of angle in respect to 003 and 006 planes. It can be seen in the Figure 5.4 that the shifting is more pronounced in the 006 planes.

The shifting can be seen better comparing the mean and standard deviation values for the peaks in the three series (Table 5.3). It is possible to see that there is approximately one degree of difference between 30 Series compared to the other series in relation to the peaks in the 003 plane. The difference is more pronounced in the 006 plane, about three degrees. The standard deviation is clearly very high for the 30 Series. It is 7.4 greater than the 20 Series for 003 and 3.4 for the 006 plane compared to 20 Series.

To discuss these observations and compare the three series results is necessary to verify if these shifts are significant. Thus a hypothesis test had to be carried out to better analyze this possibility. The results are shown in Tables 5.4, 5.5 and 5.6.

Table 5.3 Mean (\bar{x}) and Standard Deviation (s) for 003 and 006 peaks.

Plane Molar ratio (x)	003		006	
	\bar{x}	s	\bar{x}	s
0.20	11.48°	0.05°	23.07°	0.05°
0.25	11.58°	0.05°	23.32°	0.06°
0.30	10.57°	0.38°	20.04°	0.17°

Two Sample t-Tests were used as a hypothesis test to verify significant differences between the means. As a presupposition to apply this kind of test is that the compared samples have to come from a population with Gaussian distribution and the

variances have to be tested to know if they can be considered equal or not. Depending upon the variances results different equations are applied in hypothesis test. The following equations demonstrate both cases (MONTGOMERY and RUNGER, 2012):

When the variances are similar ($\sigma_1^2 = \sigma_2^2$):

$$T = \frac{\bar{x}_1 - \bar{x}_2 - (\mu_1 - \mu_2)}{S_p \sqrt{\frac{1}{n_1} + \frac{1}{n_2}}} \quad 5.1$$

where \bar{x}_1 and \bar{x}_2 are the mean values for the samples and μ_1 and μ_2 are the mean values for the populations; n_1 and n_2 are the numbers of samples. S_p is the pooled estimator calculated by the equation:

$$S_p^2 = \frac{(n_1 - 1)S_1^2 + (n_2 - 1)S_2^2}{n_1 + n_2 - 2} \quad 5.2$$

where S_1^2 and S_2^2 are the sample variances. It is a t-distribution with $(n_1 + n_2 - 2)$ degree of freedom (ν).

When the variances are different ($\sigma_1^2 \neq \sigma_2^2$):

$$T = \frac{\bar{x}_1 - \bar{x}_2 - (\mu_1 - \mu_2)}{\sqrt{\frac{S_1^2}{n_1} + \frac{S_2^2}{n_2}}} \quad 5.3$$

The degree of freedom (ν) is calculated with the following equation:

$$\nu = \frac{\left(\frac{S_1^2}{n_1} + \frac{S_2^2}{n_2}\right)^2}{\frac{\left(\frac{S_1^2}{n_1}\right)^2}{n_1 - 1} + \frac{\left(\frac{S_2^2}{n_2}\right)^2}{n_2 - 1}} \quad 5.4$$

The degree of freedom (ν) has to be rounded for the least integer according to MONTGOMERY and RUNGER (2012).

It was performed the well-known Fischer-Snedecor Test (F-test) to verify the equality of variances and Shapiro-Wilk and Kolmogorov-Smirnov tests to verify the normality of the samples. Samuel Shapiro, an American, and Martin Wilk, a Canadian, both statistical, proposed this normality test in 1965 that is based on the following equation (SHAPIRO and WILK, 1965):

$$W = \frac{\left[\sum_{i=1}^n a_i x_i \right]^2}{\sum_{i=1}^n (x_i - \bar{x})^2} \quad 5.5$$

where W is the result test compared with a critical one W_α tabulated; the parameters a_i are coefficients normalized and tabulated obtained from the ordered data observed.

Kolmogorov-Smirnov test (Andrei Kolgomorov and Vladimir Ivanovich Smirnov, both mathematicians Russian) is based in a comparison of the maximum distance between a cumulative function and a normal distribution. It is calculated by the equation (SOONG, 2004):

$$D_{calc} = \max |S_n(x_i) - F(x_i)| \quad 5.6$$

where D_{calc} is the calculated maximum distance between a cumulative distribution until i^{th} element, $S_n(x_i)$, and the theoretical cumulative value for the i^{th} element, $F(x_i)$. D_{calc} is compared with a $D_{n,\alpha}$ tabulated, where n is the number of samples and α is the significance level.

There are two possibilities:

If $D_{calc} < D_{n,\alpha}$ the null hypothesis is accepted, i.e., the sample present a Gaussian distribution;

If $D_{calc} > D_{n,\alpha}$ the null hypothesis is rejected, i.e., the sample present non-Gaussian distribution origin.

There are others normality test that could be applied, Lilliefors, Cramer-von Mises and Anderson-Darling test. Shapiro-Wilk test was chosen because is more powerful than the others. However its power test is low for small samples, thus another normality test could reinforce the results and Kolgomorov-Smirnov test was also chosen. A detailed study of the comparative powerful of these tests can be found in RAZALI and WAH (2011).

Some authors (MONTGOMERY and RUNGER, 2012; LEVINE et alli, 2012) suggest that for a few number of samples the hypothesis test could be reinforced by a non-parametric test.

Furthermore a non-parametric test is used in situations that the presupposition of normality is not confirmed, it happened to Shapiro-Wilk test of the 30 Series samples for crystallinity analysis. Thus a Wilcoxon Paired Rank Test was chosen to test de median values for paired samples.

Wilcoxon Paired Rank Test is a qualitative analysis of the difference between two median values and is based on a comparison of the observations in both set. The numbers of the two samples n_1 and n_2 are added ($n = n_1 + n_2$); all the data are ordered and is obtained T_1 and T_2 , the sum of the classifications of the samples. For any integer value n we have the following equation (LEVINE et alli, 2012):

$$T_1 + T_2 = \frac{n(n+1)}{2} \tag{5.7}$$

When n_1 and n_2 are either less or equal to 10, tables are used to supply critical values for T_1 and there are two hypotheses for a one-tale test:

H_0 : $Md_1 = Md_2$, the median of the first population is equal to the median of the second one: the null hypothesis is accepted if T_1 is less than the critical value.

H_1 : $Md_1 > Md_2$. the median of the first population is greater than the median of the second one and the alternative hypothesis is accepted if the T_1 is greater or equal to the critical value.

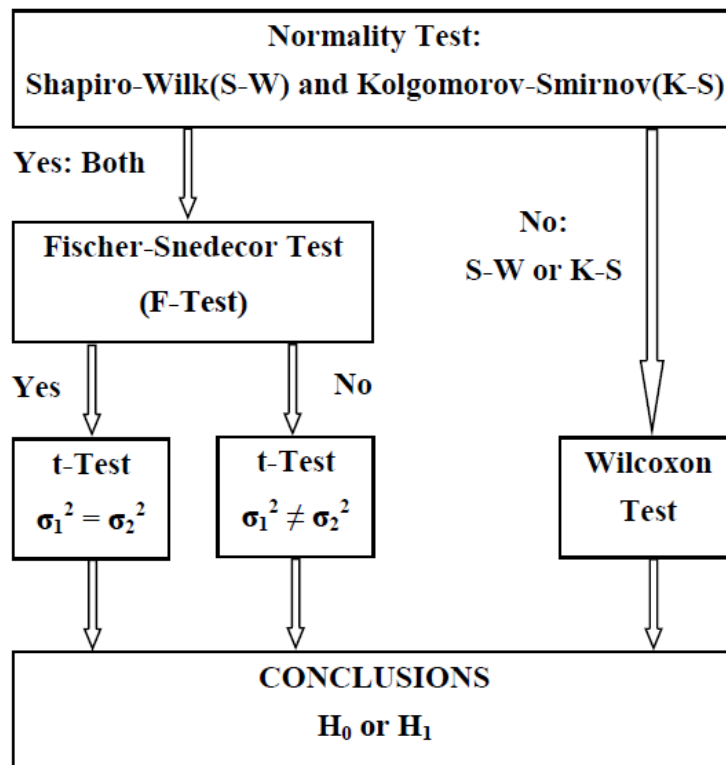
Tables 5.4 and 5.5 summarize these tests for the shift in 003 and 006 peaks, respectively, and Table 5.6 shows the result for crystallinity. σ^2 and μ are the variance and mean population, respectively.

The sequence to be analyzed in these tables is shown in the diagram from the Figure 5.9. First, the presupposition to parametric test is evaluated with normality test: Shapiro-Wilk and Kolgomorov-Smirnov test.

If at least one of the tests fails, the data is considered to present a non-Gaussian origin. Thus the non-parametric test is made, Wilcoxon Paired Rank test, and then follow the conclusion of the hypothesis test.

If both results point to Gaussian distribution, a Fischer-Snedecor test is carried out. Depending upon the results, about variances, different equations are used to t-Test (when the variances are similar ($\sigma_1^2 = \sigma_2^2$) equation 5.1 and 5.2; for different variances ($\sigma_1^2 \neq \sigma_2^2$), equations 5.3 and 5.4 are used). Then, the hypothesis test is concluded.

Figure 5.9 Diagram for hypothesis test sequence



The discussion for these results is as follows:

20 peaks shift at 003 planes

All the samples in the three series are confirmed to come from a Gaussian distribution population based on Shapiro-Wilk and Kolmogorov-Smirnov tests.

Fischer-Snedecor test (F-test) showed that the pair 0.20/0.25 presents similar variances and the result for hypothesis test shows that it does not exist a significant difference between these samples. The probability was next to unit, 0.9982. The result is also confirmed by the non-parametric test with a probability 0.9766.

Table 5.4 Applied statistics to 2 θ peaks shift at 003 planes.

Normality Test				
Molar ratio (x)	Shapiro-Wilk		Kolmogorov-Smirnov	
	Probability	Conclusion	Probability	Conclusion
0.20	0.9428	Gaussian	1.000	Gaussian
0.25	0.1619	Gaussian	0.9508	Gaussian
0.30	0.9583	Gaussian	1.000	Gaussian
Fischer-Snedecor Test				
Pairs compared	Probability	Conclusion	Probability	Conclusion
0.20/0.25	0.9670	$\sigma_1^2 = \sigma_2^2$	0.9766	$Md_1 = Md_2$
0.20/0.30	1.112×10^{-4}	$\sigma_1^2 \neq \sigma_2^2$	7.810×10^{-3}	$Md_1 > Md_2$
0.25/0.30	1.237×10^{-4}	$\sigma_1^2 \neq \sigma_2^2$	7.810×10^{-3}	$Md_1 > Md_2$
Hypothesis Test (Two Sample t-Test)				
Pairs compared	$\sigma_1^2 = \sigma_2^2$		$\sigma_1^2 \neq \sigma_2^2$	
	Probability	Conclusion	Probability	Conclusion
0.20/0.25	0.9982	$\mu_1 = \mu_2$	0.9982	$\mu_1 = \mu_2$
0.20/0.30	1.866×10^{-5}	$\mu_1 > \mu_2$	3.135×10^{-4}	$\mu_1 > \mu_2$
0.25/0.30	6.917×10^{-6}	$\mu_1 > \mu_2$	1.761×10^{-4}	$\mu_1 > \mu_2$

On the other hand F-test fails for the pairs 0.20/0.30 and 0.25/0.30 and the hypothesis test showed that both 0.20 and 0.25 molar ratio samples have the mean value significantly greater than the 0.30 molar ratio samples. The orders of the t-Test probability reinforce the differences, 3.135×10^{-4} and 1.761×10^{-4} , respectively. The non-parametric test confirmed the hypothesis test results for the two combination pairs with probability 7.810×10^{-3} , in both cases.

2θ peaks shift at 006 planes

The normality test for the samples confirmed that all of them come from a Gaussian distribution. However it is important to highlight that the probability for the Shapiro-Wilk test was just 7.85%, so it is very near a non-Gaussian distribution for this test that adopted a 5% significance level.

Table 5.5 Applied statistics to 2θ peaks shift at 006 planes.

Normality Test				
Molar ratio (x)	Shapiro-Wilk		Kolmogorov-Smirnov	
	Probability	Conclusion	Probability	Conclusion
0.20	0.8105	Gaussian	0.9854	Gaussian
0.25	0.5275	Gaussian	1.000	Gaussian
0.30	0.0785	Gaussian	0.4251	Gaussian
Fischer-Snedecor Test			Wilcoxon Paired Rank Test	
Pairs compared	Probability	Conclusion	Probability	Conclusion
0.20/0.25	0.6969	$\sigma_1^2 = \sigma_2^2$	1.000	Md ₁ = Md ₂
0.20/0.30	1.196 x 10 ⁻²	$\sigma_1^2 \neq \sigma_2^2$	7.810 x 10 ⁻³	Md ₁ > Md ₂
0.25/0.30	2.783 x 10 ⁻²	$\sigma_1^2 \neq \sigma_2^2$	7.810 x 10 ⁻³	Md ₁ > Md ₂
Hypothesis Test (Two Sample t-Test)				
Pairs compared	$\sigma_1^2 = \sigma_2^2$		$\sigma_1^2 \neq \sigma_2^2$	
	Probability	Conclusion	Probability	Conclusion
0.20/0.25	1.000	$\mu_1 = \mu_2$	1.000	$\mu_1 = \mu_2$
0.20/0.30	4.427 x 10 ⁻¹⁵	$\mu_1 > \mu_2$	2.349 x 10 ⁻¹⁰	$\mu_1 > \mu_2$
0.25/0.30	2.092 x 10 ⁻¹⁵	$\mu_1 > \mu_2$	5.137 x 10 ⁻¹¹	$\mu_1 > \mu_2$

F-test showed the same result for the combined pairs as in the 2θ peaks shift at 003 planes: it fails 0.20/0.30 and 0.25/0.30 with probabilities 1.196 x 10⁻² and 2.783 x 10⁻², respectively. It showed similar variances for the 0.20/0.25 pairs. The hypothesis test showed the same conclusion that pairs 0.20/0.25, they present the same population mean.

The 0.20 and 0.25 molar ratio samples presented a very greater mean than the 0.30 molar ratio samples. Wilcoxon Paired Rank test confirmed the hypothesis

results for the two combination pairs with the same probability for both results: 7.810×10^{-3} .

Another underline is about the order of the probability obtained in the hypothesis tests for 2θ peaks shift at 006 planes: 10^{-10} whereas the 2θ peaks shift at 003 planes is only 10^{-4} . It must come from the large differences between the 2θ angles observed in Table 5.3 that was about 3 degrees for 006 planes and about 1 degree for 003 planes.

Crystallinity

The normality test was accepted for the 0.20 and 0.25 samples but failed for the 0.30 samples in respect to the Shapiro-Wilk test. On the other hand all the pairs showed to have the same variance as confirmed by F-test. However the parametric hypothesis test may not be allowed for the 0.30 molar ratio samples paired with the others. It could be carried out if it is considered just the Kolmogorov-Smirnov normality test.

The parametric and non-parametric hypothesis test showed that the 0.20 molar ratio samples present a higher crystallinity than the 0.25. It can be considered the parametric test as we have the 0.20 and 0.30 molar ratio samples with Gaussian distribution origin. Wilcoxon Paired Rank test confirmed what was observed in the XRD graphics: the median values for 0.20 and 0.25 molar ratio samples are higher than the 0.30 molar ratio samples, and the 0.20 molar ratio present median greater than the 0.25 molar ratio samples.

The statistical hypothesis test analyses allow us to make affirmative about compared samples. Obviously the results could change if it was chosen another significance level; however 5% is the most used in statistics analysis.

Probability in Tables 5.4 and 5.5 show us that no change would happen in the results for 2θ peaks shift at 003 and 006 planes if it was used a 1% significance level. The only change would be observable in crystallinity analysis with the parametric and non-parametric results: 2.564% and 1.563% probability, respectively. Thus the 0.20 and 0.25 samples crystallinity would be the same with 1% significance level.

Table 5.6 Applied statistics to Crystallinity.

Normality Test				
Molar ratio (x)	Shapiro-Wilk		Kolmogorov-Smirnov	
	Probability	Conclusion	Probability	Conclusion
0.20	0.9948	Gaussian	1.000	Gaussian
0.25	0.2480	Gaussian	0.5430	Gaussian
0.30	6.670×10^{-3}	Non-Gaussian	0.2876	Gaussian
Fischer-Snedecor Test			Wilcoxon Paired Rank Test	
Pairs compared	Probability	Conclusion	Probability	Conclusion
0.20/0.25	0.4234	$\sigma_1^2 = \sigma_2^2$	1.563×10^{-2}	$Md_1 > Md_2$
0.20/0.30	0.5674	$\sigma_1^2 = \sigma_2^2$	7.810×10^{-3}	$Md_1 > Md_2$
0.25/0.30	0.1779	$\sigma_1^2 = \sigma_2^2$	7.810×10^{-3}	$Md_1 > Md_2$
Hypothesis Test (Two Sample t-Test)				
Pairs compared	$\sigma_1^2 = \sigma_2^2$		$\sigma_1^2 \neq \sigma_2^2$	
	Probability	Conclusion	Probability	Conclusion
0.20/0.25	2.564×10^{-2}	$\mu_1 > \mu_2$	2.683×10^{-2}	$\mu_1 > \mu_2$
0.20/0.30	1.067×10^{-7}	$\mu_1 > \mu_2$	1.749×10^{-7}	$\mu_1 > \mu_2$
0.25/0.30	3.420×10^{-5}	$\mu_1 > \mu_2$	9.280×10^{-5}	$\mu_1 > \mu_2$

It can be observed that Shapiro-Wilk test is more rigorous than Kolmogorov-Smirnov normality test. Even if Shapiro-Wilk test was not used this would not change the result because there were a confirmation with Wilcoxon paired rank test in crystallinity analysis.

The final conclusion is that: it can be affirmed, with 5% of significance level, that there were a shift in the basal planes in 30 Series compared to the other series and the 20 Series present more crystallinity than 25 Series and thereafter the 25 Series shows more crystallinity than the 30 Series.

After this discussion a question can be raised: what does this shift possibly mean? Let us use the Bragg's law (equation 3.1), $n\lambda = 2 d_{hkl} \sin\theta$. Substituting $n = 1$; $\lambda = 0.1542$ nm and the correspondent angles to the 003 and 006 peaks plane it is possible to calculate the parameter c for the series using a 2θ mean value.

The parameter c can be calculated as three times the distance d_{003} ($c = 3 d_{003}$) or six times d_{006} ($c = 6 d_{003}$). Thus we calculate the theoretical parameter c (Table

5.7), the first column of c is relative to the parameter from the Rietveld refinement and the second and third one was obtained from the Bragg's law equation. The calculated values for 20 and 25 Series are very close to the results obtained from the refinement.

Table 5.7 Parameter c for the 30 Series.

Plane		003		006	
x	c	2θ	$c = 3d_{003}$	2θ	$c = 6d_{006}$
0.20	2.326 nm	11.48°	2.313	23.07°	2.313
0.25	2.296 nm	11.58°	2.293	23.32°	2.289
0.30	-	10.57°	2.511	20.04°	2.659

The c cell parameter estimated for the 30 Series present a mean of 2.585 nm. However these results are contradictory to what was expected as mentioned before because the molar ratio increases as the parameter c decreases (NODA PÉREZ et alli, 2004; PÉREZ et alli, 2009; KUSTROWSKY et alli, 2005). It can be concluded that occurred an enlargement in c cell parameter of the 30 Series that justify the shift observed in the basal planes.

Another possibility to explain this shift is associated to defects. Small crystal or grain size can be seen as lattice imperfection (CULLITY and STOCK, 2001), dislocation, vacancies, interstitials, substitutional, small and large-angle boundaries, stacking faults, twins, can strain the lattice (BALZAR, 1999). All of them can broad the peaks and are associated to micro or macrostress. Microstress and microstrain vary from one grain to another whereas the macrostress can be quite uniform over large distances and may cause a shift to lower angles (CULLITY and STOCK, 2001).

Thus the samples from 30 Series may probably present an uniform strain over large distances other than grains that may be the cause to the shift in the 003 and 006 peaks. According to CULLITY and STOCK (2001) the shift occurs by the reasons explained before but no other change could happen to the diffraction pattern. So the reduction in crystallinity is not yet explained.

SHARMA et alli (2007) developed a research with hydrotalcite and their goal was to study crystallinity and crystallite size effect obtained with different molar ratio, 0.22, 0.25, 0.29, and 0.33. They affirmed that occurred a significantly increasing in crystallinity and crystallite size but they did not show statistically the results to

confirm it. Furthermore it is observed from their XRD pattern result a shift in 003 and 006 planes and this observation were not approached by the authors.

5.5 FIT Function

The crystallinity was evaluated for the 21 analyzed samples and a 3D Surface color map and hypsometric was constructed and showed in Figure 5.10, and the color scale is drawn together with the hypsometric curve. The crystallinity function analyzed the intensity of the 003 peaks for all the samples and the graphic was constructing with a matrix considering the values zero for crystallinity in the molar ratios **0.17** (ALEJANDRE et alli, 1999; SILVA, 2008) and **0.33** (FERREIRA, 2001; CHANG et alli, 2005; RODRIGUES, 2007; PÉREZ et alli, 2009).

These values 0.33 and 0.17 were mentioned in literature as the limits, minimum and maximum to obtain pure hydrotalcite. The crystallinity was analyzed the same way in previous research (LIMA et alli, 2012) with integral intensities of the 003 peaks.

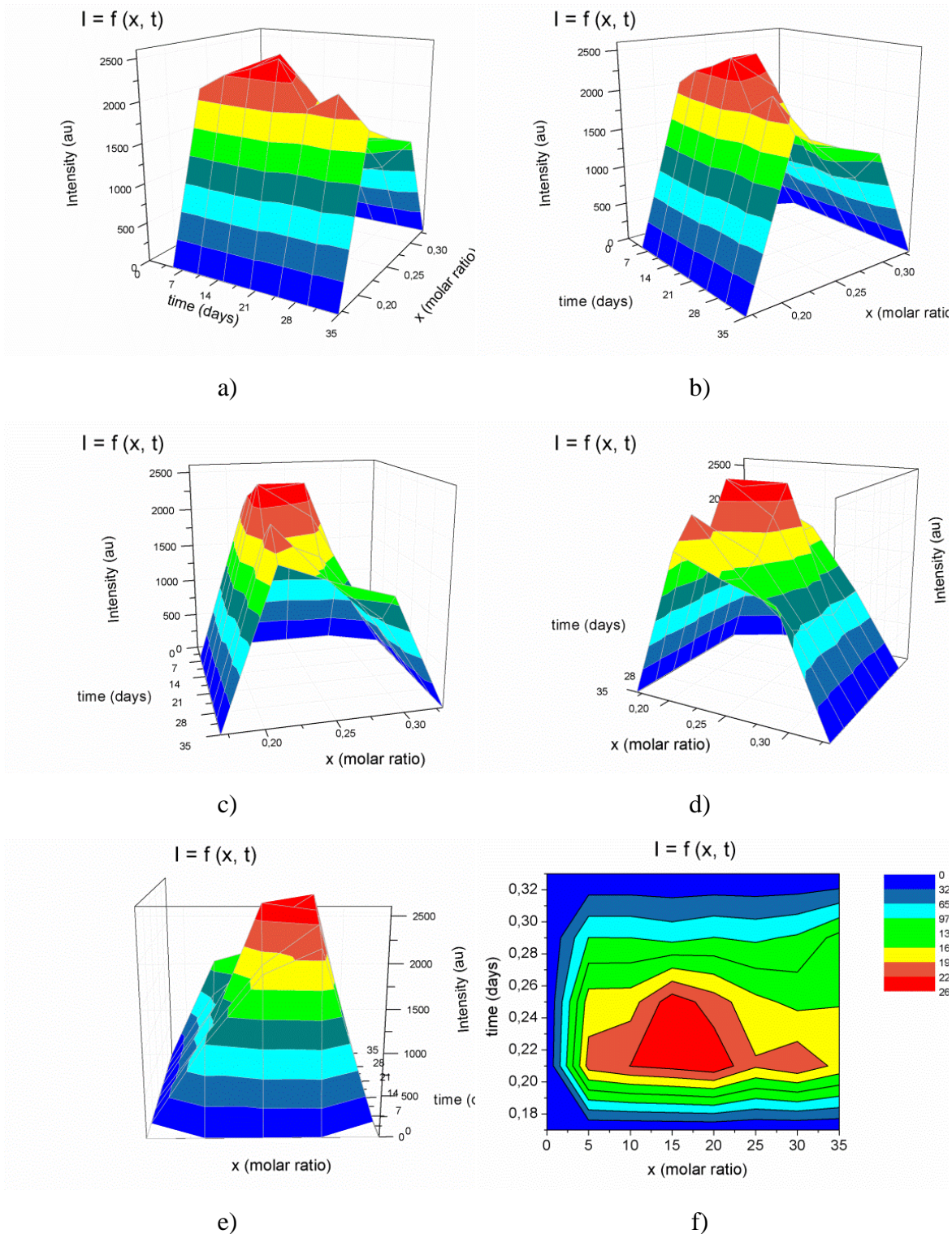
Thus the matrix of input data consisted of five lines, including the limits above explained, correspondent to molar ratios (0.17, 0.20, 0.25, 0.30 and 0.33) and eight times (0, 2, 4, 7, 14, 21, 28 and 35 days) to obtain the intensity function, $I = f(x,t)$, depending upon molar ratio and time.

Although it was found another phase in two of the 20 Series, it is possible to measure the crystallinity and affirm that it is just relative to hydrotalcite as the peak used was just the 003.

This fit function presents two presuppositions: the mass of all the samples analyzed were equal and the function measures the intensity of the “material” hydrotalcite. The second consideration means that the obtained hydrotalcite present a behavior of an engineering material with different chemical characteristic as the molar ratio changes. In a chemical view they are different compounds.

The graphics in Figure 5.10 shows a region of maximum crystallinity between 10 and 21 days and in-between 0.20 to 0.25 molar ratios. It is asymmetric with respect to the molar ratio with a tendency to be higher in regions near to values in 0.20 molar ratios. It is better visualized in the hypsometric surface by the very together lines in this region.

Figure 5.10 3D Surface Color Map (a, b, c, d, e) and hypsometric (f) for $I=f(x,t)$.



The crystallinity was statistically proof to be significantly greater in 20 Series than 25 Series and thereafter greater than 30 Series. Maybe the crystallinity

continues to grow or begins to decrease as the molar ratio decreases. Another synthesis need to be carried out to verify it.

Some functions were analyzed to fit the graphic: power, polynomial, Gauss, Lorentz and Rational, among others. The better adjust was found in a Rational function that presents the follow general equation:

$$z = \frac{z_0 + a_0x + b_0y + b_1y^2 + b_2y^3}{1 + a_1x + a_2x^2 + a_3x^3 + b_3y + b_4y^2} \quad 5.8$$

where the parameters z_0 , a_0 to a_3 and b_0 to b_4 depends upon the function fit and the parameters x and y .

The function to better represent the fit results can be shown in equation 5.9 and was obtained using the program Origin Pro 8.0. The parameters obtained for the fit are shown in Table 5.10 with a coefficient of determination R^2 , 88.96%. This result shows that it was a good fit of the data.

$$I(x,t) = \frac{I_0 + a_0t + b_0x + b_1x^2 + b_2x^3}{1 + a_1t + a_2t^2 + a_3t^3 + b_3x + b_4x^2} \quad 5.9$$

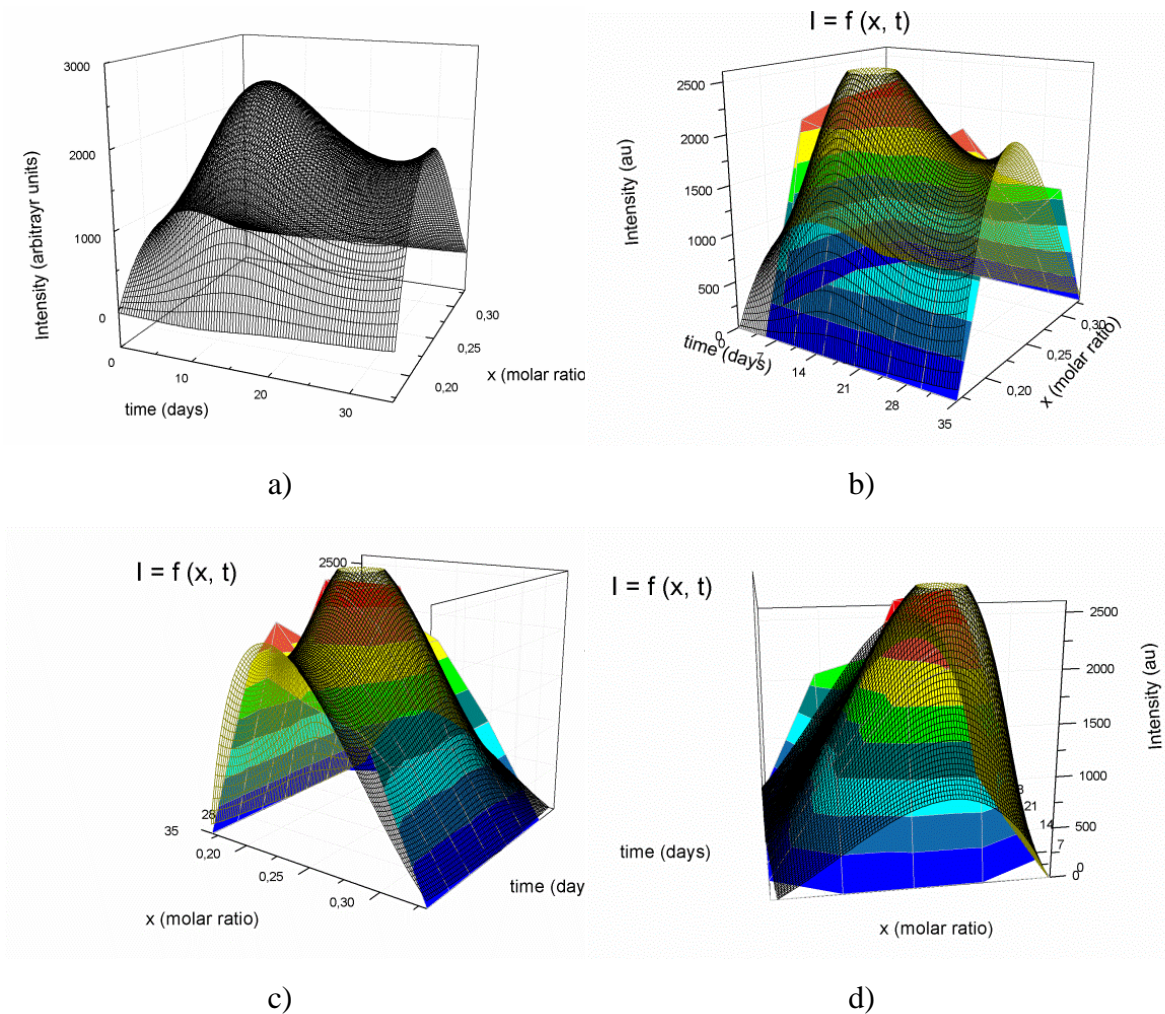
where I_0 is a constant related to initial intensity; the a_i parameters are associated with the time (t) and the b_i constants are related to the molar ratio variable (x).

Table 5.8 Parameters for the fit function.

I₀	a₀	a₁	a₂	a₃
-7.01x10 ⁴	7.33x10 ⁰	-3.81x10 ⁻¹	1.91x10 ⁻²	-2.79x10 ⁻⁴
b₀	b₁	b₂	b₃	b₄
8.01x10 ⁵	-2.84x10 ⁶	3.18x10 ⁶	1.66x10 ¹	-2.47x10 ¹

Figure 5.11 shows the rational function that better fitted the results in three different perspectives. There is a good fit in the regions limited by molar ratio next the extremes 0.17 and 0.33.

Figure 5.11 Function fit: Rational only (a) fit with $I = f(x, t)$ (b, c, d).



It is possible to observe in this figure (b and d) that the fit was not so good for the extremes with relation to the time. The rational function does not get zero in time zero and grow at long times differently that what is observed in the results obtained.

5.5.1 FIT Function possible applications

The proposed function in equation 5.9 can be used to preview the crystallinity of a LDH with others different molar ratio and time. For example, applying values $(x, t) = (0.27, 10)$ the Intensity $I(0.27, 10) = 1197$ counts; for $(x, t) = (0.32, 50)$ the intensity would be $I(0.32, 50) = 11$ counts; and a value next to low extreme molar ratio $(x, t) = (0.21, 10)$, $I(0.21, 10) = 2389$ counts.

We could preview for a fixed molar ratio, like 0.20, 0.25 and 0.30, and calculate how much time the crystallinity would get zero: in 43, 45 and 44 days, respectively.

According to SHARMA and co-workers (2007) crystallinity is associated with particles size, or rather, high crystallinity mean large particles and the opposite is true, low crystallinity would mean small particles. For a specific application like adsorption, it is known that larger particle implies in low values of specific surface area. Thus the better hydrotalcite would be synthesized with molar ratio close to 0.30 and in initial times after synthesis or in times next to 44 days of aging.

Some LDH and hydrotalcite are used as biomaterials and one of the possible applications is the intercalation of drugs to be controlled their releasing in the body. The intercalation occurs in the lamellae, so it is necessary the maximum crystallinity to retain the drugs inside (CUNHA et alli, 2009).

It was seen in previous chapter that some parameters are important in LDH textural characteristics: obtaining method, M^{+2} and M^{3+} nature and ratio, the interlamellar anion, pH synthesis and temperature, aging time, temperature of aging, reagent concentration, speed reagent addition (CARJA et alli, 2001; OH et alli, 2002; NODA PEREZ et alli, 2004; SHARMA et alli, 2007; HOSNI and SRASRA, 2009; SAIAH et alli, 2009; BERBER et alli, 2013).

The obtaining methods also play an important role in this characteristics: co-precipitation at variable pH (NODA PEREZ et alli, 2004; KOVANDA et alli, 2005; SHARMA et alli, 2007; KOVANDA et alli, 2009;) and co-precipitation at constant pH (NODA PEREZ et alli, 2004; KUSTROWSKI et alli, 2005); urea procedure (BENITO et alli, 2008; MEIS, 2010) and reconstruction method (LI et alli, 2010; CHANG^a et alli, 2011).

LDH industrial applications depend on their textural properties, crystallinity, particle size distribution, surface area and porosity (OH et alli, 2002; NODA PÉREZ et alli, 2004; BENITO at alli, 2010). These characteristics have been studied for some authors to try to find a synthesis path that could give specific properties to LDH obtained (OH et alli, 2002; BRAVO-SUAREZ et alli, 2004; SHARMA et alli, 2007; SAIAH et alli, 2009; BENITO at alli, 2010; BERBER et alli, 2013). However, none of them has proposed a path to this kind of synthesis or a function to predict these properties as it was proposed in this work.

The obtained rational fit function is restricted only to the initial and temporal conditions studied in this research: co-precipitation method, ions Mg^{+2} , Al^{+3} and CO_3^{-2} , temperature and pH synthesis. However it can be seen as the beginning of a study to get more complex function that could preview textural properties using the other synthesis parameters and procedures.

5.6 The non-Expected Brucite

Figure 5.12 shows the XRDP for the samples 20 Mg-Al 28 (a) and 20 Mg-Al 35 (b). The presence of brucite is confirmed by the peaks observed: 001, 101, 102 and 110. Table 5.9 shows the cell parameters and the crystallite size obtained through their refinement.

Table 5.9 Cell parameters and crystallite size for the samples with brucite.

Samples	Cell parameters		Crystallite size			
	<i>a</i>	<i>c</i>	D_{001}	D_{101}	D_{102}	D_{110}
	nm					
20 Mg-Al 28	0.314	0.483	14.7 ± 0.2	15.2 ± 0.2	15.9 ± 0.3	16.4 ± 0.3
20 Mg-Al 35	0.317	0.482	55.0 ± 1.2	19.4 ± 0.3	7.9 ± 0.1	5.9 ± 0.1
Brucite*	0.313	0.475	-	-	-	-

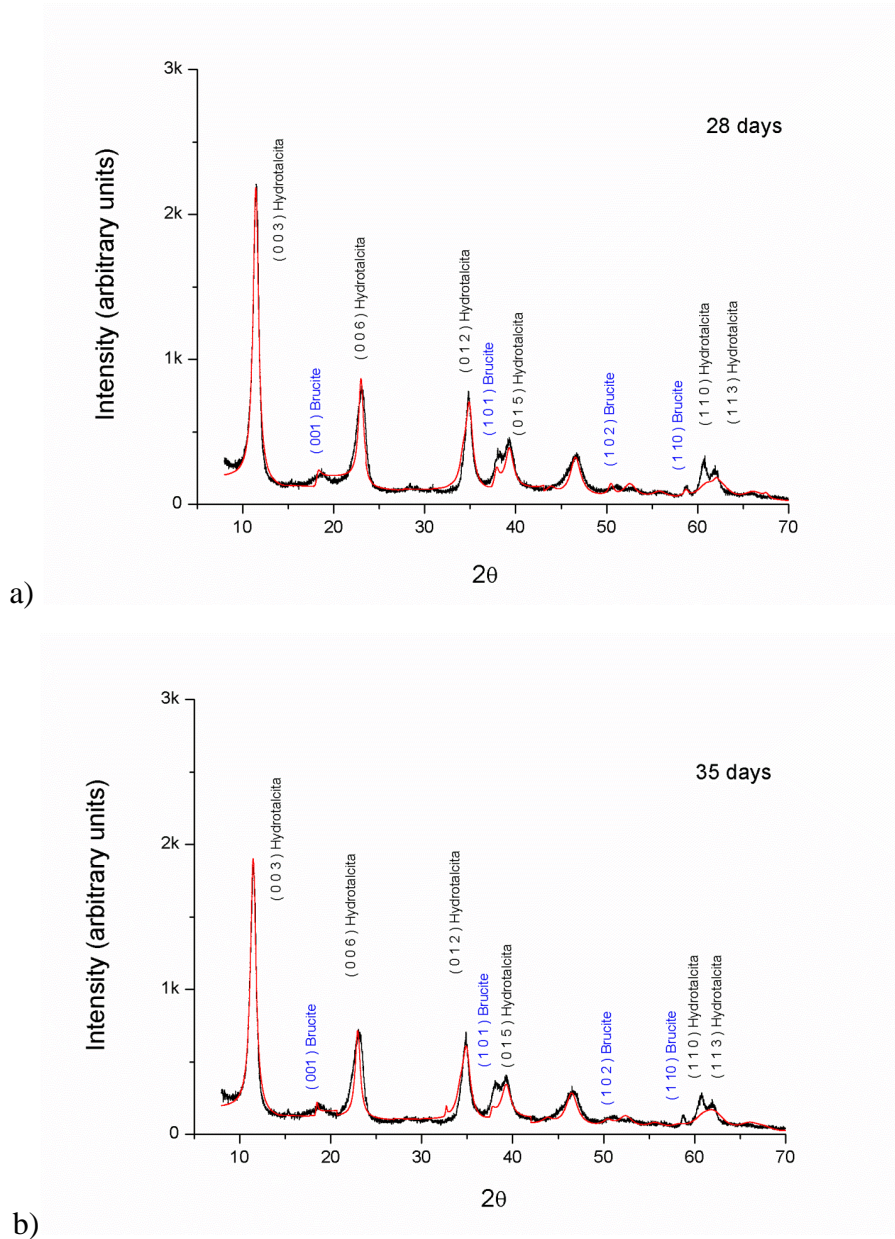
The results with (*) are from HANAWALT et alli (1938). Brucite has a hexagonal crystal system and belongs to a space group P-3m1, number 164. The cell parameters from the samples present little differences between them and the reference.

The crystallite size showed great differences mainly in planes 001. D_{001} for 20 Mg-Al 35 is 3.7 greater than the 20 Mg-Al 28. The crystallite size for the four planes showed values with some proximity for the 20 Mg-Al 28, the mean 15.6 nm and the standard deviation just 0.75 nm whereas for the 20 Mg-Al 35 the mean was 22.1 nm and standard deviation 22.76 nm.

The mass percentage of brucite in 20 Mg-Al 28 was 10.94% whereas for 20 Mg-Al 35 was just 1.85%. These results are not expected as the mentioned literature affirms that with the molar ratio 0.20 it would be obtained just pure LDH (CAVANI et

alli, 1991; ALEJANDRE et alli, 1999; FERREIRA, 2001; NODA PÉREZ et alli, 2004; CHANG et alli, 2005; RODRIGUES, 2007; SILVA, 2008; PÉREZ et alli, 2009).

Figure 5.12 XRD samples with brucite: 20 Mg-Al 28 (a) and 20 Mg-Al 35 (b).



It is important to highlight that the arise of the non-expected brucite appear to be related with hydrothermal treatment aging, so the system probably is changing their structure, crystallinity and phases.

6 THERMOGRAVIMETRY, INFRA-RED AND MICROGRAPHY

The results in this chapter are discussed in the sequence of the title and it is carried out a comparison among the three molar ratios groups. They complete the informations necessary to make conclusions about the samples studied in this research.

All the thermo gravimetric and infra-red analysis was shown in this chapter but just some micrograph was chosen to present as the results are very similar and in some cases not conclusive.

6.1 Thermo Gravimetric Analysis

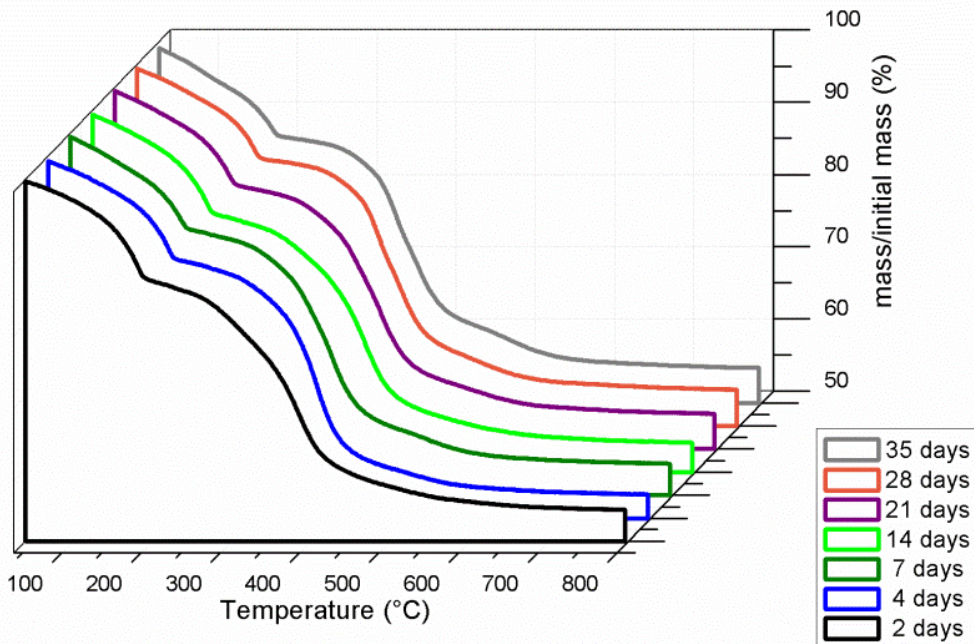
Figures 6.1, 6.2 and 6.3 shows the thermo gravimetric analyses of the 20, 25 and 30 Series and their first derivative. Thermo gravimetric plots show two distinct stages of mass loss through LDH structure decomposition. The first one corresponds to the loss of the physically adsorbed and the interlayer water. The second stage is associated with the dehydroxylation, carbonate decomposition and consequent collapse of the lamellar structure yielding the formation of magnesium and aluminum oxides. Similar results are found in literature (FERREIRA, 2001; NODA PÉREZ et alli, 2004; CHANG et alli, 2005; RODRIGUES, 2007; SILVA, 2008; PÉREZ et alli, 2009; AGUIAR et alli, 2012; LIMA et alli, 2012).

Thermal decomposition patterns depend on their interlayer anion and the energy between the bonds of the structure analyzed (BENITO et alli, 2010). Thus their evaluation can give us the indication of the possible structure formed in the synthesis and under the period of ageing established in the research.

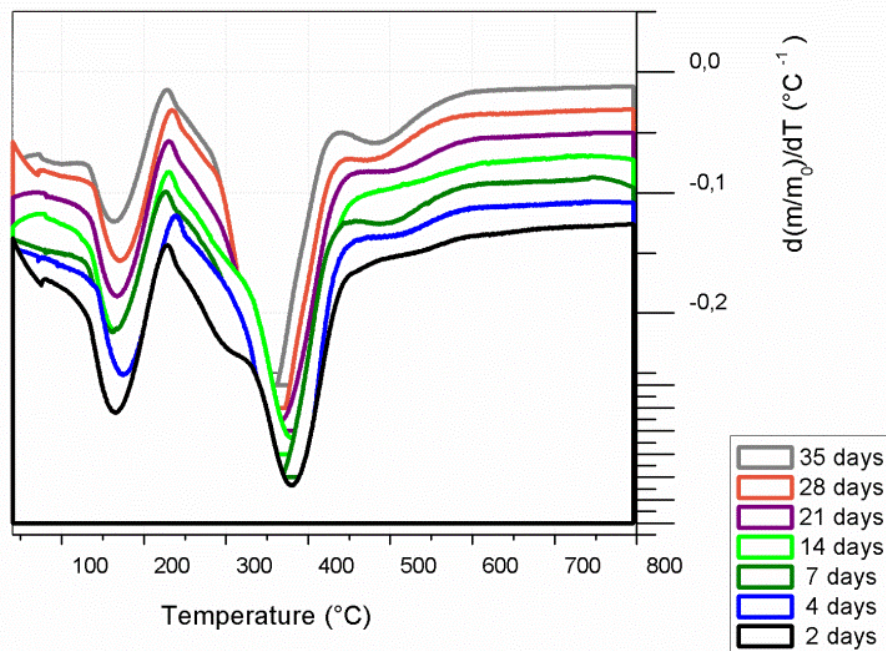
Thermo gravimetric analyses of the 20, 25 and 30 Series are shown in perspective as the same sequence that was shown the XRD. The shape of the three curves is similar for the three series, but is evident that the mass loss above 700 °C is more pronounced in the 30 Series.

Derivative of TG shows two peaks that indicate the beginning of the stages. However the position of minima depends upon the composition of the interlayer anion and the lamellar structure (BENITO et alli, 2006). Thus the values of the temperature and the percentage of final mass were identified and allocated in Table 6.1 and 6.2 correspondents to the first and second stages, respectively. These tables show the mean (\bar{x}), standard deviation (s) and the Pearson Coefficient of Variation (CV).

Figure 6.1 Thermo Gravimetric (a) and derivative (b) for the 20 Series.

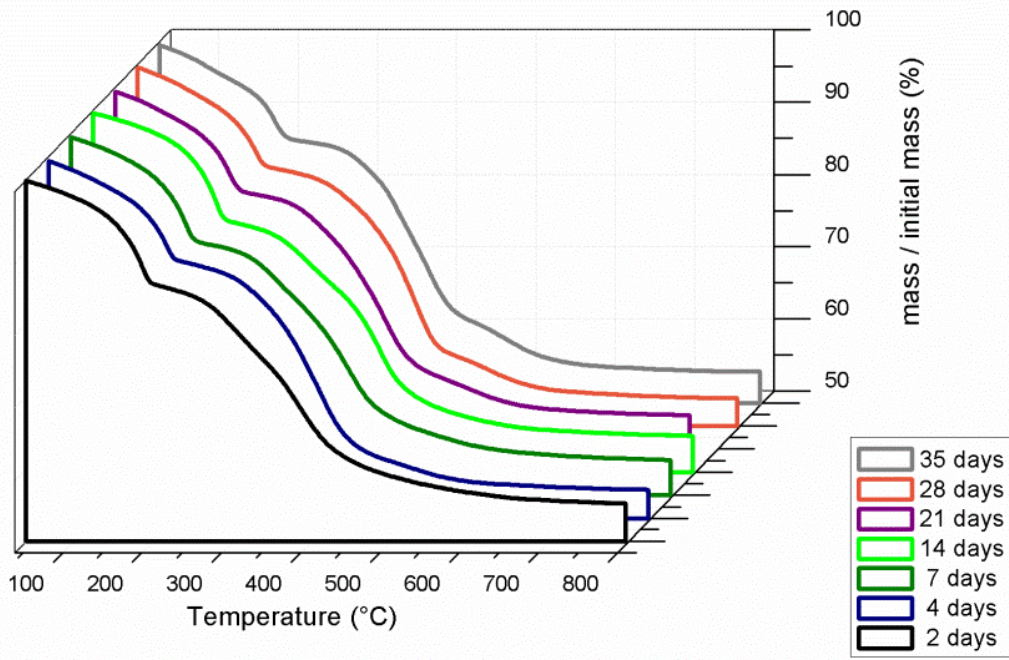


a)

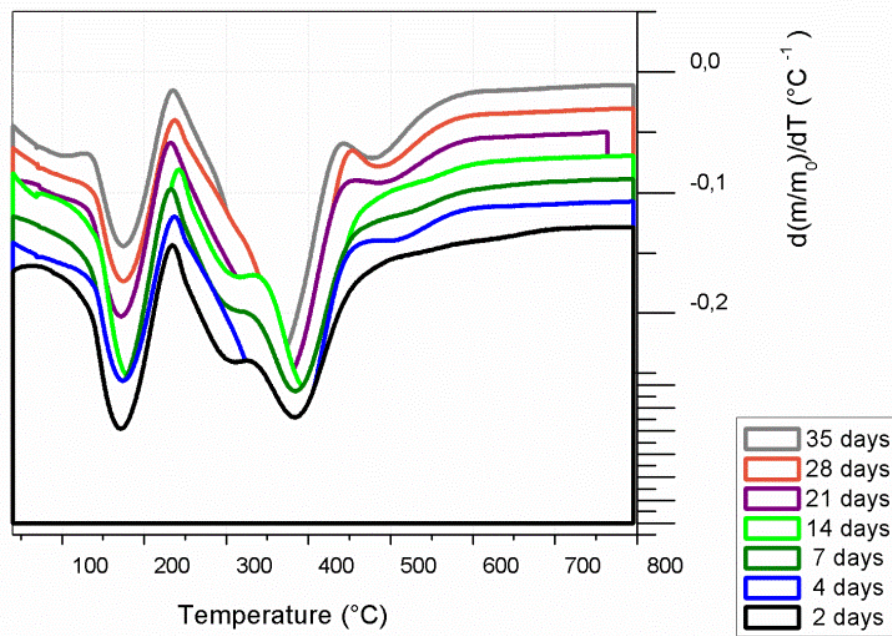


b)

Figure 6.2 Thermo Gravimetric (a) and derivative (b) for the 25 Series.

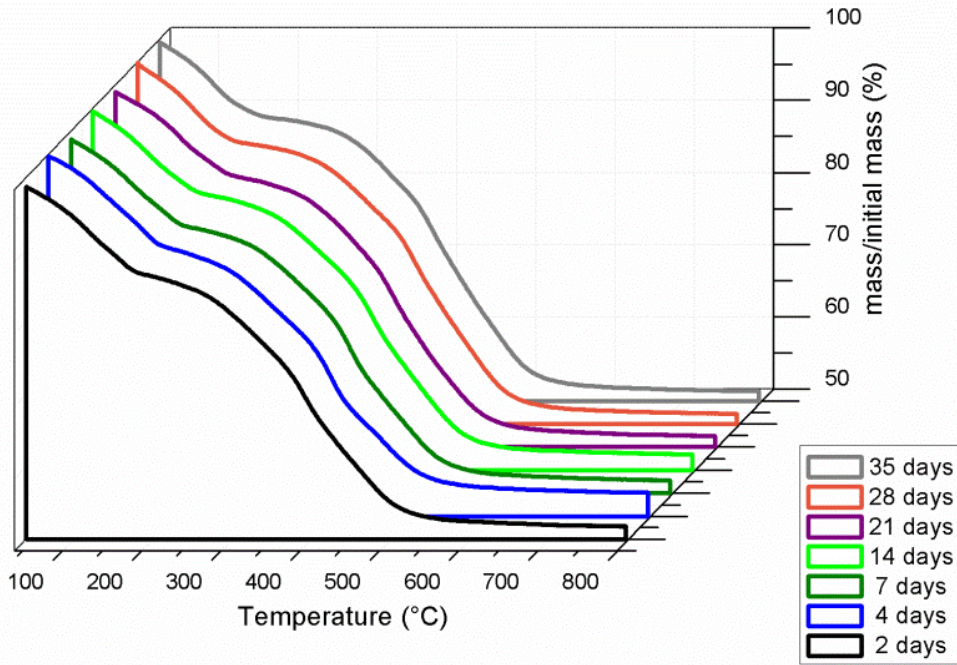


a)

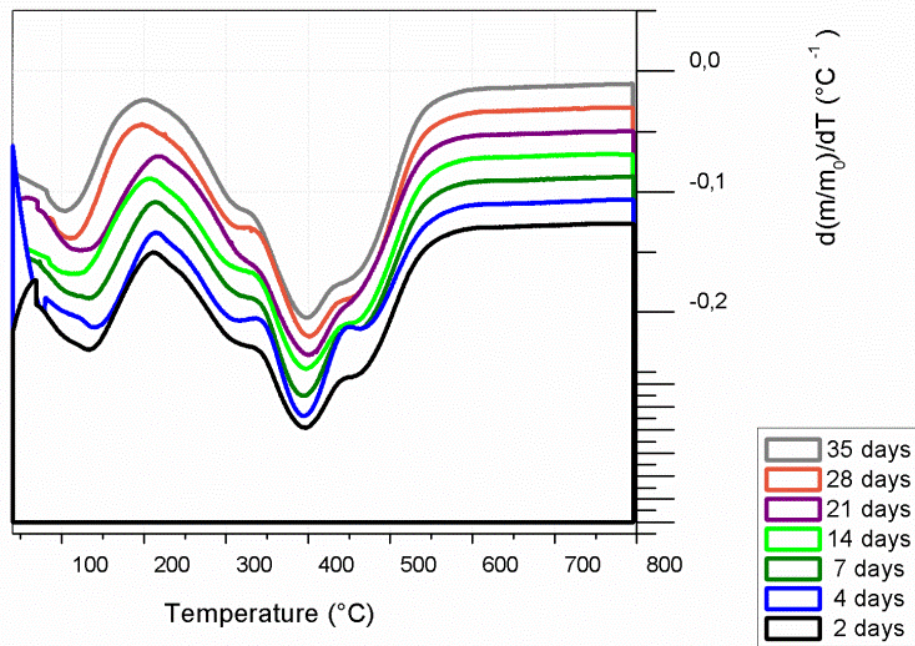


b)

Figure 6.3 Thermo Gravimetric (a) and derivative (b) for the 30 Series.



a)



b)

Table 6.1 shows the results for the beginning of the first stage and it ranged from 163.0 to 176.7 °C for the 20 Series, the mean was 167.6 °C and for the 25 Series the range was 171.0 to 181.2 and a mean of 174.0 °C. The mean for the 25 Series is greater than the 20 Series for almost 6.5 °C with the same result for the mass loss. Thus it was more difficult to begin the first stage to the 25 Series. It was necessary to give more energy to begin the loss of the physically adsorbed and the interlayer water.

Thus this fact can be explained and correlated to the XRD results the 25 Series present more charge in their lamellae, evidenced for the *c* cell parameter that were less than 20 Series. It means that there exist more electrostatic attraction between the lamellae and the interlayer anion causing a difficulty of the interlayer water to be expelled.

Table 6.1 Mass loss in the first stage.

Time	Molar ratio (x)					
	0.20		0.25		0.30	
	T (°C)	m/m ₀ (%)	T (°C)	m/m ₀ (%)	T (°C)	m/m ₀ (%)
2	165.5	91.2	171.4	91.2	133.2	91.1
4	176.7	90.2	173.9	90.6	138.9	91.7
7	163.0	90.8	171.0	90.6	132.6	91.2
14	166.1	90.6	181.2	90.7	115.6	93.1
21	167.3	90.8	171.8	90.5	122.7	92.7
28	171.4	91.1	174.5	90.6	110.3	93.6
35	163.0	90.7	174.5	90.9	103.7	94.3
\bar{x}	167.6	90.8	174.0	90.7	122.4	92.5
s	4.9	0.3	3.5	0.2	13.1	1.2
CV (%)	3.0	0.4	2.0	0.3	10.7	1.3

On the other hand the 30 Series show a difference approximately in 1.7% less mass loss in the first stage than the other two series. However, the major difference is in the beginning of the first stage with a mean of 122.4 °C. This means that there are 45 and 51 °C (in round numbers) of difference between the 20 and 25 Series, respectively.

The derivative of this 30 Series, showed in Figure 6.3 b, present less definition in its first peak, differently from the other two series that are sharper. If we compare the three peaks, the third one, looks more like a shoulder and may be an evidence of a weakly held water in the LDH structure. Maybe there is another phase not identified in this series by the XRD that could present a structure easier to be broken.

There is another remark to highlight, the statistical parameters for the 30 Series. The standard deviation for the mass loss is 3.7 and 5.1 greater than the 25 and 20 Series, respectively, and greater results also happen for the temperature. Combining the standard deviation with the mean, the Pearson Coefficient of Variation shows that for the temperature of the beginning of the first stage for the 30 Series is much more dispersive than the others; more than 10% is considered a medium dispersive data where the others are classified as low dispersive one.

Table 6.2 shows results for the beginning of the second stage. The first consideration is about the mass loss that presents almost the same results. The greatest difference is about 1.3% between 20 and 25 Series. It was found a growing in the temperature of this stage as the molar ratio increases. NODA PÉREZ et alli (2004) found similar results to hydrotalcite at pH 13 of synthesis for the molar ratios 0.20, 0.25 and 0.33.

Table 6.2 Mass loss in the second stage.

Time	Molar ratio (x)					
	0.20		0.25		0.30	
	T (°C)	m/m ₀ (%)	T (°C)	m/m ₀ (%)	T (°C)	m/m ₀ (%)
2	380.3	68.6	383.8	68.7	397.7	68.5
4	376.4	69.2	374.2	69.2	394.4	69.6
7	362.1	71.2	384.2	68.5	394.4	69.6
14	380.7	68.6	396.7	67.9	398.1	70.0
21	366.0	71.2	371.6	69.7	400.2	69.0
28	359.5	72.3	382.6	69.2	401.2	70.1
35	351.1	72.5	364.0	71.6	398.3	70.8
\bar{x}	368.0	70.5	379.6	69.3	397.8	69.7
s	11.4	1.7	10.6	1.2	2.6	0.8
CV (%)	3.1	2.4	2.8	1.7	0.7	1.1

The temperature difference between 25 and 20 Series is 11.6 °C whereas the difference between 25 and 30 Series is 18.2 °C. The difference from the first stage to the second stage is 200.4, 205.6 and 275.3 °C, respectively for the 20, 25 and 30 Series.

Any of the three series studied by NODA PÉREZ et alii (2004) showed so great difference as the 30 Series. They found a 193 °C difference between the two stages in a 0.20 molar ratio with pH 10 of synthesis. It is important to underline that the first stage for the 30 Series was very low, increasing this range. Their sample showed another phase beside the hydrotalcite, the hydromagnesite ($4\text{MgCO}_3 \cdot \text{Mg}(\text{OH})_2 \cdot 4\text{H}_2\text{O}$). However they just pointed the phases in their XRD pattern. They did not present the amount of this phase that could help in finding a relation with its decomposition with temperature. On the other hand their DTA showed a third peak at 517 °C evidencing this phase.

The growing in temperature and in the difference from the stages may be due to the fact that the lamellae are more electrostatically attracted as the molar ratio increases. All of the series showed low values for CV and the data shows that the 30 Series presented the lowest values for CV for temperature and mass loss.

Finally we can conclude that the 30 Series probably present another different phase than what was shown in their pattern. Thus if it is true this possible phase must to be an amorphous phase. Let us analyze the infra-red to try to make this conclusion.

6.2 Infra-Red Spectroscopy

The infra-red spectra for all the samples are shown in Figures 6.4, 6.5 and 6.6 respectively for the 20, 25 and 30 Series.

All the series present the same common hydrotalcite infra-red profiles with some slight variations in some peaks positions. There is a broad band near 3460 cm^{-1} associated to the hydroxyls stretching; another well-defined peak at $1380\text{-}1385\text{ cm}^{-1}$ showing the presence of carbonate, and peaks from $400\text{ to }1000\text{ cm}^{-1}$ indicating region that there are some bands related to the oxygen metal bond vibration, (Mg-O e Al-O) (CAVANI et al, 1991; CORNEJO et alii, 2000; KLOPROGGE et alii 2004; REIS, 2004; SILVÉRIO, 2004; BENITO et alii, 2006; RODRIGUES, 2007; SILVÉRIO et alii, 2008).

Figure 6.4 Infra-Red for 20 Series samples.

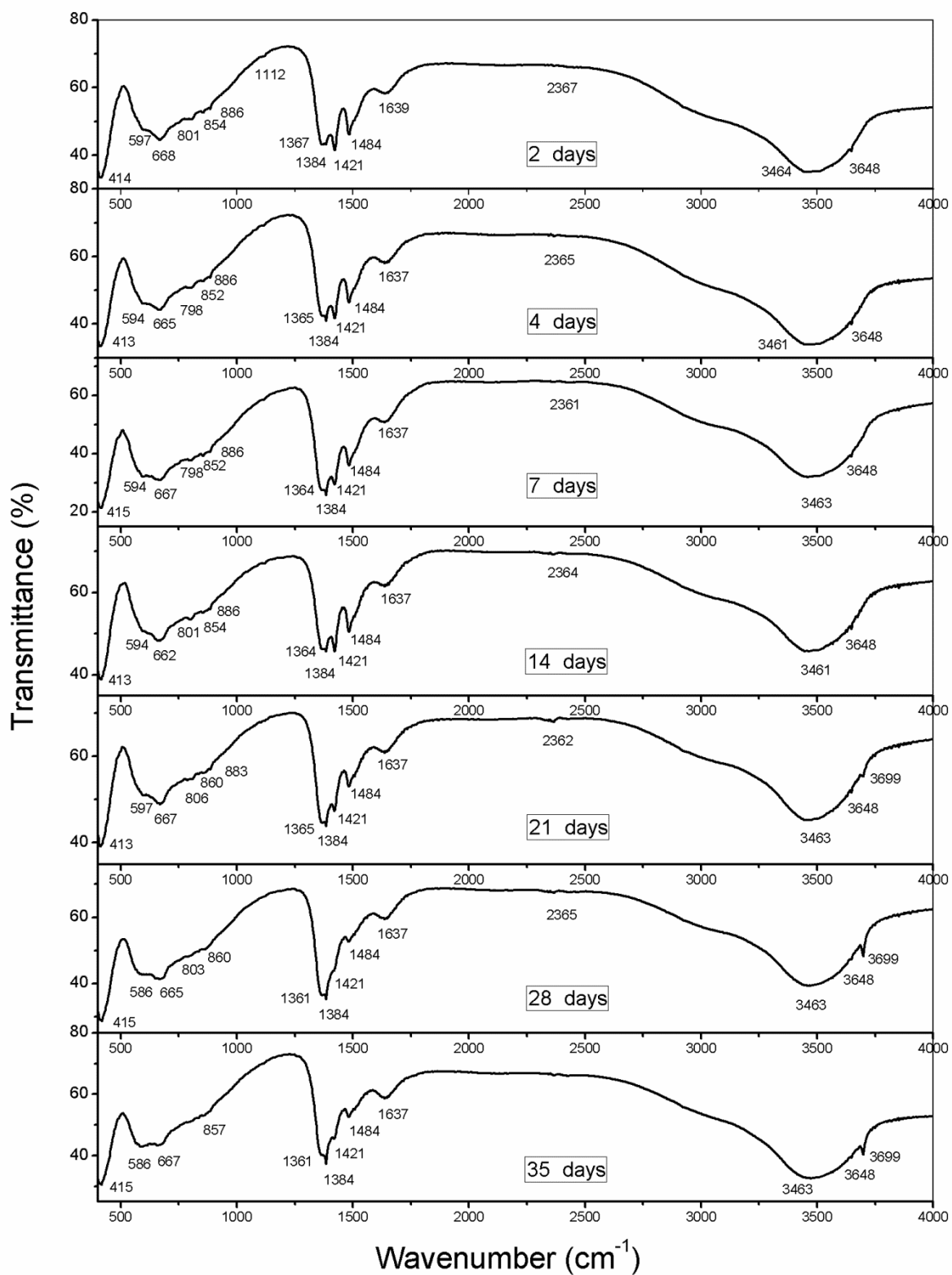


Figure 6.5 Infra-Red for 25 Series samples.

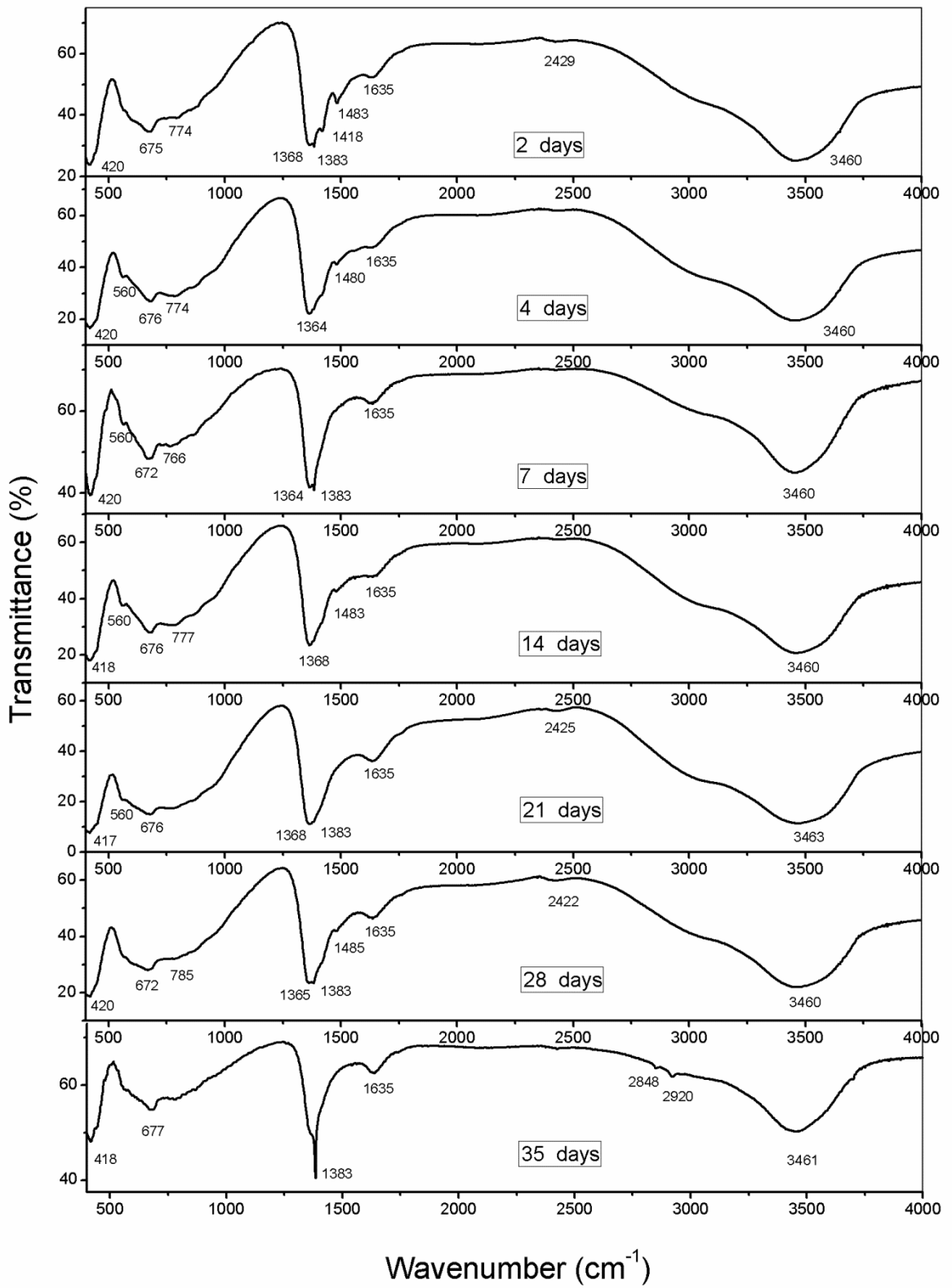


Figure 6.6 Infra-Red for 30 Series samples.

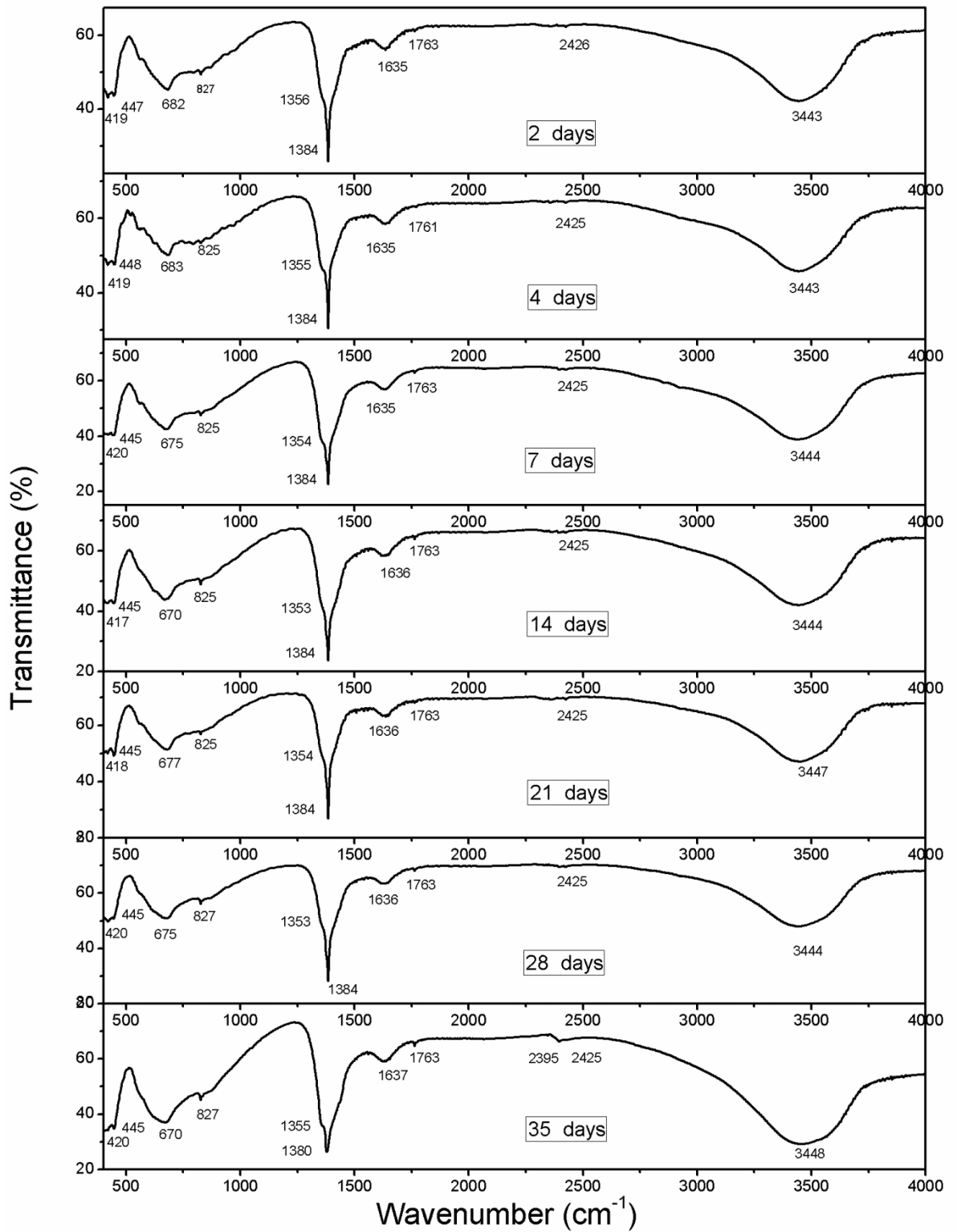


Figure 6.4 shows the 20 Series samples where it can be seen a more pronounced and sharp peaks in the region between 1360 cm^{-1} to 1640 cm^{-1} than the other series. The peak at 1637 and 1639 cm^{-1} is related to the bending of water molecules (BENITO et alli, 2006) and this peak is present in all the other samples with a slight difference. Two peaks at 1421 and 1484 cm^{-1} appears in all this 20 Series and a double band or a split at 1384 cm^{-1} .

These peaks are attributed to a lowering of the symmetry of the carbonate and to the disorder in the interlayer (CAVANI et alli, 1991). The split and a little peak in the same region were observed in a hydrotalcite-like compound by ÁLVAREZ et alli (2013). The same peaks can be observed in the 25 Mg-Al 2 and a split in 25 Mg-Al 7. As the carbonate is more free in the 20 Series than the others, this may cause another possibility of vibration or stretching in their bonds that is not possible in the other series.

The samples 20 Mg-Al 28 and 35 presented vibration band at 3699 cm^{-1} that correspond to a stretching in the hydroxyl from brucite (FROST and KLOPROGGE, 1999). This result reinforces the presence of brucite showed in XRD. The 20 Mg-Al 21 also shows this band with a low intensity and these samples did not show the correspondent peaks in XRDP. The segregation of brucite from the lamellae is probably favored by aging.

The 30 Series did not show any split in its bands as the others did and there were a broad in the band correspondent to the OH stretching in the interlayer water molecules at 3444 to 3448 cm^{-1} (BENITO et alli, 2006). Furthermore, this band was shifted about 15 cm^{-1} compared to the others series.

6.3 Scanning Electronic Microscopy and Energy Dispersive Spectroscopy

The Scanning Electronic Microscopy (SEM) and Energy Dispersive Spectroscopy (EDS) were carried out in two samples of 20 and 25 Series and in five samples of 25 Series. The EDS gave a qualitative distribution of the constituents through the element map that were shown for the seven samples.

6.3.1 Micrographs and EDS for the 20 Series

The scanning electron micrograph of the samples obtained from the 20 Series (Figure 6.7) indicates that the hydrotalcite are formed by particles without a defined shape and with an irregular surface.

Figure 6.7 Micrographs: (a) 20Mg-Al 4 (b) 20Mg-Al 35

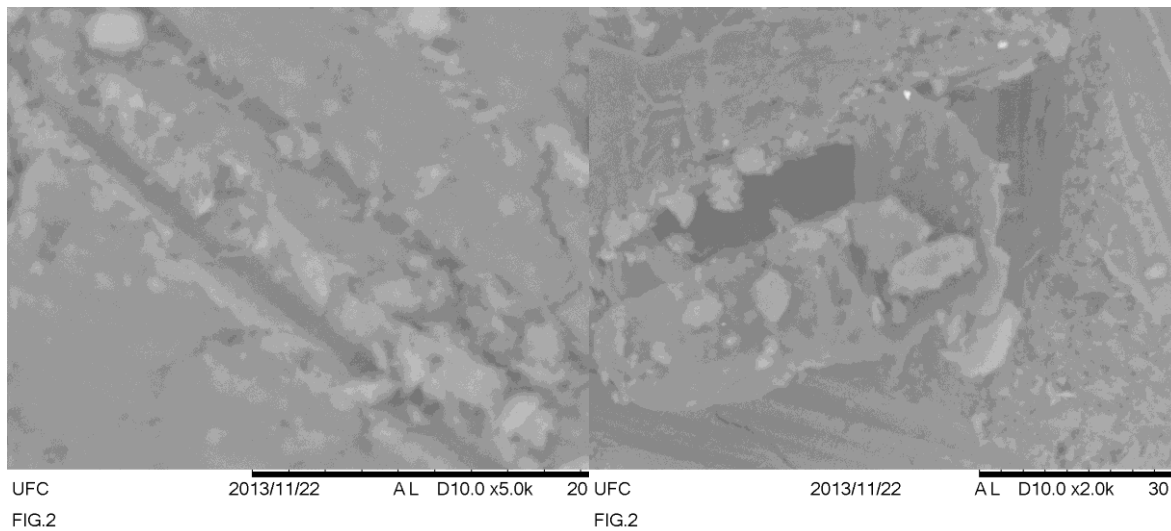
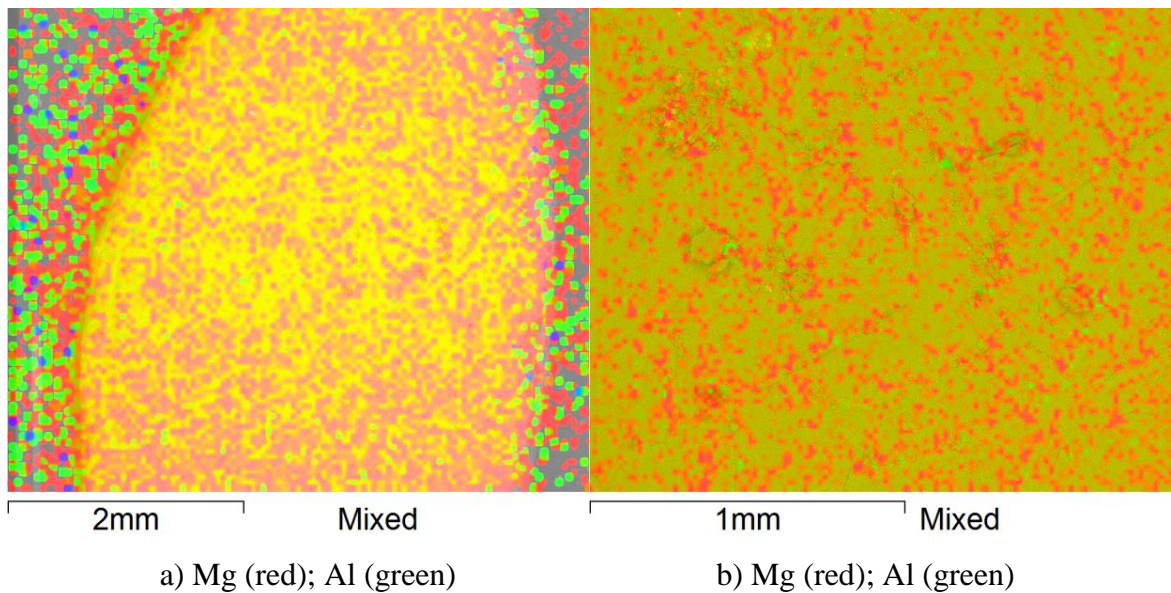


Figure 6.8 Element maps for: a) 20 Mg-Al 4 and b) 20 Mg-Al 35



The obtained results from EDS for the two samples showed a molar ratio of 0.19 for the 20Mg-Al 4 and 0.20 for 20Mg-Al 35. Although there is a dispersion of the values measured by EDS the molar ratio for these series is confirmed. The magnification is 5,000 x in the first sample and 2,000 x in the second sample.

Figure 6.8 shows the element maps for the samples a) 20 Mg-Al 4 and b) 20 Mg-Al 35. They show a quite homogenous distribution of the elements magnesium and aluminum in the two samples analyzed with four and thirty five days of aging.

6.3.2 Micrographs and EDS for the 25 Series

Figure 6.9 Micrographs: a) 25Mg-Al 4; b) 25Mg-Al 14; c) 25Mg-Al 21; d) 25Mg-Al 28.

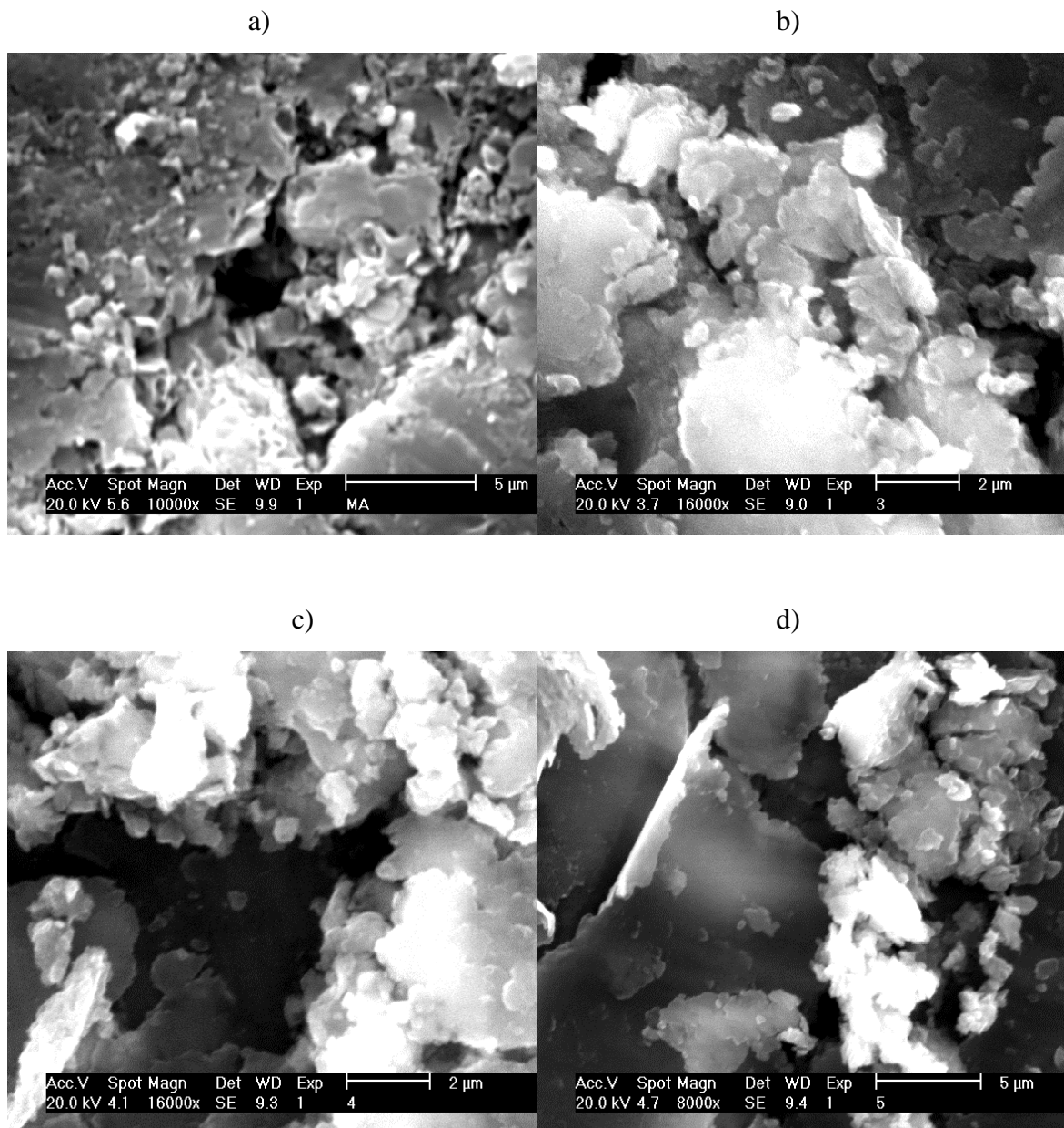


Figure 6.9 shows the micrographs for some samples of the 25 Series with different magnification, 8,000; 10,000 and 16,000 x.

It can be seen that all the hydrotalcite samples are formed by imperfect laminar particles without a well-defined shape. Furthermore the laminar particles may have been formed by the process of grinding by the mortar.

Apparently there are no significant differences between the samples related to their shape. None of the samples showed hexagonal shapes in their particles.

Figure 6.10 Micrographs for 25 Mg Al 4 sample without grinding. Magnification: a) 800 x; b) 1,000 x; c) 2,000 x; d) 5,000 x

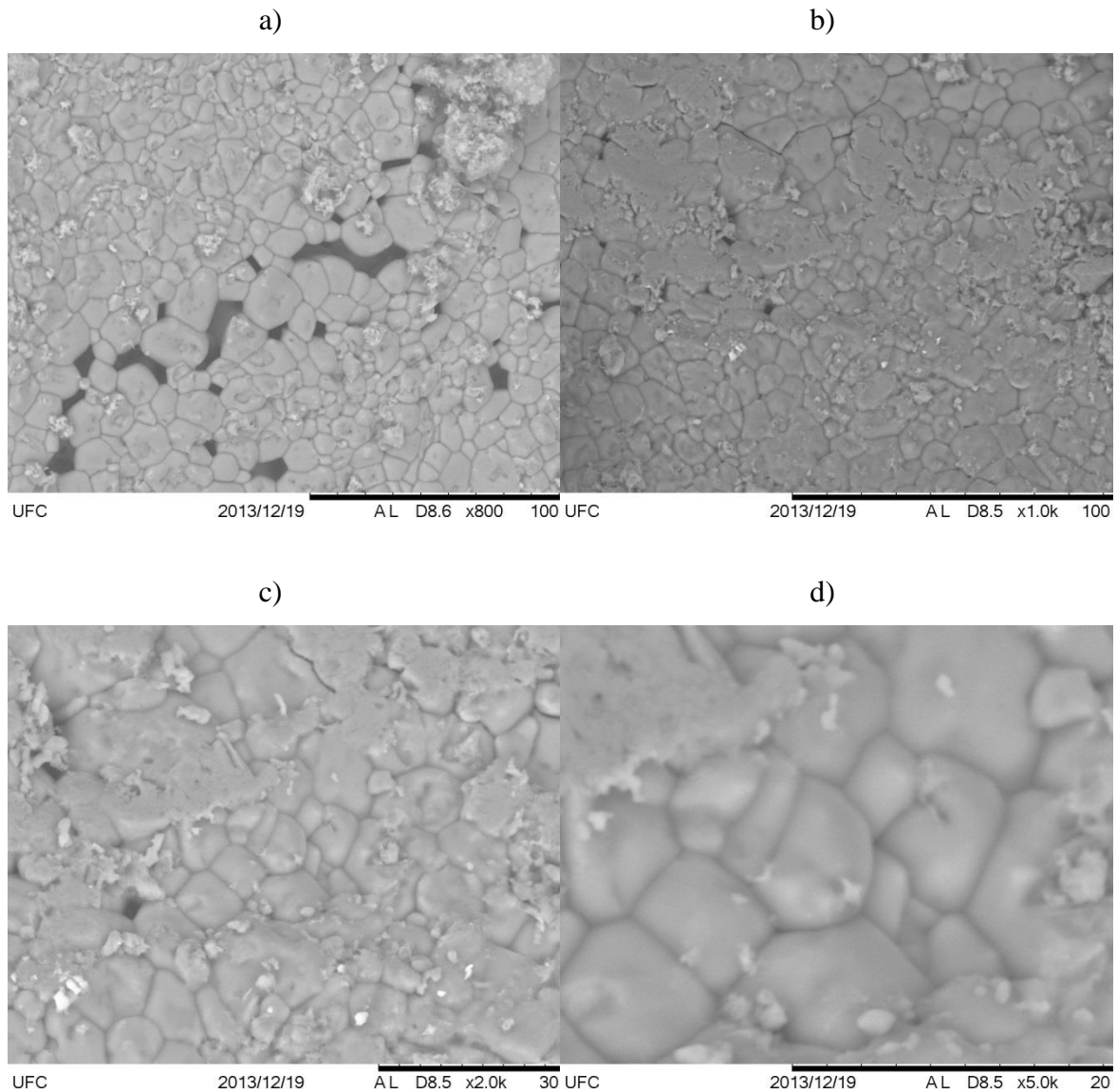


Figure 6.10 shows different magnifications for the scanning electron micrographs from the non-ground 25 Mg Al 4 sample; these images show that the hydrotalcite are formed by irregular particles with different sizes. It can be observed that the particles are very different from the others that were ground.

They present a non-uniform shape with length and width approximately the same dimension for the majority of them.

There are some holes together forming a track in Figure 6.10 (a) that permit to see the depth of some particles and conclude that they are differently from the other samples that present plate-like shape. It was not possible identify any particle with a hexagonal-shaped in all the samples, neither in the ground samples, nor in the non-ground samples.

Probably the temperature of synthesis and hydrothermal treatment are the major responsible for the crystal growth. SHARMA et alli (2007) carried out a research with hydrotalcite in different aging and at 110 °C they did not find a well-defined and hexagonal-shaped crystal whereas BENITO et alli (2006) synthesized hydrotalcite with temperature of aging 125 °C and they identified particles with a hexagonal shape. In both works similar procedure of synthesis were used.

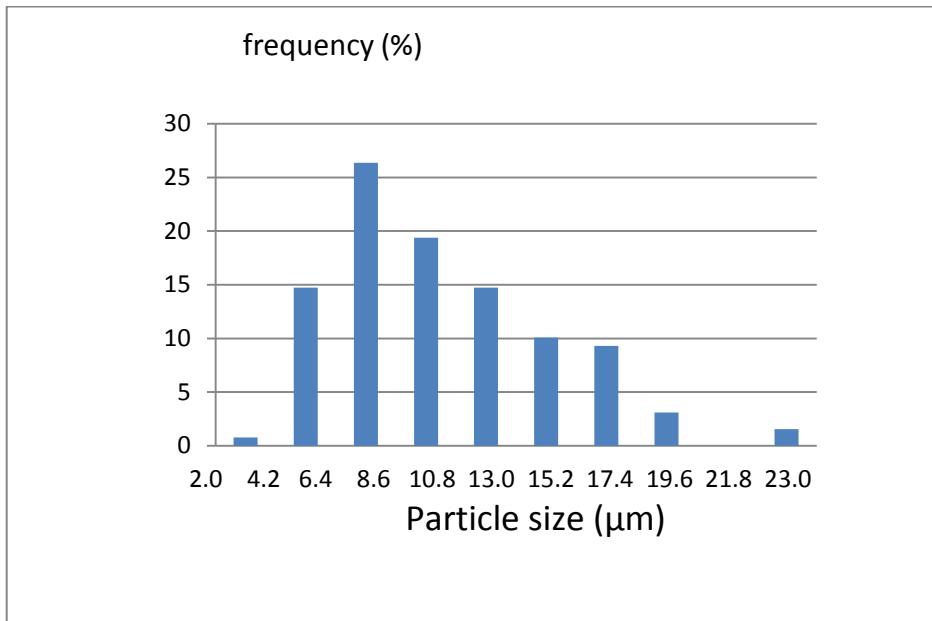
SAIAH et alli (2009) synthesized a hydrotalcite-like compound with nickel and iron and aged them in different temperatures, 100, 120, 140, 160, and 180 °C. They have found a better crystallinity and very well defined hexagonal-shaped particles as the temperature of aging was increased.

The procedure used in this research, described in chapter 4 Material and Methods, follows some authors (VILLANUEVA, 2000 and 2005; SILVÉRIO, 2004; RODRIGUES, 2007) that includes the grinding of the obtained LDH after synthesis. Thus this process of comminution is probably the responsible for the obtained flake-like shape of LDH.

The particles width displayed in the Figure 6.10 were measured with an appropriate program Image J. The measures were done in Figure 6.10 (a) just in the horizontal direction for approximately 120 particles. Figure 6.11 shows a histogram for the distribution.

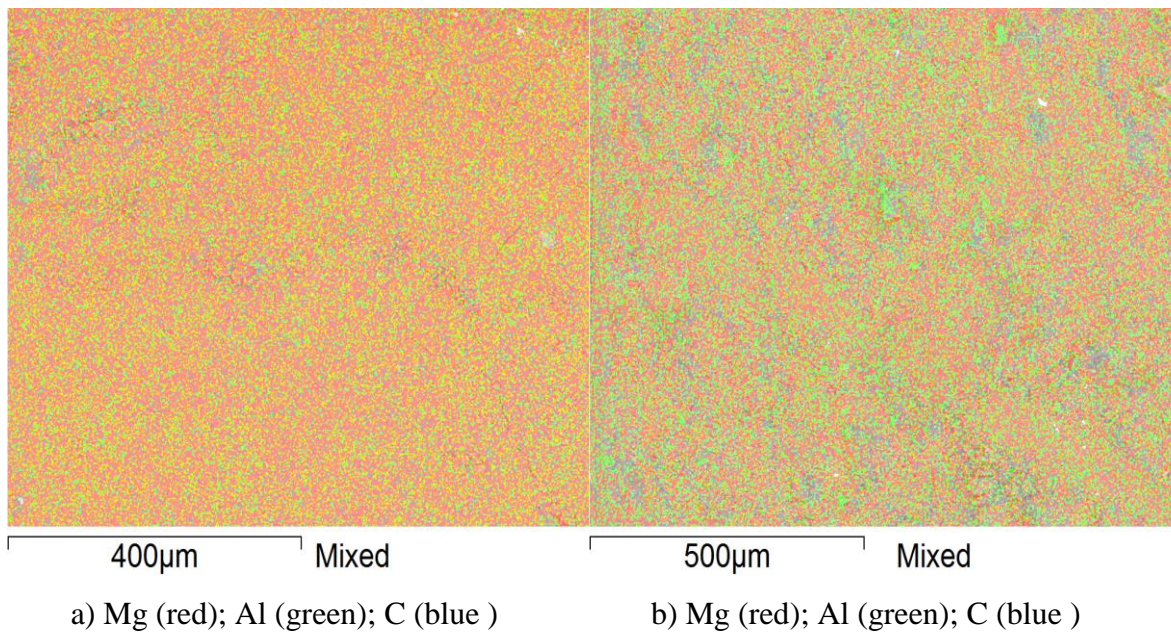
The distribution of particle size in the non-ground four days aging sample of the 25 Series shows result of approximately 25 % of the particles present a size between 6.4 and 8.6 μm and almost 60% of the particles are below 10.8 μm .

Figure 6.11 Distribution of particle size in the not ground sample 25 Mg-Al 4.



The element maps for two non-ground samples are in Figure 6.12 and they show a homogenous distribution of the elements magnesium and aluminum in both samples analyzed with four and thirty five days of aging. There are also some narrow regions of blue colors in both samples evidencing a high concentration of carbon element. Apparently it is more pronounced in the 35 days aging sample.

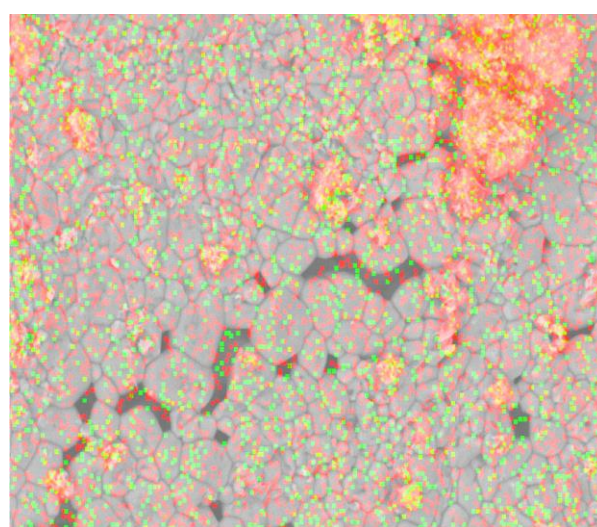
Figure 6.12 Element maps for: a) 25 Mg-Al 4 and b) 25 Mg-Al 35



Element map for the non-ground 4 days aging sample is shown in Figure 6.13. The sample shows reddish regions that indicate an elevated concentration of magnesium. EDS indicated, in this region, a molar proportion of 5.1 Mg:Al and a consequent molar ratio 0.16. The ground samples showed a 0.26 molar ratio, obtained from a mean of 0.27 and 0.25, respectively for 25 Mg-Al 4 and 35.

The surface of these reddish regions is greater than the other ones in the non-ground samples; the grinding can be responsible for the quite homogenous distribution of elements in the Figures 6.12.

Figure 6.13 Element maps for 25 Mg-Al 4 (without grinding)

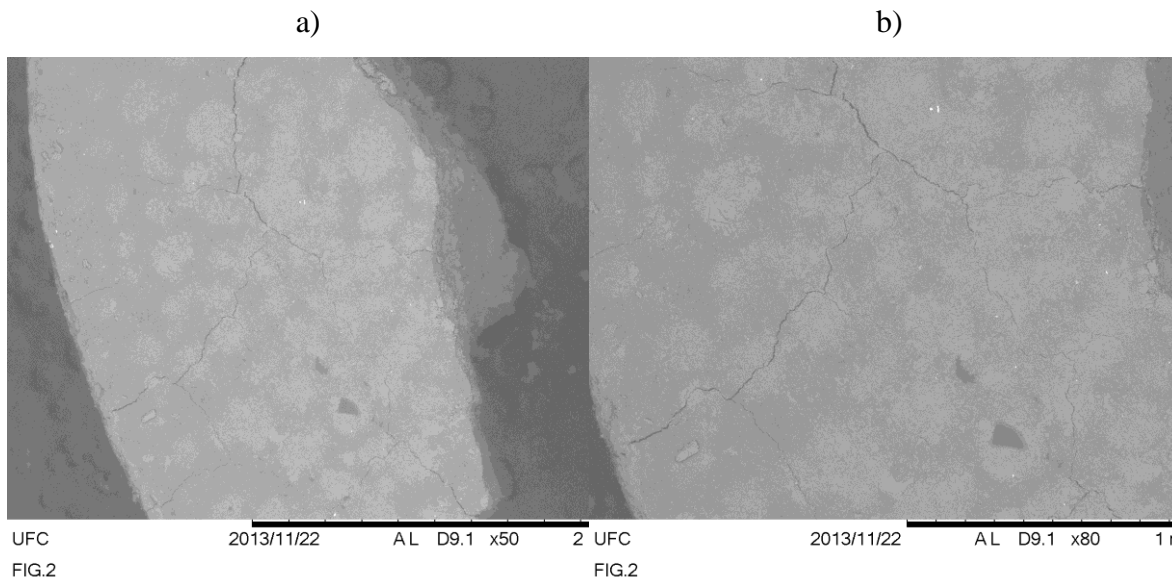


100µm Mixed
Mg (red); Al (green); C (blue)

6.3.3 Micrographs and EDS for the 30 Series

Figure 6.14 show the micrographs for a sample with 4 days of aging. It can be observed two dark regions almost in the bottom of the figure. EDS analyses were carried out to investigate this possible phase. Figure 6.15 shows the results atomic composition for these two dark regions.

Figure 6.14 Micrographs for 30 Mg-Al 4 sample. Magnification: a) of 50x; b) 80x.



The atomic composition shows differences between the dark regions and the non-dark region. This possible phase present the element carbon as the majority component in both regions. If we think about a phase it would be an amorphous one as it was not shown another phase than hydrotalcite in all the 30 Series samples.

In the previous chapter it was proof statistically that the 30 Series showed the poorest crystallinity of all the series studied and the difference is significant. This possible new non-crystalline phase would explain the reduction in the 30 Series crystallinity and the broad in all peaks.

The EDS showed a molar ratio of 0.27, 0.32 and 0.28, respectively for the Figure 6.13 a), b) and c). Although, the difference shown in atomic composition, the molar ratio did not present differences among the points analyzed in the samples. There was just a great difference in the carbon atomic composition in the three points: they showed a proportion of 2.6 : 2.4 :1, respectively for spectrum 1, 2 and 3 in figures 6.15 a, b and c.

Figure 6.15 EDS for 30 Mg-Al 4 sample in different regions (a, b, c).

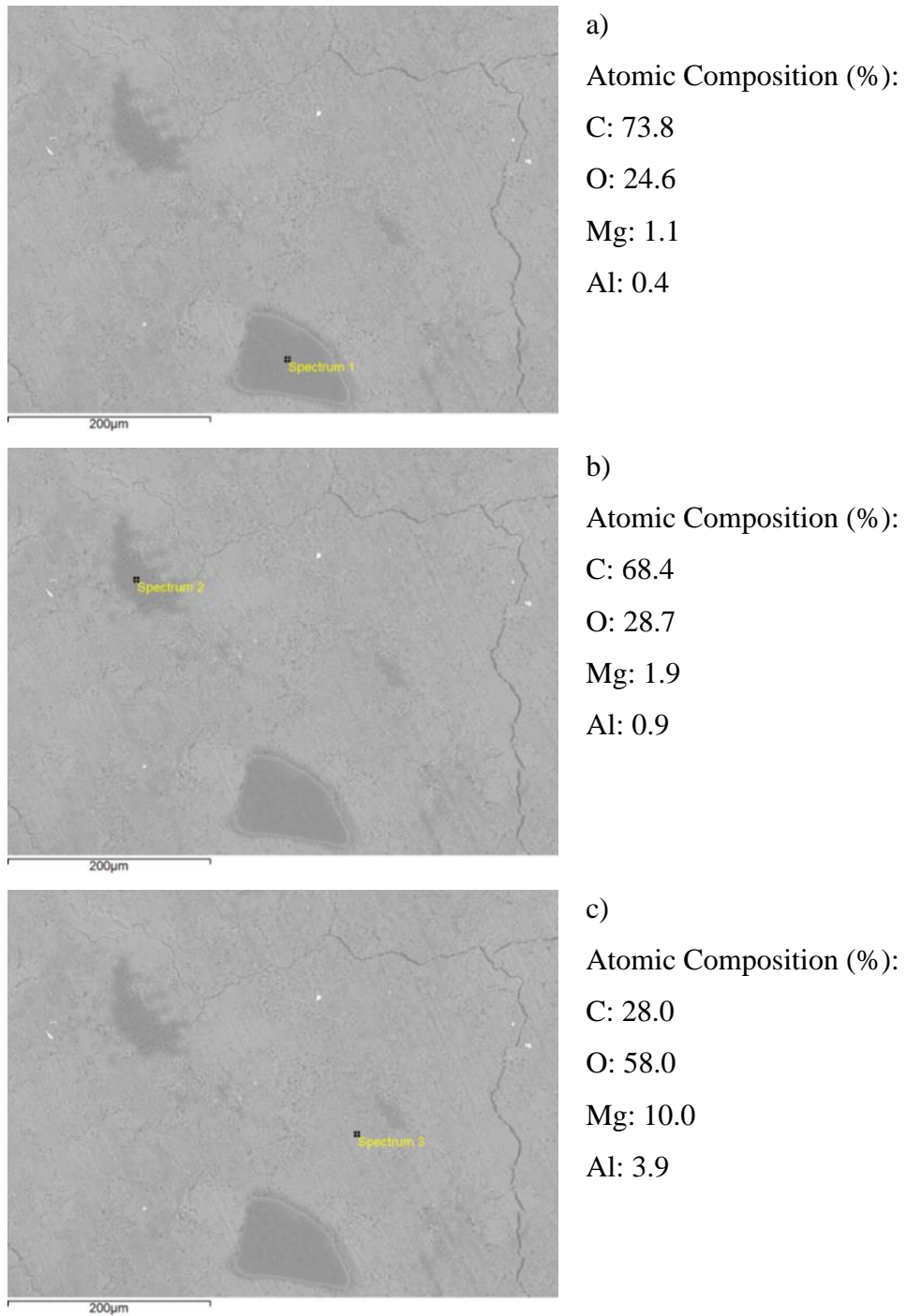
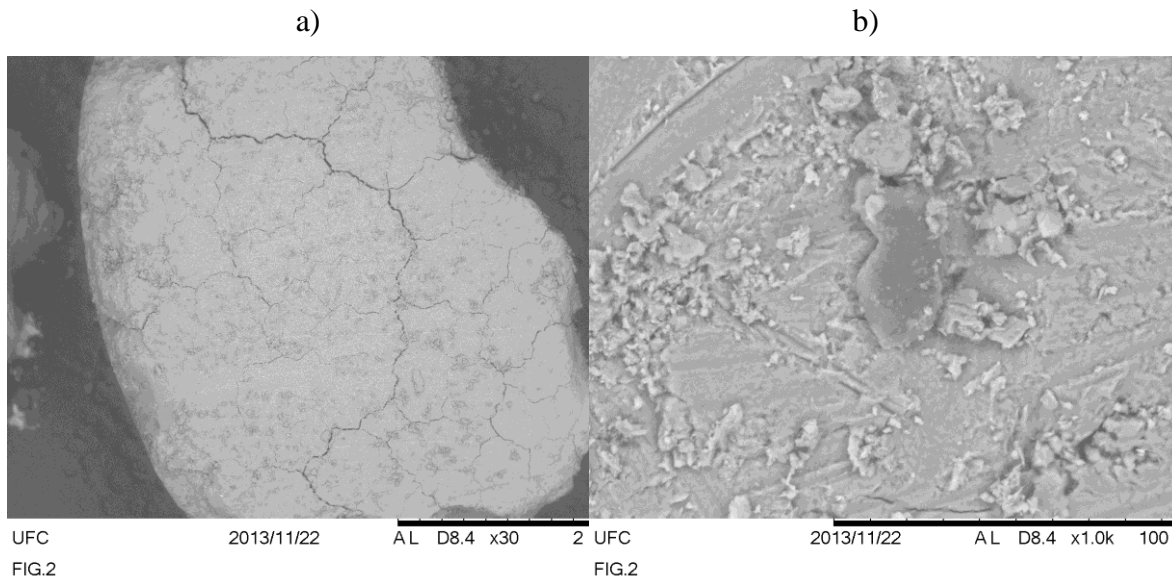


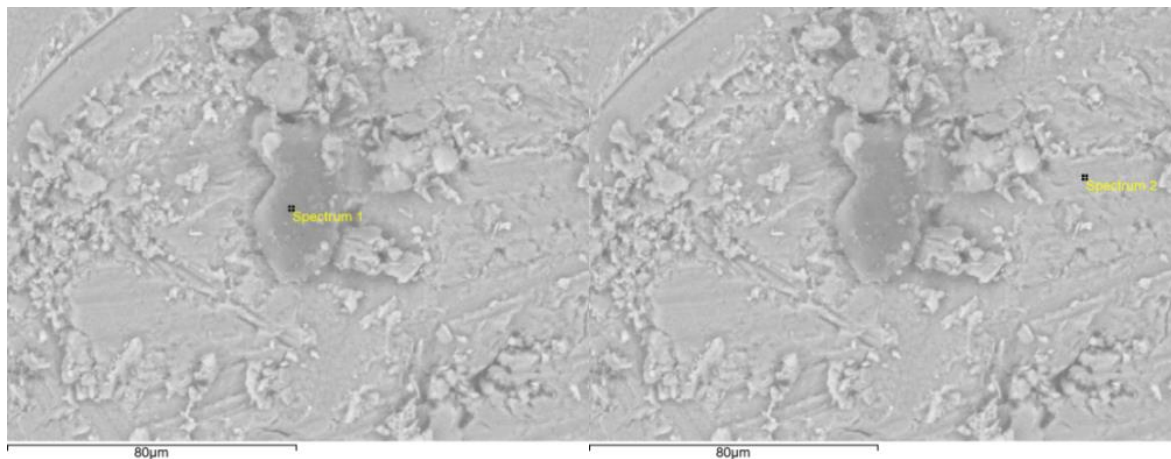
Figure 6.16 a) shows the micrographs for a sample with 35 days aging and Figure 6.14 b) showing a dark region that was analyzed by EDS. Figure 6.17 shows the results atomic composition for this two dark region. The EDS showed a molar ratio 0.34 and 0.30, respectively, for the spectrum 1 and 2 in Figures 6.17 a) and b).

Figure 6.16 Micrographs for 30Mg-Al 35 sample. Magnification: (a) of 30x; (b) 1,000x.



It is important to highlight that there were results about the differences in carbon atomic compositions. It was not so marked as the 4 aging sample. A relation 1.2:1 is found from the results obtained from EDS in 35 aging sample. The micrographs show regions with different compositions and probably represent another phase as shown in the 4 days aging sample.

Figure 6.17 EDS for 30 Mg-Al 35 samples in different regions (a, b).

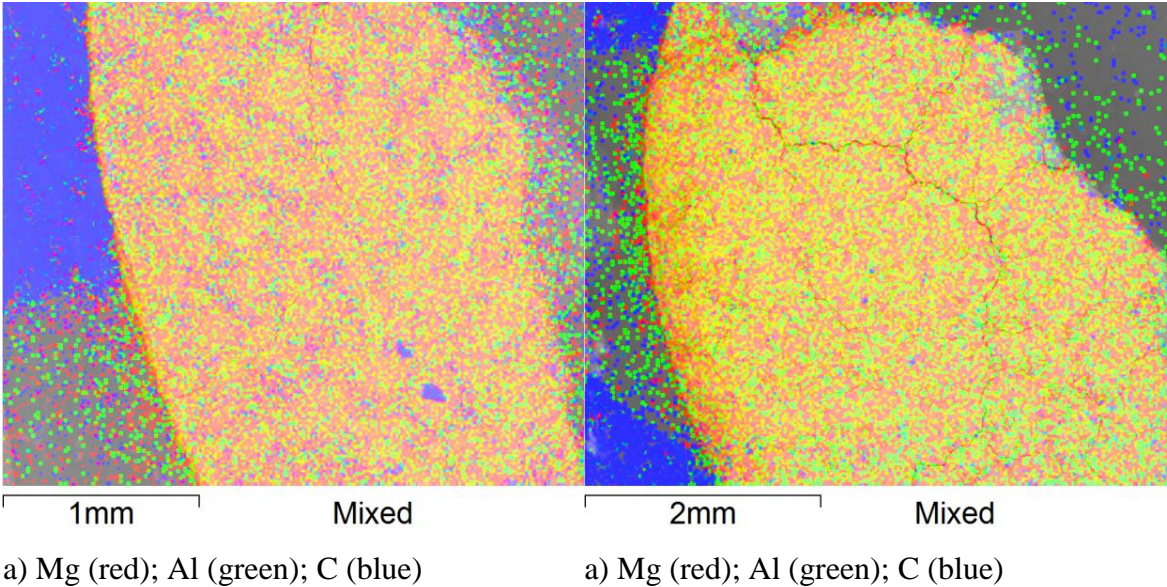


a) Atomic Composition (%):
C: 70.7; O: 24.8; Mg: 2.9; Al: 1.5

b) Atomic Composition (%):
C: 57.9; O: 36.8; Mg: 3.5; Al: 1.5

The element maps for the samples for the 4 and 35 days of aging are in Figure 6.18 a) and b) respectively; they show a homogenous distribution of the elements magnesium and aluminum, however it is possible to see regions with high concentration of carbon evidenced by the bluish color. These regions are more pronounced in the first sample.

Figure 6.18 Element maps for: a) 30 Mg-Al 4 and b) 30 Mg-Al 35.



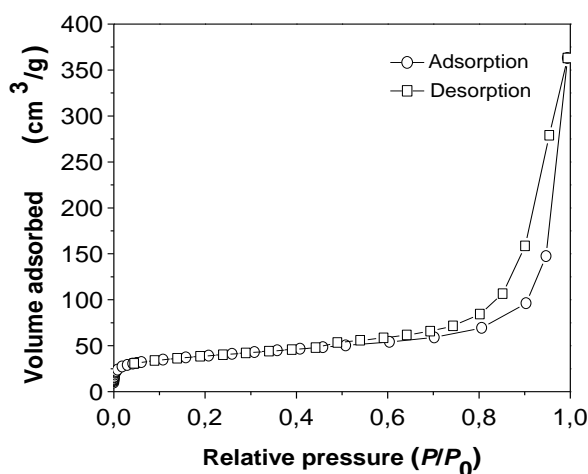
7 ADSORPTION APPLICATIONS

This chapter describes adsorption application in three samples of the 25 Series with 4, 14 and 28 days of aging. The objective was to evaluate their performance as a dye adsorbent and make an attempt of comparison with the crystallinity fit function. The 25 series was chosen because there are many results in literature to compare.

7.1 Adsorption-Desorption Isotherm

An analysis of adsorption-desorption isotherm was carried out to know some LDH textural properties. Figure 7.1 shows the adsorption-desorption isotherm at 77 K of the 25 Mg-Al 4 sample.

Figure 7.1. N₂ adsorption-desorption isotherm of 25Mg-Al 4 at 77 K.



This resembles a type IV isotherm established by IUPAC. The isotherms of type IV are found in many measures of adsorption. The turning point or "knee" present in this isotherm corresponds to the occurrence formation of first adsorbed layer that covers the entire surface of the material. A steep slope for small values of P/P_0 indicates the presence micropores whereas the hysteresis is linked to the process of filling by capillary condensation. It is a typical characteristic of mesoporous materials (MARSH and REINOSO, 2006).

BET analysis showed that hydrotalcite sample presents a $125 \text{ m}^2\text{g}^{-1}$ of surface area. This result are in agreement with literature (AUXILIO et alli, 2009), which demonstrates a considerable area available for adsorption.

Typical values of the specific surface area measured by BET technique range from 20 to $85 \text{ m}^2\text{g}^{-1}$ (Del ARCO et alli, 1994). For Mg–Al LDH containing simple anions such as carbonate, chloride, and nitrate, the surface area is mostly less than $100 \text{ m}^2/\text{g}$ (HUSSEIN et alli, 2001; INACIO et alli, 2001).

7.2 Dyes Adsorption

Adsorption procedures were carried out in two dyes Reactive Blue 4 (RB 4) and Acid Blue 25 (AB 25) using three LDH samples as adsorbent: 25Mg-Al 4, 25Mg-Al 14 and 25Mg-Al 25.

The results were compared with the follows adsorption models: Langmuir, Freundlich, Langmuir-Freundlich and Toth. Figure 7.2 shows the experimental results only whereas the Table 7.2 shows them with the fit models.

A comparison among the experimental results is shown in Table 7.1. It is possible to see a great difference in the results with aging. They showed much higher adsorption results for 4 days of aging for both dyes, compared with 14 and 28.

Table 7.1 Relative comparison among the experimental results.

Aging time	AB 25	RB 4
4 days	100%	100%
14 days	57.8%	35.3%
28 days	36.4%	29.3%

These results apparently did not show relation with the crystallinity nor with the crystallite size D_s evaluated in Chapter 5. Both parameters increases with time and get a maximum about 14 days aging and then there is a reduction whereas adsorption showed just a reduction with aging. Probably not only the crystallinity and crystallite size has to be analyzed to predict adsorption with these dyes.

According to SHARMA et alli (2007) it is an expected result considering that the aging time promotes the growth of the crystals and hence the reduced surface area available for adsorption.

Figure 7.2 Experimental adsorption results in a) AB 25 and b) RB 4.

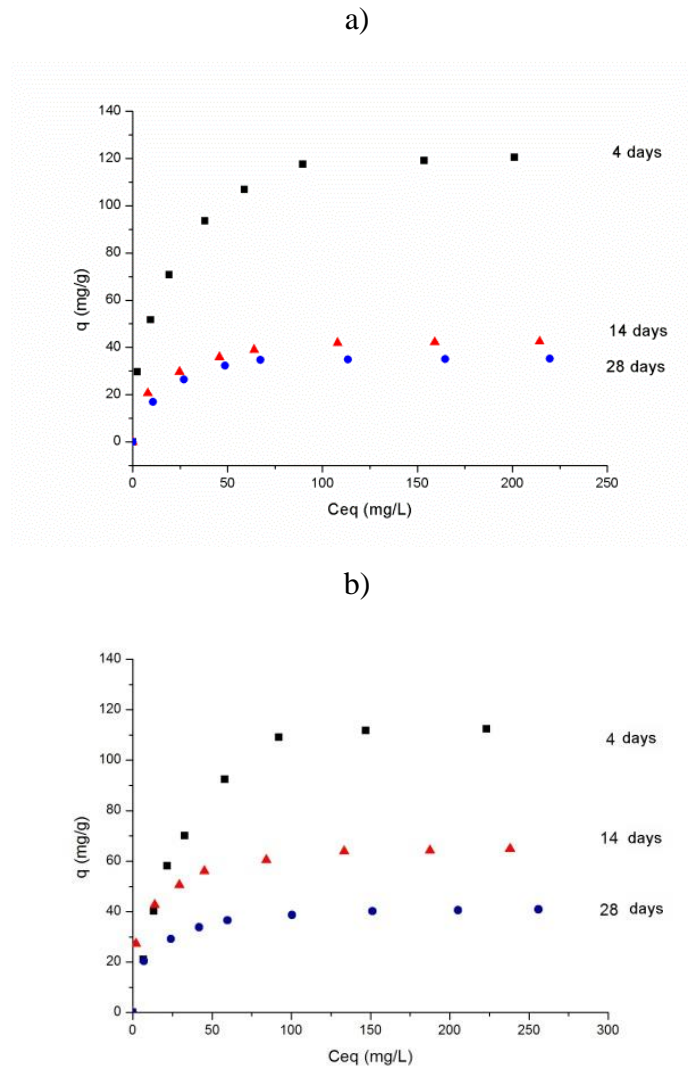
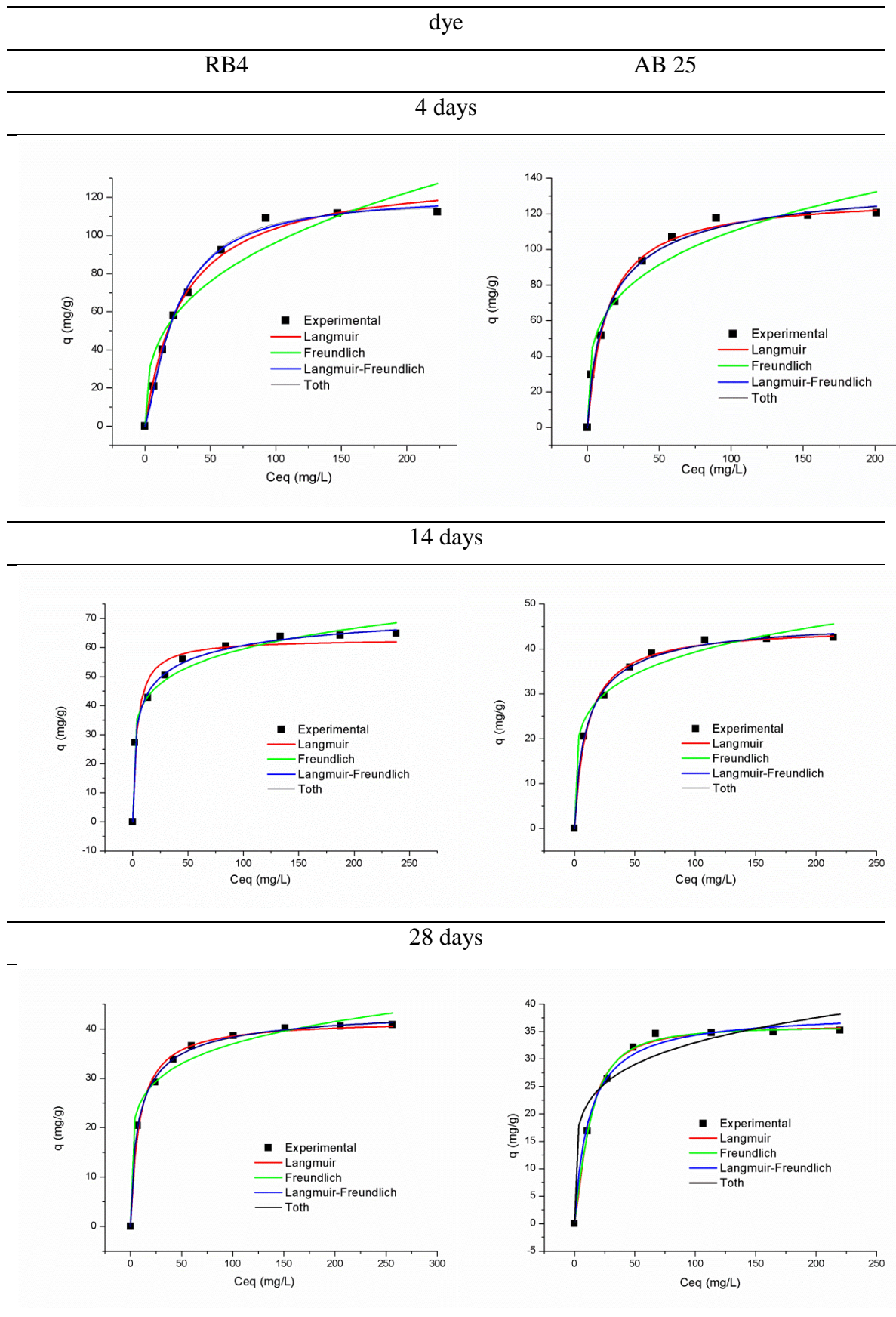


Table 7.3 shows the parameters obtained with the fit for the models used in the experimental results. Freunlich presented the worst results in fit for both dyes and aging that can be seen in Table 7.2 (green line). It also presented low values for determination coefficient and their k_F constant is not compatible with the obtained results.

Table 7.2 Fit for dyes adsorption in LDH samples.



Toth model presented good fit for the dyes, except for the result in 4 days of aging. It presented a great error for both dyes. Langmuir-Freundlich model also presented great error in Acid Blue 25 in 4 days of aging and Langmuir presented a low value of determination coefficient in reactive blue 4 in 14 days.

Thus Langmuir and Langmuir-Freundlich models were suitable to describe the adsorption behavior. LDH presented a quasi-homogenous distribution in adsorption sites for these two dyes. It can be observed Langmuir-Freundlich model that the heterogeneous factor is approximate of unity in all the samples except the Reactive Blue 4 with 14 days of aging. This indicates the tendency to Langmuir model.

Table 7.3 Isotherms parameters adsorption: Langmuir (L), Freundlich (F), Langmuir-Freundlich (LF) e Toth (T) for Acid Blue 25 (AB 25) and Reactive Blue 4(RB 4).

Model		AB 25			RB 4		
		4 days	14 days	28 days	4 days	14 days	28 days
L	q_{max}	130.3±3.7	45.0±0.7	38.5±1.0	133.6±4.5	63.0±2.2	41.9±0.6
	k_L	0.07±0.01	0.09±0.01	0.08±0.01	0.04±0.01	0.3±0.1	0.12±0.01
	R^2	0.9900	0.9958	0.9912	0.9912	0.9634	0.9955
F	k_F	32.3±5.2	16.0±2.1	14.0±2.9	19.7±5.0	28.2±2.1	17.2±1.7
	n	3.8±0.5	5.1±0.8	5.4±1.3	2.9±0.5	6.2±0.6	6.0±0.8
	R^2	0.9573	0.9700	0.9435	0.9290	0.9848	0.7960
LF	q_{max}	140.9±9.3	47.1±2.0	36.3±0.8	121.8±3.9	80.7±5.3	44.7±1.1
	k_{LF}	9.5±1.9	7.6±1.8	34.8±15.0	59.1±18.0	2.7±0.2	5.3±0.7
	b	0.8±0.1	0.8±0.1	1.4±0.2	1.3±0.2	0.5±0.06	0.8±0.1
	R^2	0.9934	0.9971	0.9968	0.9963	0.9976	0.9987
T	q_{max}	143.3±13.6	47.3±2.4	35.9±0.7	117.9±3.4	87.7±9.6	45.1±1.4
	k_T	0.11±0.04	0.13±0.04	0.05±0.01	0.027±0.002	4.5±4.5	0.2±0.05
	m_T	0.7±0.2	0.8±0.2	1.7±0.2	1.7±0.3	0.3±0.1	0.7±0.1
	R^2	0.9923	0.9970	0.9974	0.9972	0.9971	0.9986

CONCLUSIONS

The 21 samples corresponding to the three series with different molar ratios (0.20, 0.25 and 0.30) were synthesized successfully and characterized by X-Ray Diffraction, Thermo Gravimetric, Infra-Red Spectroscopy, Scanning Electron Micrograph and Energy Dispersive Spectroscopy.

X-Ray Diffraction patterns revealed that hydrotalcite was the only phase synthesized in just five samples of the 20 Series; two of them, with 28 and 35 days of aging, showed another phase brucite that was refined and quantified with approximately 11 and 2%, respectively. This result has not been observed in literature and could be a new contribution for LDH and hydrotalcite studies (ALEJANDRE et alli, 1999; FERREIRA, 2001; NODA PÉREZ et alli, 2004; CHANG et alli, 2005; RODRIGUES, 2007; SILVA, 2008; PÉREZ et alli, 2009).

It is relevant that CAVANI et alli (1991) had predict theoretically the formation of brucite in the presence of excess magnesium in the lamellae.

All the samples from the 25 Series showed just the hydrotalcite phase only whereas the 30 Series probably present an amorphous phase evidenced by the reduction in its crystallinity and the broadening in all peaks. SEM and EDS show evidences of this possible phase. Some authors affirm that it is only possible to obtain an amorphous phase only above 0.33 molar ratios. This phase could be bohemite (γ -AlO(OH)) and/or gibbsite (Al(OH)₃) that would be segregated by the lamellae containing an excess of aluminum with this molar (CAVANI et alli, 1991; NODA PÉREZ et alli, 2004; PÉREZ et alli, 2009). However an amorphous phase was detected with the molar ratio below this limit by some authors (NODA PÉREZ et alli, 2004; PÉREZ et alli, 2009).

Cell parameters and their crystallite size were calculated for two complete series (0.20 and 0.25). Unfortunately the last series could not be refined by the program used. Probably the program did not recognize this series as hydrotalcite because they presented a great shift in the basal plane peaks. This was the reason why it was not possible to fit a surface to predict the crystallite size before synthesis.

The shift in the basal plane peaks has proof to be significant compared to the other series by applying appropriate hypothesis test. The shift was about one degree and three degrees, respectively for the 003 and 006 planes. Furthermore, crystallinity of the 21 samples was evaluated and the three series were compared proof statistically that

the 20 Series presented more crystallinity than the 25 Series and thereafter the 25 Series shows more crystallinity than the 30 Series.

SHARMA et alli (2007) affirmed that the crystallinity and crystallite size of hydrotalcite samples analyzed presented significant difference among them as the aging time increases, but they did not show it statistically.

The results obtained for crystallinity were used to generate a surface that was fit to predict these characteristics before synthesis according to conditions used in this research: 0.20, 0.25 and 0.30 molar ratios; magnesium and aluminum atoms and carbonate as ion and the conditions of fixed temperature of 80 °C for hydrothermal treatment. Furthermore the synthesis of co-precipitation at variable pH; the rate of reagent addition and the temperature of synthesis are also to be the same as used in this research.

3D and hypsometric graphics were drawn to aid in the understanding and visualization of the results of crystallite size and the surface fit.

Thermo gravimetric analysis showed characteristics of hydrotalcite with two distinct stage of mass loss that were identified by the first derivative of TG. Comparison of results indicated that the behavior of the 30 Series suggested the presence of another phase due to the difference in the final loss of mass and the difference in the beginning of the stages between the others series.

All the samples presented the same common hydrotalcite infra-red profiles with slight variations in some peaks positions. The results from the samples 20 Mg-Al 28 and 35 presented a vibration band at 3699 cm^{-1} that corresponds to a stretching in the hydroxyl from brucite (FROST and KLOPROGGE, 1999). This result reinforces the presence of brucite showed in the X-ray diffraction pattern. The 20 Mg-al 21 also shows this band but with a low intensity and that sample did not show the corresponding peaks in the X-ray diffraction pattern. The segregation of brucite from the lamellae is probably favored by aging.

The scanning electron micrographs of the 20 Series samples indicate that the hydrotalcite is formed by particles without a defined shape and with an irregular surface. A mixed map carried out by Energy Dispersive Spectroscopy showed a homogeneous distribution of the atoms of aluminum and magnesium in 4 and 35 days of aging. The molar ratio were also confirmed by this analysis.

Scanning electron micrograph of two of 25 Series samples, with and without grinding, were analyzed. The images showed that the non-ground hydrotalcite is formed

by irregular particles with various sizes, and which were very different from the particles that were ground. They present a non-uniform shape with length and width approximately the same dimension for some of them and did not show a plate-like shape as the others.

The element maps showed a homogenous distribution of the elements magnesium and aluminum in two ground samples with different aging. Energy Dispersive Spectroscopy showed a 0.26 molar ratio for the non-ground samples analyzed in the 25 Series.

Micrographs for a 30 Series showed dark regions with different composition for different samples analyzed. Energy Dispersive Spectroscopy showed a phase that presented the element carbon as the major component in both regions. This could be an amorphous phase, as it was not identified by the X-ray diffraction.

A kind of grid was observed in the samples that could suggest a type of defect, associated with the amorphous phase, could be the responsible for the low crystallinity, broadening in all peaks and the shift in the basal planes peaks observed in all the samples from the 30 Series.

Finally, adsorption procedures were carried out in two different types of dyes Reactive Blue 4 and Acid Blue 25 using three LDH samples from the 25 Series. The results were fit and the Langmuir and Langmuir-Freundlich models were suitable to describe the adsorption.

Experimental results showed a great difference in the results with aging. They showed much higher adsorption results for 4 days of aging for both dyes, compared with 14 and 28 days. These results are not in accordance with the crystallinity evaluated by surface fit in this research. Probably not only the crystallinity has to be analyzed for this dyes adsorption to make a preview.

Most probably, analysis of crystallinity alone is not enough in order to allow for a reliable prediction of dye adsorption using hydrotalcite.

PROPOSALS FOR FUTERES RESEARCH

There are some suggestions that could be carried out to continue and improve this fit function proposed:

Try to find a new suitable program of refinement to get the information of the 30 Series parameters and propose a fit function to preview the crystallite size of LDH before synthesis.

Enlarge the range of molar ratio from 0.10 to 0.50 and verify how the fit function behaves with these results. The step could be lesser than 0.5; a 0.1 or 0.2 could promote a known of more details in-between the step 0.5.

Analyze adsorption in all 21 samples with the dyes studied and with other different dyes belong to other classes.

Synthesize four times each of the series and analyze four samples of the three series instead just one used here. Thus we would have 336 characterization results and could make a better statistical approach using ANOVA or a linear multiple regression.

Synthesize and collect samples longer, as months or years. Maybe there are reactions occurring as the time goes by that could be discovered with the characterization analysis.

It was proposed a two variable function $I = f(x, t)$, with crystallinity (I) and molar ratio (x) and time (t). A more complete function could preview other textural property (P) characteristics like surface specific area, particle size, particle distribution, pores volume etc.

The fit function can be proposed to preview the textural properties with other parameters, e.g.: kind of synthesis (kS) (co-precipitation at constant pH with different values); temperature of synthesis (TS) (from room ambient to 100°C in step of ten Celsius degree); hydrothermal temperature treatment (T) (from 60 °C to 200 °C in step of ten Celsius degrees); so the fit function could be a function of multiple variables like $P = f(kS, TS, T, t...)$

REFERENCES

- ABDELKADER, E.; NADJIA, L.; AHMED, B. **Degradation study of phenazin neutral red from aqueous suspension by paper sludge.** *J. Chem. Eng. Process. Technol.*, 169: 231-238 (2011).
- AGUIAR, J.E.; BEZERRA, B.T.C.; BRAGA, B.M.; LIMA, P.D.S.; NOGUEIRA, R.E.F.Q.; LUCENA, S.M.P.; SILVA JR., I.J. **Adsorption of Anionic and Cationic Dyes from Aqueous Solution on non-Calcined Mg-Al Layered Double Hydroxide: Experimental and Theoretical Study.** *Separation Science and Technology*, volume 48, issue 15, 2013. DOI: 10.1080/01496395.2013.804837.
- ALLEN, S. J.; MCKAY, G.; PORTER, J.F. **Adsorption Isotherms Models for Basic Dye Adsorption by Peat in Single and Binary Component Systems.** *Journal of Colloid and Interface Science* 280(2004) 322-333.
- ALLMAN, R., JEPSEN, H.P. (1969) **Die Struktur des Hydrotalkits: Neus Jahrb. Mineral Monatsh.**, 544-551.
- ÁLVAREZ, A.; TRUJILLANO, R.; RIVES, V. **Differently aged gallium-containing layered double hydroxides.** *Applied Clay Science* 80-81 (2013) 326-333.
- AL-DEGS, Y.; KHRAISHEH, M.A.M.; ALLEN, S.J.; AHMAD, M.N.A. **Sorption behavior of cationic and anionic dyes from aqueous solution on different types of activated carbons.** *Sep. Sci. Technol.*, 36: 91-102 (2001).
- ALEJANDRE, A.; MEDINA, F.; RODRIGUEZ, X.; SALAGRE, P.; SUEIRAS, J.E. **Preparation and Activity of Cu-Al Mixed Oxides via Hydrotalcite-Like Precursors for the Oxidation of Phenol Aqueous Solutions.** *Journal of Catalysis* 188, 311-324 (1999).
- ALLERA, G.; CORRADINI, P.; ELIAS, H.G.; GEIL, P.H.; KEITH, H.D.; WUNDERLICH, B. **Definitions of Terms Relating to Crystalline Polymers.** *Pure & Appl. Chem.* Vol. 61, No. 4, pp 769-785, 1989.
- AMIGÓ, J.M.; BATISDA, J.; SANZ, A.; SIGNES, M.; SERRANO, J. **Crystallinity of Cretaceous kaolinites of Teruel (Spain).** *Applied Clay Science* 9 (1994) 51-69.
- APARICIO, P. and GALÁN, E. **Mineralogical Interference on Kaolinite Crystallinity Index Measurements.** *Clays and Clay Minerals*, Vol. 47, N° 1, 12-27, 1999.
- ARAÚJO, M.C. **Utilização de Hidrotalcitas Mg/Co/Al na Conversão de Etanol.** Dissertação de Mestrado. UNICAMP. 2003.
- AUXILIO, A. R.; ANDREWS, P. C.; JUNK, P. C.; SPICCIA, L. **The Adsorption Behaviour of C.I. Acid Blue 9 onto Calcined Mg-Al Layered Double Hydroxides.** *Dyes and Pigments* 81 (2009) 103-112.

- BALZAR, D. **Voigt-function model in diffraction line-broadening analysis.** Microstructure Analysis from Diffraction. International Union of Crystallography. 1999.
- BENITO, P.; HERRERO, M.; BARRIGA, C.; LABAJOS, F.M.; RIVES, V. **Microwave-Assisted Homogeneous Precipitation of hydrotalcites by Urea hydrolysis.** Inorg. Chem. 2008, 47, 5453-5463.
- BENITO, P.; HERRERO, M.; LABAJOS, F.M.; RIVES, V. **Effect of post-synthesis microwave-hydrothermal treatment on the properties of layered double hydroxides and related materials.** Applied Clay Science 48 (2010) 218-227.
- BERBER, M.R.; HAFEZ, I.H.; MINAGAWA, K.; KATOH, M.; MORI, T.; TANAKA, M. **Uniform nanoparticles of hydrotalcite-like materials and their textural properties at optimized conditions of urea hydrothermal treatment.** Journal of Molecular Structure 1033(2013) 104-112.
- BLEICHER, L.; SASAKI, J.M.; PAIVA SANTOS, C.O. **Development of a graphical interface for the Rietveld refinement program DBWS.** Journal of Applied Crystallography, 2000.
- BOUDIAF, H.Z.; BOUTAHALA, M.; ARAB, L. **Removal of methyl orange from aqueous solution by uncalcined and calcined MgNiAl layered double hydroxides (LDHs).** Chem.Eng. J., 187: 142–149 (2012).
- BRAVO-SUAREZ, J.J.; PAEZ-MOZO E.A.; OYAMA, S.T. **Microtextural properties of layered double hydroxides: a theoretical and structural model.** Microporous and Mesoporous Materials 67 (2004) 1-17.
- CALLISTER JR., W.D. and RETHWISCH, D.G. **Ciência e Engenharia de Materiais uma introdução.** Rio de Janeiro: LTC, 8^o ed. 2012.
- CARJA, G.; NAKAMURA, R.; AIDA, T.; NIIYAMA, H. **Textural Properties of Layered Double Hydroxides: Effect of Magnesium Substitution by Copper or Iron.** Microporous and Mesoporous Materials 47 (2001) 275-284.
- CAVANI, F.; TRIFIRÒ, F.; VACCARI, A. **Hydrotalcite-type Anionic Clays: Preparation, Properties and Application.** Catalysis Today, 11(1991) 173-301.
- CHANG, Z.; EVANS, D.G.; DUAN, X.; VIAL, C.; GHANBAJA, J.; PREVOT, V.; DE ROY, M.; FORANO, C. **Synthesis of [Zn-Al-Co₃] Layered Double Hydroxides by a Coprecipitation Method under Steady-State Conditions.** Journal of Solid State Chemistry 178(2005) 2766-2777.
- CHANG^a, Q.; ZHU, L.; LUO, Z.; LEI, M.; ZHANG, S.; TANG, H. **Sono-assisted preparation of magnetic magnesium-aluminum layered double hydroxide and their application for removing fluoride.** Ultrasonics Sonochemistry 18 (2011) 553-561.

CHANG^b, X.; ZHANG, X.; CHEN, N.; WANG, K.; KANG, L.; LIU, Z. **Oxidizing synthesis of Ni²⁺-Mn³⁺ layered double hydroxide with good crystallinity**. *Materials Research Bulletin* 46 (2011) 1843-1847.

CHUANG, Y.H.; TZOU, Y.M.; WANG, M.K.; LIU, C.H.; CHIANG, P.N. **Removal of 2-Chlorophenol from Aqueous Solution by Mg/Al Layered Double Hydroxides (LDH) and Modified LDH**. *Ind. Eng. Chem. Res.* 2008, 47, 3813–3819.

CONCEIÇÃO, L.; PERGHER, S.B.C.; MORO, C.C.; OLIVEIRA, L.C.A. **Compósitos Magnéticos Baseados em Hidrotalcitas para a Remoção de Contaminantes Aniônicos em Água**. *Quim. Nova*, Vol. 30, Nº 5, 1077-1081, 2007.

CONSTANTINO, U.; MARMOTTINI, F.; NOCCHETTI, M.; VIVANI, R. **New Synthetic Routes to Hydrotalcite-Like Compounds - Characterisation and Properties of the Obtained Materials**. *Eur. J. Inorg. Chem.* 1998, 1439-1446.

CORNEJO, J.; CELIS, R.; PAVLOVIC, I.; ULIBARRI, M.A.; HERMOSÍN, M.C. **Structural Changes in Phenol-Intercalated Hydrotalcite Caused by Heating**. *Clay Minerals*(2000) 35, 771-779.

COSTA, D.G. **Cálculos Ab Initio da Energia de Formação de Compostos Tipo-Brucita**. Dissertação. UFJF-MG, 2007.

CREPALDI, E.L. and VALIM, J. B. **Hidróxidos Duplos Lamelares: Síntese, Estrutura, Propriedades e Aplicações**. *Química Nova*, 21(3) 1998.

CUNHA, V.R.R.; FERREIRA, A.M.C.; CONSTANTINO, V.R.L.; TRONTO, J.; VALIM, J.B. **Hidróxidos Duplos Lamelares: Nanopartículas Inorgânicas para Armazenamento e Liberação de Espécies de Interesse Biológico e Terapêutico**. *Quim. Nova*, Vol. XY, No. 00, 1-13, 2009.

CULLITY, B.D. **Elements of X-Ray Diffraction**. Massachusetts: Addison-Wesley, 1956.

CULLITY, B.D.; STOCK, S.R. **Elements of X-Ray Diffraction**. New Jersey: Prentice Hall, 3^o ed. 2001.

Del ARCO, M.; RIVES, V.; TRUJILLANO, R. **Surface and textural properties of hydrotalcitelike materials and their decomposition products**. *Studies in Surface Science and Catalysis*, 87 (Characterization of Porous Solids III), 507–515.1994.

FARIAS, S.B.P.; CHIARO, S.S.X.; DINIZ, R. **Síntese, Caracterização e Avaliação do Grau de Cristalinidade de Hidrotalcitas**. 19^o Associação Brasileira de Cristalografia, 2009.

FERREIRA, O.P. **Desenvolvimento de Materiais Porosos Bidimensionais, à Base de Al³⁺ E M²⁺ (Zn E Mg), para Uso na Remediação de Efluentes da Indústria Têxtil**. Dissertação. UNICAMP. 2001.

FRONDEL, C. **Constitution and polymorphism of the pyroaurite and sjögrenite groups.** The American Mineralogist, Journal of the Mineralogical Society of America. 1941, vol. 26, number 5 (295-315).

FROST, L. and KLOPROGGE, J. **Infrared emission spectroscopic study of brucite.** Spectrochimica Acta Part A: Molecular and Biomolecular Spectroscopy. Volume 55, Issue 11 (1999) 2195-2205.

GÉRAUD, E.; BOUHENT, M.; DERRICHE, Z.; LEROUX, F.; PRÉVOT, V.; FORANO, C. **Texture effect of layered double hydroxides on chemisorption of Orange II.** Journal of Physics and Chemistry of Solids 68 (2007) 818-823.

GOLDANI, E. **Utilização de Argilas na Remoção de Mn e Fe de Efluentes Gerados pela Atividade Mineradora de Carvão.** Dissertação. UFRS. 2007.

GUARANTINI, C.C.I. and ZANONI, M.V.B. **Corantes Têxteis: Revisão.** Química Nova, 23(1)(2000).

GUELF, L. R and SCHEER, A. P. **Estudo de Adsorção para Purificação e Separação de Misturas na Indústria Petrolífera.** UFPR. 2007.

HALMA, M. **Síntese e Caracterização de Ferroporfirinas Imobilizadas em Hidróxidos Duplos Lamelares: Estudo de Diferentes Estratégias de Imobilização e Investigação da Atividade Catalítica.** Dissertação. UFPR. 2004.

HANAWALT J.D.; RINN, H.W.; FREVEL, L.K. **Chemical Analysis by X-ray Diffraction.** Industrial and Engineering Chemistry, Analytical Edition, 10(9), 457-512 (1938).

HAMMOND, C. **The Basics of Crystallography and Diffraction.** IUCr, Oxford: New York, 3° ed. 2009.

HE, B.B. **Two-Dimensional X-Ray Diffraction.** New Jersey: John Wiley & Sons, 2009.

HE, J.; WEI, M.; LI, B.; KANG, Y.; EVANS, D.G.; DUAN, X. **Preparation of Layered Double Hydroxides.** Springer-Verlag Berlin Heidelberg, 2005.

HERRERO, M.; BENITO, P.; LABAJOS, F.M.; RIVES, V. **Stabilization of Co⁺² in layered double hydroxides (LDHs) by microwave-assisted ageing.** Journal of Solid State Chemistry 180 (2007) 873-884.

HOSNI, K. and SRASRA, E. **Simplified synthesis of layered double hydroxide using a natural source of magnesium.** Applied Clay Science 43 (2009) 415-419.

HUNGER, K. **Industrial Dyes, Chemistry, Properties, Applications.** Ed. Wiley-Vch, Frankfurt, Germany. 2003.

HUSSEIN, M.Z.B.; ZAINAL, Z.; CHOONG, E.M. **Structure and surface transformations of humic-adsorbed synthetic hydrotalcite-like materials.** Journal of Porous Materials 8, 219–226. 2001.

INACIO, J.; TAVIOT-GUÉHO, C.; FORANO, C.; BESSE, J.P. **Adsorption of MCPA pesticide by MgAl-layered double hydroxides.** Applied Clay Science 18, 255–264. 2001.

IQBAL, M. **Textile Dyes.** Ed. Rahber. Pakistan, 2008.

JENKINS, R. and SNYDER, R. Introduction to X-Ray Powder Diffractometry. Wiley. Volume 138. Chemical Analysis. 1996.

KAGUNYA, W. and JONES, W. **Aldol Condensation of Acetaldehyde Using Calcined Layered Double Hydroxides.** Applied Clay Science 10 (1995) 95-102.

KANNAN, S.; NARAYANAN, A.; SWAMY, C.S. **Effect of composition on the physicochemical properties of nickel aluminum hydrotalcites.** Journal of Materials Science 31(1996) 2353-2360.

KAVESH, S. and SCHULTZ, J.M. **Meaning and Measurement of Crystallinity in Polymers: A Review.** Polymer Engineering and Science, September, 1969, Vol. 9, N°5.

KLOPROGGE, J.T.; HICKEY, L.; FROST, R.L. **FT-Raman and FT-IR Spectroscopy Study of Synthetic Mg/Zn/Al-Hydrotalcites.** Journal of Raman Spectroscopy, 35. pp. 967-974. 2004.

KOVANDA, F.; KOLOUŠEK, D.; CÍLOVÁ, Z.; HULÍNSKÝ, V. **Crystallization of synthetic hydrotalcite under hydrothermal conditions.** Applied Clay Science 28 (2005) 101-109.

KOVANDA, F.; KOLOUŠEK, D.; ROJKA, T.; BEZDIČKA, P.; JIRÁTOVÁ, K.; OBALOVÁ, L.; PACULTOVÁ, K.; BASTL, Z.; GRYGAR, T. **Effect of hydrothermal treatment on properties of Ni-Al layered double hydroxides and related mixed oxides.** Journal of Solid State Chemistry. 182 (2009) 27-36.

KÜHNEL, R.A.; ROORDA, H.J.; STEENSMA, J.J. **The crystallinity of minerals - A new variable in pedogenetic process: a study of goethite and associated silicates in laterites.** Clays and Clay Minerals, vol. 23, pp.349-354. Pergamon Press 1975.

KUSTROWSKI, P.; SULKOWSA, D.; CHMIELARZ, L.; RAFALSKA-LASOCHA, A.; DUDEK, B.; DZIEMBAJ, R. **Influence of thermal treatment conditions on the activity of hydrotalcite-derived Mg-Al oxides in the aldol condensation of acetone.** Microporous and Mesoporous Materials 78 (2005) 11-22.

KYZAS, G.; FU, J.; MATIS, K.A. **The Change from Past to Future for Adsorbent Materials in Treatment of Dyeing Wastewaters.** Materials 2013, 6, 5131-5158.

KYZAS, G.Z. and LAZARIDIS, N.K. **Reactive and Basic Dyes Removal by Sorption onto Chitosan Derivatives.** Journal of Colloid and Interface Science 331(2009) 32-39.

LEVINE, D.M.; STEPHAN, D.F.; KREHBIEL, T.C.; BERENSON, M.L. **Estatística Teoria e Aplicações**. Rio de Janeiro: LTC, 6° ed. 2012.

LENG, Y. **Materials Characterization Introduction to Microscopy and Spectroscopic Methods**. Singapore: John Wiley & Sons (Asia), 2008.

LI, K.W.; KUMADA, N.; YONESAKI, Y.; TAKEI, T.; KINOMURA, N.; WANG, H.; WANG, C. **The pH Effects on the Formation of Ni/Al Nitrate form Layered Double Hydroxides (LDHs) by Chemical Precipitation and Hydrothermal Method**. *Materials Chemistry and Physics* 121(2010) 223-229.

LIMA, P.D.S.; BEZERRA; AGUIAR, J.E.; SILVA JR., J.I.; NOGUEIRA, R.E.F.Q.; LUCENA, S.M.P.; **Síntese e Caracterização de Hidróxidos Duplos Lamelares em Diferentes Tempos de Maturação Visando Adsorção de Corantes**. Búzios: COBEQ 2012.

LOW, K.S. and LEE, C.K. **Quaternized rice husk as sorbents for reactive dyes**. *Bioresour. Technol.*, 61: 121–125 (1997).

MEIS, N.N.A.H.; BITTER, J.H.; JONG, K.P. **Support and Size Effects of Activated Hydrotalcites for Precombustion CO₂ Capture**. *Ind. Eng. Chem. Res.* 2010, 49, 1229-1235.

MARANGONI, R. **Imobilização de Nano Partículas de Ferro em Óxidos Isolantes e Semicondutores**. Dissertação. UFPR, 2005.

MARSCH, H. and REINOSO, F.R. **Activated Carbon**. Elsevier, 2006.

MEIRA, D. M.; CORTEZ, G.G. **Estudo da Influência da Composição Química nas Propriedades Físico-químicas de Catalisadores VO_x/MOO_x/Mg_{0,5}AlO_x**. VII Encontro Latino Americano de Pós-Grauação-Universidade do Vale do Paraíba, 2007.

MIOTTO, N.; RIGOTI, E.; PENHA, F.G.; PERGHER, S.B.C.; DALLAGO, R.M. **Aplicações de Hidrotalcitas Hidrofóbicas na Remoção de Corantes Têxteis em Soluções Aquosas**. XVI Encontro de Química da Região Sul. 2008.

MONTGOMERY, D.C. and RUNGER, G.C. **Estatística Aplicada e Probabilidade para Engenheiros**. Rio de Janeiro: 5° ed. LTC. 2012.

MOUZDAHIR, Y.E.; ELMCHAOURI, A.; MAHBOUB, R.; GIL, A.; KORILI, S.A. **Equilibrium Modeling for the Adsorption of Methylene blue from Aqueous Solutions on Activated Clay Minerals**. *Desalination* 250 (2010) 335-338.

NAIME FILHO, J.F.; SILVÉRIO, F.; REIS, M.J.; VALIM, J.B. **Adsorption of Cholate Anions on Layered Double Hydroxides: Effects of Temperature, Ionic Strength and pH**. *J. Matter Sci.*(2008) 43:6986-6991.

NODA PÉREZ, C.; PÉREZ, C.A.; HENRIQUES, C.A.; MONTEIRO, J.L.F. **Hydrotalcites as Precursors for Mg,Al-mixed Oxides used as Catalysts n the Aldol**

Condensation of Citral with Acetone. Applied Catalysis A: General 272(2004) 229-240.

OH, J.M.; HWANG, S.H.; CHOY, J.H. **The effect of synthetic conditions on tailoring the size of hydrotalcites particles.** Solid State Ionics 151 (2002) 285-291.

PAIVA-SANTOS, C.O. **Aplicações do Método Rietveld.** Instituto de Química da UNESP (2001).

PEREIRA, M.F.R.; SOARES, S.F.; ORFÃO, J.J.M.; FIGUEIREDO, J.L. **Adsorption of dyes on activated carbons: influence of surface chemical groups.** Carbon, 41: 811-821 (2003).

PÉREZ, C.N.; MONTEIRO, J.L.F.; LÓPEZ NIETO, J.M.; HENRIQUES, C.A. **Influence of Basic Properties of Mg,Al-Mixed Oxides on their Catalytic Activity in Knoevenagel Condensation between Benzaldehyde and Phenylsulfonylacetonitrile.** Quim. Nova, Vol. 32, Nº 9, 2341-2346, 2009.

PERRY, R.H. and GREEN, D.W. **Perry's Chemical Engineers' Handbook.** 8th edition. 2008. McGraw-Hill.

POLATO, C.M.S.; MONTEIRO, J.L.F.; HENRIQUES, C.A. **Efeito da Composição das Correntes do Conversor das Unidades de FCC no Desempenho Catalítico de Ativos DeSO_x.** Quim. Nova, Vol. 32, No. 1, 38-44, 2009.

PONRAJ, M.; GOKILA, K.; ZAMBARE, V. **Bacterial Decolorization of Textile Dye-Orange 3R.** International Journal of Advanced Biotechnology and Research. Vol. 2, Issue 1, 2011, pp 168-177.

RAHAMAN, M.N. **Ceramic Processing and Sintering.** 2^o ed. Marcel Dekker. New York. 2003.

RAZALI, N.M. and WAH, Y.B. **Power comparisons of Shapiro-Wilk, Kolgomorov-Smirnov, Lilliefors and Anderson-Darling tests.** Journal of Statistical Modeling and Analysis, vol.2 No. 1, 21-33, 2011.

REED, J.S. **Introduction to the Principles of Ceramic Processing.** John Wiley & Sons. 1988.

REIS, M.J. **Estudo da Adsorção de Tensoativos Aniônicos Sulfonados em Hidróxidos Duplos Lamelares.** Dissertação. USP, 2004.

REIS, M.J. **Síntese e Caracterização de HDL Preparados na Presença de Polímeros Orgânicos ou com Macromoléculas Intercaladas.** Tese. USP, 2009.

RIBEIRO, C. **Intercalação de Ânion Enalaprilato em Hidróxido Duplo Lamelar Recoberto com Xiloglucana: Estudos de Liberação in Vitro.** Dissertação. UFPR, 2008.

RIBEIRO, T.S. **Caracterização por difração de raios-x e espectroscopia Mossbauer de nanopartículas de SnO₂ dopadas com ferro.** Dissertação de Mestrado. UFC. 2010.

RODRIGUES, J.C. **Síntese, Caracterização e Aplicações de Argilas Aniônicas do Tipo Hidrotalcita.** Dissertação. UFRS. 2007.

RUTHVEN, D.M. **Principles of Adsorption and Adsorption Processes.** John Wiley & Sons, 1984.

SAIAH, F.B.D.; SU, B.; BETTAHAR, N. **Nickel-Iron Layered Double Hydroxide(LDH): Textural Properties upon Hydrothermal and Application on Dye Sorption.** Journal of Harzadous Materials 165(2009) 206-217.

SANTOS, A.F.X.G. **Catalisadores Heterogêneos para a Produção de Biodiesel Metanólise de Óleo de Soja sobre Hidrotalcites de Magnésio e Alumínio Modificadas.** Dissertação. Instituto Superior Técnico de Lisboa. 2007.

SHAPIRO, S.S. and WILK, M.B. **An Analysis of Variance Test for Normality (Complete Samples)** Biometrika, vol. 52, No. 3 and 4 (Dec., 1965), pp. 591-611.

SHARMA, S. K.; KUSHWAHA, P.K.; SRIVASTAVA, V.K.; SHARAD, D.; BHATT, S.D.; JASRA, R.V. **Effect of Hydrothermal Conditions on Structural and Textural Properties of Synthetic Hydrotalcites of Varying Mg/Al Ratio.** *Ind. Eng. Chem. Res.* 2007, 46, 4856-4865.

SILVA, V.A. **Estudo da Síntese da Chalcona 1(4'-N-Fenil-Sulfonilamidafenil)-3-(4-Metilfenil)-2e-Propen-1-Ona.** Dissertação. UnUCET. 2008.

SILVA, L.P.R. and VALIM, J.B. **Estudo da Intercalação do Ânion do Ácido Cólico em Hidróxidos Duplos Lamelares de Mg⁺² E Al⁺³.** 30º Reunião Anual da Sociedade Brasileira de Química – SBQ. 2007.

SING, K.S.W; EVERETT, D.H.; HAUL, R.A.W.; MOSCOU, L.; PIEROTTI, R.A.; ROUQUEROL, J.; SIEMIENIEWSKA, T. **Reporting physisorption data for gas-solid systems.** Pure and Applied Chemistry. Vol. 57, N°4, pp. 603-619, 1985.

SINGH, V.; SHARMA, A.K.; SANGHI, R. **Poly(acrylamide) Functionalized Chitosan: An Efficient Adsorbent for Azo Dyes from Aqueous Solutions.** Journal of Hazardous Materials 161(2009) 955-966.

SILVERIO, F. **Adsorção de Aminoácidos em Hidróxidos Duplos Lamelares: Efeito da Temperatura, pH e Força Iônica do Meio.** Dissertação. USP Ribeirão Preto. 2004.

SILVÉRIO, F.; REIS, M.J.; TRONTO, J.; VALIM, J.B. **Adsorption of Phenylalanine on Layered Double Hydroxides: Effect of Temperature and Ionic Strength.** J Mater Sci (2008) 43:434-439.

SOONG, T.T. **Fundamentals of probability and statistics for engineers.** John Wiley & Sons, 2004.

THEVENOT, F.; SZYMANSKI, R.; CHAUMETTE, P. **Preparation of Al-Rich Zn-Al Hydrotalcite-Like Compounds.** Institut Français du Pétrole. Clays and Clay Minerals, vol.37, No. 5, 396-402, 1989.

TRONTO, J. **Síntese, Caracterização e Estudo das Propriedades de Hidróxidos Duplos Lamelares Intercalados com Polímeros Condutores.** Tese. USP, 2006.

VILLANUEVA, S.B.L. **Reações de Etanol sobre Hidrotalcitas Calcinadas.** Dissertação. UNICAMP. 2000.

VILLANUEVA, S.B.L. **Preparação e Caracterização de Hidrotalcitas Mg/Al Calcinadas e suas Propriedades Catalíticas para Reações de Conversão de Etanol.** Tese. UNICAMP. 2005.

ZAMBONI, S.; CONCEIÇÃO, L.; PERGHER, S.B.C. **Estudo dos Ciclos de Adsorção de Contaminantes Aniônicos Aquosos de Indústrias Têxteis Utilizando Hidrotalcita Calcinaada.** 28º Reunião Anual da SBQ, 2005.

ZHU, M.X.; LI, Y.P.; XIE, M.; XIN, H.Z. **Sorption of an anionic dye by uncalcined and calcined layered double hydroxides: a case study.** *J. Hazard. Mater.* B,120: 163–17. (2005)

WASEDA, Y.; MATSUBARA, E.; SHINODA, K. **X-Ray Diffraction Crystallography Introduction, Examples and Solved Problems.** Springer-Verlag Berlin Heidelberg, 2011.

WOOLFSON, M.M. **An Introduction to X-Ray Crystallography.** Cambridge: Cambridge University Press, 2º ed. 1997.

YOUNG, R.A. **The Rietveld Method.** New York: ed. OXFORD University Press, 1993.

APPENDIX

A. SCIENTIFIC PRODUCTION

AGUIAR, J.E.; BEZERRA, B.T.C.; BRAGA, B.M.; LIMA, P.D.S.; NOGUEIRA, R.E.F.Q.; LUCENA, S.M.P.; SILVA J.R., I.J. **Adsorption of Anionic and Cationic Dyes from Aqueous Solution on non-Calcined Mg-Al Layered Double Hydroxide: Experimental and Theoretical Study.** Separation Science and Technology, volume 48, issue 15, 2013. DOI: 10.1080/01496395.2013.804837.

AGUIAR, J.E.; BEZERRA, B.T.C.; BRAGA, B.M.; LIMA, P.D.S.; LUCENA, S.M.P.; SILVA J.R., I.J. **Adsorção de Corantes Aniônicos e Catiônicos de Soluções Aquosas em Hidróxido Duplo Lamelar (Mg-Al) não Calcinado: Estudo Experimental e Teórico.** XXXVI Congresso Brasileiro de Sistemas Particulados. UFAL, Maceió, 2013.

LIMA, P.D.S.; BEZERRA, B.T.C.; SILVA J.R., I.J.; NOGUEIRA, R.E.F.Q.; LUCENA, S.M.P.; **Síntese e Caracterização de Hidróxidos Duplos Lamelares em Diferentes Tempos de Maturação Visando Adsorção de Corantes.** XIX Congresso Brasileiro de Engenharia Química, COBEQ. Búzios, RJ, 2012.

ALBUQUERQUE, J.S.V.; LIMA, P.D.S.; ALVES, E.R.; NOGUEIRA, R.E.F.Q. **Influência da Razão Ca/P na Síntese de β -Fosfato Tricálcio Nanométrico.** XIX Congresso Brasileiro de Engenharia Química, COBEQ. Búzios, RJ, 2012.

BRAGA, B.M.; LIMA, P.D.S.; LUCENA, S.M.P.; **Validação de Modelo de Hidróxido Duplo Lamelar via Simulação Molecular.** XIX Congresso Brasileiro de Engenharia Química, COBEQ. Búzios, RJ, 2012.

AGUIAR, J. E. ; BEZERRA, B. T. C.; LIMA, P. D. S.; LUCENA, S. M. P.; SILVA JR., I. J. **Remoção de Corantes Têxteis Utilizando Hidróxido Duplo Lamelar.** IN: IX Encontro Brasileiro de Adsorção / I simpósio Ibero-Americano sobre Adsorção. Recife. IX encontro Brasileiro de Adsorção / I simpósio Ibero-Americano sobre Adsorção, 2012.

BEZERRA, B. T. C.; AGUIAR, J. E. ; LIMA, P. D. S.; LUCENA, S. M. P.; SILVA JR., I. J. **Remoção De Corantes Têxteis por Adsorção em Argila do Tipo Hidróxido Duplo Lamelar (HDL)**. In: IX Congresso Brasileiro De Engenharia Química - Iniciação Científica. Maringá. IX Congresso Brasileiro De Engenharia Química - Iniciação Científica, 2011.

BEZERRA, B. T. C.; AGUIAR, J. E. ; LIMA, P. D. S.; NOGUEIRA, R. E. F. Q.; LUCENA, S. M. P.; SILVA JR., I. J. **Estudos De Adsorção Em Tanques Agitados Do Corante Reativo Preto 5 Em Materiais Nanoporosos**. In: XXXV Congresso Brasileiro de Materiais Particulados. Vassouras. XXXV Congresso Brasileiro de Materiais Particulados, 2011.

MOTA, R.C.; LIMA, P.D.S.; SASAKI, J.M.; NOGUEIRA, R.E.F.Q. **Influência na Adição de Borra Branca nas Características Físicas e Mecânicas de Argilas de Formação Secundária**. Revista de Geologia (Fortaleza), v.22, p.242-249, 2009.

B. PRESENTATION

LIMA, P.D.S. **Aplicações de Argilas Tipo Hidróxido Duplo Lamelar na Adsorção de Corantes Industriais**. III Mostra de Pesquisa em Ciência e Tecnologia DeVry Brasil. Fortaleza, 2012.